Colour changing electro active polymer systems

Hediyeh Zahabi

SUBMITTED IN PARTIAL FULFILLMENT OF THE REQUIREMENTS OF THE DEGREE OF DOCTOR OF PHILOSOPHY

School of Engineering and Materials Science

Queen Mary University of London

September 2016

Declaration

I, Hediyeh Zahabi, confirm that the research included within this thesis is my own work or that where it has been carried out in collaboration with, or supported by others, that this is duly acknowledged below and my contribution indicated. Previously published material is also acknowledged below.

I attest that I have exercised reasonable care to ensure that the work is original, and does not to the best of my knowledge break any UK law, infringe any third party's copyright or other Intellectual Property Right, or contain any confidential material.

I accept that the College has the right to use plagiarism detection software to check the electronic version of the thesis.

I confirm that this thesis has not been previously submitted for the award of a degree by this or any other university.

Signature:

Hediyeh Zahabi

Date

Acknowledgements

This thesis, like many others, required the input of many people, most of whom selflessly helped me during the course of my research.

First and foremost, I would like to extend my gratitude to my first supervisor Professor James Busfield for giving me the opportunity to carry out this PhD in the soft matter group. I am wholeheartedly grateful for his encouragement, supervision and support throughout my research. I would like to also thank him for allowing me to attend the many workshops and conferences during my PhD that gave me a great opportunity to broaden my knowledge and strengthen my ability to communicate with so many interesting people from all around the world.

I wish to express my gratitude to my second supervisor Dr Federico Carpi for his constant help, motivation and guidance he has provided throughout my PhD. It was an absolute pleasure to be a member of his group.

I have been extremely lucky to have such incredible supervisors who responded to my questions and queries so promptly, and who cared so much about my work.

This work is done with collaboration with Martyn Bennett and Mike Harral from ARTIS and Avon Rubber PLC respectively. I would like to thank ARTIS for their generous support and in particular Martyn Bennett for his support, patience and his valuable suggestions. I would like to also acknowledge the Principal's scholarship of QMUL, for the financial support of my research.

I am most grateful to Dr Olivier Picot for his endless ideas and support from the beginning of my research without whom the divergence into the field of liquid crystals would have been twice as difficult. It was an absolute pleasure to work with him.

I would like to thank Professor Cees Bastiaansen whose monthly meetings I looked forward to as his wisdom and advice was invaluable to this PhD.

I extend my sincere thanks to all the staff in the School of Engineering and Materials Science as well as Nanoforce Technology Ltd. for use of their facilities.

I would like to thank all the members of soft matter group, the source of many life-long friends, and some acquaintances. To be at the centre of such a bright and talented collection of individuals has been a real privilege.

Also I want to thank all my friends for their encouragement and emotional support.

I would like to dedicate this thesis to my father, mother and sister. No matter how far they were from me all these years, they have always provided me endless love and compassion and without their support I would have never been able to overcome all the difficulties I encountered during my PhD. I would like to especially thank my father, Mr. Hooman Zahabi for the motivation and financial support he provided me all these years, I can never thank you enough for all you have done for me. You are all my inspiration and I love you.

I would finally like to acknowledge the love and even greater patience of my darling fiancé Dr Jakub Kadlcak, another reason to be thankful for the soft matter group.

Abstract

Dielectric elastomers are electroactive polymers, which change size and shape in response to an electrical field. Dielectric elastomer actuators (DEAs) are highly promising new technologies in optical applications such as tuneable optical lenses, diffraction gratings and active camouflage. This thesis aims to develop a new approach to create a strain actuated compliant colour changing device that is controlled using DEAs as they offer stretchability, low weight, high efficiency, low cost and the possibility for miniaturisation. Conventional DEAs use transparent elastomeric materials with no significant colour change with strain. Conversely, liquid crystal materials are known to display dynamic colour changing behaviour, thereby making them good candidate materials. The thesis examines both the potential for colour changing soft actuators and the upcoming challenges in this field as well as the key concepts around liquid crystals that exhibit colour change.

An initial approach was aimed at creating colour changes using dielectric elastomer actuators that drove a masked positioner. This method showed colour change since the mask changes the colour visualisation.

The second approach used polymer dispersed liquid crystals, such as a nematic liquid crystal within a reactive silicone resin. The immiscibility of these compounds resulted in a dispersion of the liquid crystal droplets in the silicone matrix. However, the optical properties could not be controlled through mechanical deformation alone and the alignment of resulting LC droplets in the PDLC films was sensitive to the substrate used to perform the actuation.

The next approach used reactive cholesteric liquid crystals (CLC) instead. A thin film coating process was preferred to carefully control the film's thickness by stretching. In

free standing films a planar cholesteric alignment was obtained with mesogens aligned parallel to the substrate and colour was achieved based on the selective reflection of light. A transfer print technique was introduced to combine CLC coatings with elastomeric substrates that can be stretched. However, no colour change was achieved in response to mechanical deformation primarily due to the modulus and strength mismatch between the thin film and the elastomeric susbstrate material.

Finally, lightly crosslinked liquid crystal elastomers using a combination of reactive and non-reactive liquid crystals were produced that were compatible with elastomer substrate materials. In free standing films planar cholesteric alignment was obtained with mesogens aligned parallel to the substrate. Successfully a reversible colour change based on selective reflection of light was achieved in response to a mechanical deformation.

Contents

List of Figures

List of Tables

List of Symbols and Abbreviations

A	Area
n	Average refractive index
Δn	Birefringence
C	Capacitance
cm	Centimeter
cm^2	Centimeter squared
Q	Charge
CCD	Charge Coupled Device
CLC	Cholesteric Liquid Crystal
C	Concentration of chiral dopant
ccp	Cubic closed-pack
DI	De-ionised
°C	Degrees celsius
DE	Dielectric Elastomer
DEA	Dielectric Elastomer Actuator
ε_0	Dielectric permittivity of vacuum
DSC	Differential Scanning Calorimetry
$\hat{n}$	Director
E	Electric field
U_e	Electrical energy
EAP	Electroactive Polymer

EMI	Electromechanical instability
n_e	Extraordinary index
FGS	Functionalized Graphene Sheet
Tg	Glass transition temperature
HTP	Helical Twisting Power
IR	Infrared
kPa	kilopascal
kV	Kilovolt
kW	Kilowatt
LHCPL	Left Handed circularly Polarised Light
LC	Liquid Crystal
LCE	Liquid Crystal Elastomer
LCP	Liquid Crystal Polymer
LSCE	Liquid single crystal elastomers
p	Maxwell stress
MJ	Megajoule
MPa	Megapascal
MV	Megavolts
m^3	Meter cubed
µm	Micrometer
µs	Microsecond
mm	Millimeter
ms	millisecond
mW	milliwatt

nm	Nanometer
OM	Optical Microscopy
S	Order parameter
n_o	Ordinary index
Pa	Pascal
%	percentage
P	Pitch
PEDOT	Poly 3,4-ethylenedioxythiophene
PDMS	Polydimethylsiloxane
PI	Polyimide
PDLC	Polymer dispersed liquid crystal
n_p	Polymer refractive index
PIPS	Polymerisation Induced Phase Separation
PS	Polystyrene
PSS	Polystyrenesulfonate
PVA	Polyvinylalcohol
ε_r	Relative dielectric constant
RHCPL	Right Handed circularly Polarised Light
rpm	Round per minute
SEM	Scanning Electron Microscopy
s	Second
SIPS	Solvent Induced Phase Separation
$\Delta\lambda$	Spectral bandwith
SRI	Stanford Research Institute

TIPS	Thermally Induced Phase Separation
t	Thickness
z	Thickness
TN	Twisted Nematic
UV/Vis	Ultraviolet/Visible
Vol	Volume
λ	Wavelength
λ_0	Wavelength of reflected light
wt.%	Weight percentage
W	Work done
E_{0x}	x component of the amplitude of electric field
E_{0y}	Y component of the amplitude of electric field

Chapter 1: Introduction

Ongoing developments in engineering technology and progress in the field of materials science means that tuneable colour devices are becoming very popular as they can potentially be used in various fields such as communication, fashion, camouflage and architecture.

A huge amount of the research has been done attempting to understand how the structural colour seen in nature can be adopted for the development of novel materials that can change colour (Vukusic and Sambles, 2003, Kinoshita and Yoshioka, 2005, Parker, 2000, Zhao et al., 2012, Fudouzi, 2016, Kolle et al., 2010). Recently Zhang and Chen (2015) reported a breakthrough where they had mimicked the blue colour in *Morpho* butterfly wings by developing a novel nanofabrication process (Zhang and Chen, 2015). Rossiter

et al. (2012) studied the colour change as a result of rapid response of the chromatophores in the skins of fish and cephalopods (Rossiter et al., 2012). Sharma et al. (2009) investigated the structural origin of circularly polarised irradiance in jewelled beetles (Sharma et al., 2009).

Dielectric elastomers are an important class of Electroactive Polymers (EAPs) with highest achievable active strains and stresses, above 100% strain and 1 MPa respectively (Carpi and De Rossi, 2005). They can be used as actuators when sandwiched between two compliant electrodes followed by the application of high voltage difference between the electrodes. Dielectric Elastomer Actuators (DEAs) are considered as highly promising new technologies as they offer stretchability, low weight, high efficiency, low cost and the possibility for miniaturisation. They have been studied for optical applications such as, tuneable focus optical lenses (Carpi et al., 2011, Son et al., 2012), tuneable transmission gratings and variable diffraction gratings (Aschwanden et al., 2008, Fang et al., 2010) and active camouflage (Rossiter et al., 2012). In a review paper, Carpi and De Rossi (2005) explained the multifunctionality of EAPs and EAP based actuators, showing they can be very promising for the development of wearable flexible devices (Carpi and De Rossi, 2005). They highlighted the flexibility of tube and rolled DEAs with linear actuation functionalities making them potentially suitable for completely wearable electronic textiles and flexible displays.

Inspired by the structural colour in nature the aim of this thesis is to develop a new approach to create a colour changing device that is strain activated whereby the strain is achieved using dielectric elastomer actuators.

Conventional DEAs use transparent elastomeric materials that do not provide significant colour change with strain. For this reason in this work the DEA was considered to only be used as the driving mechanism to achieve a strain in the colour changing or potentially

tuneable colour display device. Consequently, we need a novel soft material that has some sort of structural organisation that can produce spectral colour and is compatible with elastomer substrate materials used in a DEA. Hence, dynamic colour changing behaviour of liquid crystals, makes them a good candidate for the proposed soft material.

Chapter 2 of this thesis contains a three-part literature survey that begins by examining the existing colour changing technologies that exist using a range of different technological approaches. The focus of this thesis is on underlying technologies that are based on soft materials that produce colour under the application of a mechanical strain. The second part of the literature review describes the fundamental behaviour of DEAs, the upcoming challenges in this field and the state of the art in the area of optics. The third part of the literature review describes the key concepts around liquid crystal materials with a particular focus on a cholesteric liquid crystal's structure and optical properties.

This thesis is composed of four experimental chapters starting with chapter 3 that introduces an initial approach to create a colour changing device using dielectric elastomer actuators that drove a masked positioner.

In chapter 4 polymer dispersed liquid crystals (PDLCs) are introduced whereby nematic liquid crystals are mixed together with a reactive silicone resin. The immiscibility of these compounds results in a dispersion of the liquid crystal droplets in the silicone matrix. To create a suitable film, the alignment of the different dispersed liquid crystal droplets is verified using LCs with different molecular chemistries. The effect of mechanical deformation and the effect of layering the films onto different elastomeric materials that are capable of being actuated is also investigated.

In chapter 5, reflective thin films are introduced by coating a Cholesteric Liquid Crystal (CLC) mixture on an aligned sacrificial polymer substrate using a spray deposition

technique. It demonstrates how the colour is achieved based on the selective reflection of light and how the colour can be tuned by changing the thickness of the thin film. Transfer print techniques are developed which allow the CLC coatings to be combined with these elastomeric substrates that have the potential to be stretched.

Finally, in chapter 6 we demonstrate a novel soft material that can produce a reversible colour change based on selective reflection of light in response to a mechanical deformation. The soft material is made of a lightly crosslinked liquid crystal elastomer using a combination of reactive and non-reactive liquid crystals that are compatible with elastomer substrate material.

Chapter 7 discusses the key findings in this thesis and maps out a series of future works that will allow these materials to be developed into a functioning, robust, strain activated colour changing devices.

Chapter 2: Literature Review

2.1 Colour Changing Technologies

A great deal of scientific research has been done towards the possibility of producing structural colour inspired by the colour in nature that comes from inherent colours of materials or colour that has purely physical origins such as from the diffraction of light. This literature review will focus on a few examples of different colour changing technologies that are based on soft materials that can change colour through the application of mechanical deformation.

Fudouzi et al. (2006) demonstrated tuneable and reversible structural colour using a photonic elastomer rubber sheet for the application of smart sensing. The sheet is composed of a thin layer of cubic closed-packed, ccp, colloidal monodispersed

polystyrene (PS) spheres embedded in polydimethylsiloxane (PDMS) elastomer (Figure 2.1) (Fudouzi and Sawada, 2006).

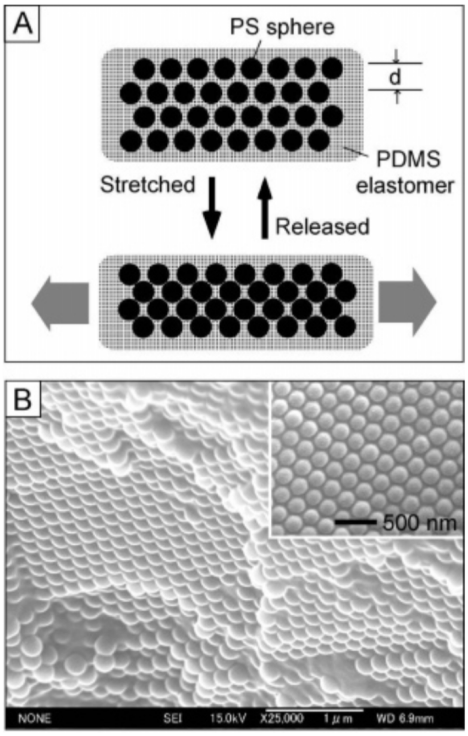

Figure 2.1- (a) schematic representation of reversible tuning lattice distance of PS array embedded in a PDMS, elastomer matrix due to stretching and shrinking, (b) Scanning Electron Microscopy (SEM) images of the surface and cross section of the PS spheres arrayed with cubic close packing (ccp) in a PDMS elastomer (Fudouzi and Sawada, 2006).

They showed that the Bragg's diffraction peak of the photonic rubber sheet was linearly tuned as a function of mechanical strain up to 20%. Figure 2.2 shows in the circled area, that the colour shifted in the visible spectrum from red to green resulting from a decrease in the centre-to-centre distance between the spheres shown in (Figure 2.1).

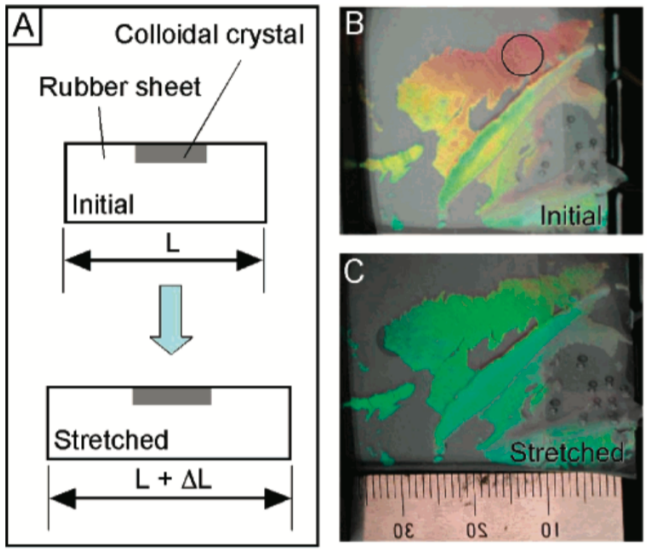

Figure 2.2- Structural colour change of photonic elastomer sheet (a) schematic representation of elastic deformation when rubber sheet is stretched by applying a mechanical strain, (b) photonic image of the sheet at initial length and (c) photonic image of the stretched sheet (Fudouzi and Sawada, 2006).

Shieh et al. (2013) developed PS/PDMS photochromic films for the application of security devices and decorative paints. The film was formed by adding PDMS pre-polymer around the self-assembled polystyrene microspheres on a PDMS substrate followed by curing. PS microspheres were synthesised using emulsifier-free emulsion polymerisation and then they were self-assembled into an ordered periodic structure by the dip-drawing method. The reflected structural colour was stabilised as a result of the close match in the refractive index of the PDMS and the PS microspheres. A low viscosity PDMS pre-polymer was used to surround the vacant spaces between the spheres and was also used as a protective layer. It had the ability to increase the optical transmittance of the film to 95%. Reflected structural colour was observed when the film was tilted at a particular angle of view (Shieh et al., 2013).

Zhu et al. (2010) demonstrated the fabrication of a highly stretchable plasmonic structure consisting of a monolayer array of gold-coated PS spheres on an elastic PDMS substrate through self-assembly and transfer printing technique. In conventional plasmonic

structures, surface plasmons (charge density oscillations bound at metallic surfaces) are used to achieve optical properties not seen in nature (Raether, 1988).

In this experiment the structure shows Surface Plasmon Resonances (SPRs) which is a phenomenon that occurs when polarized light hits a metal surface at the interface of two media with different refractive indices. This technique generates electron charge density waves called 'Plasmons', which then reduces the intensity of reflected light at a specific angle in proportion to the mass on a sensor surface (Richard, 2007). Upon stretching, the lattice of the PS microsphere is deformed, causing a large wavelength shift of the surface plasmon resonances that leads to a reversible colour change. Hence these tuneable plasmon structures can be used in sensing and display applications (Zhu et al., 2010).

Suzumori et al. (2011) investigated soft diffraction gratings for the application of soft sensor-actuator using a silicone rubber moulded against commercial diffraction gratings. The films were fabricated with a high accuracy having the same pitch and height as the master gratings (Figure 2.3).

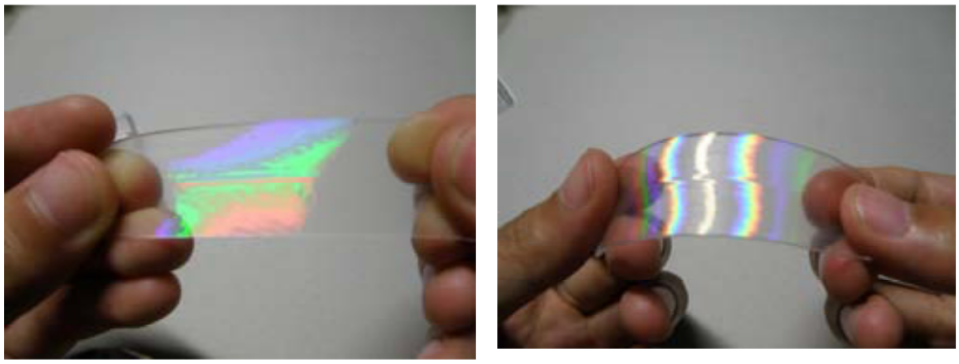

Figure 2.3- Image of the soft diffraction grating sheets (Suzumori et al., 2011).

Incident light (white light) was irradiated through a slit from an LED into a darkroom at a fixed angle and the colour change was observed from blue to red by extending the rubber

diffraction grating sheet up to 30% as a result of increase in the pitch length of the moulded flexible grating (Figure 2.4) (Suzumori et al., 2011).

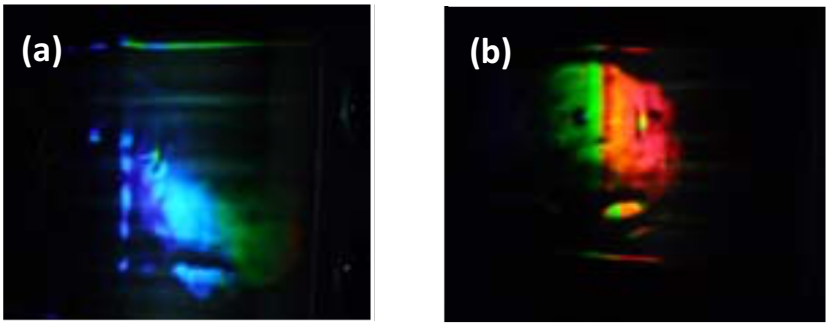

Figure 2.4- Soft diffraction grating sheet at (a) 0% extension and (b) 30% extension (Suzumori et al., 2011).

Shibaev et al. (2008) established a highly viscous cholesteric material that changes colour under uniaxial strain suitable for the application of sensors and tuneable lasers. This cholesteric material is produced by mixing 3 different types of silicone-based cholesteric liquid crystal materials with a nematic liquid crystal. Each of these silicone based cholesteric liquid crystals have a selective reflection band depending on the amount of chiral moieties inside the compound. Hence by mixing these components together, it was possible to make a cholesteric liquid crystal that has a selective reflection band. The cholesteric liquid crystal was then sandwiched between two transparent silicone strips (Figure 2.5). With applied uniaxial strain, the film induces a shift of the selective reflection band from longer wavelength towards a shorter wavelength. This shift is accompanied by colour changes that depend on the degree of stretching and the composition of the cholesteric material. The resulting colour is demonstrated to be related to the reduction in the cholesteric helix's pitch due to the contraction of the sample in the direction perpendicular to the applied force. They demonstrated a large shift of the selective reflection band of around 250 nm (Shibaev et al., 2008).

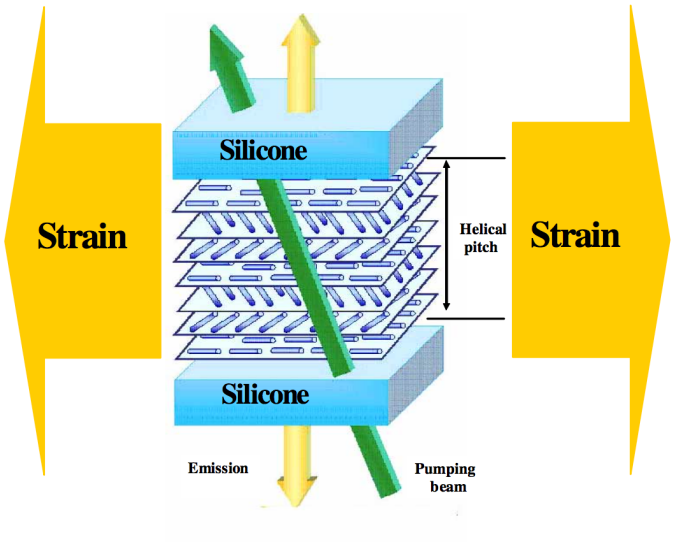

Figure 2.5- Schematic representation of the cholesteric helix, its deformation and optically pumped lasing (Shibaev et al., 2008).

2.2 Dielectric Elastomer Actuators

Dielectric Elastomers (DEs) are an important class of Electroactive Polymers (EAPs), when used as actuators they show large area strains (up to 100%), high energy densities (up to 1 MJ/m^3) and fast responses (down to 0.1 ms) (Carpi et al., 2008). A dielectric elastomer actuator consists of an elastomeric polymer film sandwiched between two compliant electrodes. By applying a voltage difference between the electrodes, the film is compressed in thickness and stretched in area. As the electrodes are bonded to the elastomer, they must be able to sustain large cyclic deformations but also remain conductive, without increasing the stiffness of the soft elastomer in order to enable electrostatic actuation. For this configuration the *Maxwell stress* (Pelrine et al., 2000) is given as:

$$p = \varepsilon_0 \varepsilon_r E^2 = \varepsilon_0 \varepsilon_r \left(\frac{V}{t}\right)^2 \quad (2\text{-}1)$$

Where ε_0 is the dielectric permittivity of vacuum, ε_r is the relative dielectric constant, E is the electric field, V is the applied voltage and t is the thickness of the elastomer. When an electric field is applied between the electrodes, the electrostatic attraction between the opposite charges on opposing electrodes results in a reduction in thickness and a concomitant increase in area since the material is virtually incompressible. Similarly, repulsion of like charges on a single electrode generates stress on the film, which causes an increase in area and a concomitant reduction in thickness (Pelrine et al., 2000, Carpi et al., 2008). Figure 2.6 represents the actuation mechanism of a dielectric elastomer actuator.

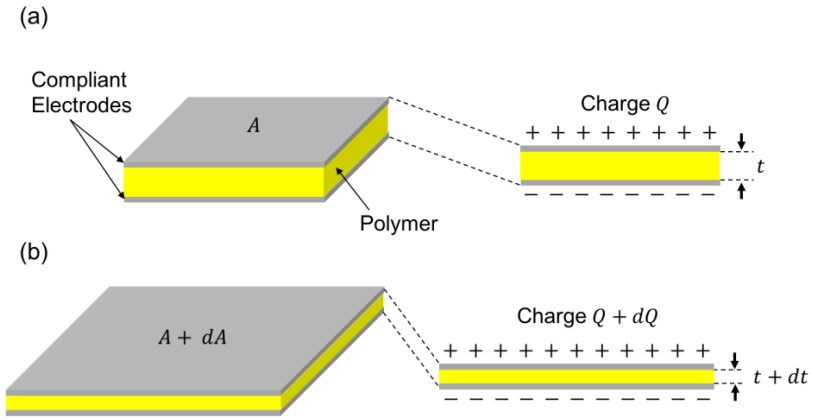

Figure 2.6- DE film actuation, (a) in an initial state and (b) in final stage (incrementally change state).

2.2.1 Fundamentals of dielectric elastomer transduction

The dielectric elastomer film which is sandwiched between two compliant electrodes is recognised electrically as a capacitor. The electrical and mechanical energy of the system can be conserved by making the following assumptions:

1. The ideal structure has zero resistance in the electrode and infinite resistance in the polymer.
2. The polymer is a perfect dielectric with relative dielectric constant ε and perfectly elastic with no dissipative mechanical losses.

Hence the capacitance of dielectric elastomer is calculated as (Carpi et al., 2008):

$$C = \frac{\varepsilon_0 \varepsilon_r A}{z} \tag{2-2}$$

In the above equation, ε_0 is the permittivity of free space, ε_r is relative permittivity or dielectric constant, A is the area where opposite electrodes overlap, which is also known as active area and z is the polymer thickness.

Following this equation, the electrical energy of a capacitor U_e with charge Q can be calculated using (Carpi et al., 2008):

$$U_e = \frac{0.5\ Q^2}{C} = 0.5z(\varepsilon_0 \varepsilon_r A)^{-1} Q^2 \tag{2-3}$$

Using the above equation, the change in the electrical energy (dU_e) under actuation is calculated as :

$$dU_e = \left(\frac{Q}{C}\right) dQ + U_e \left\{\left(\frac{1}{z}\right) dz - \left(\frac{1}{A}\right) dA\right\} \quad (2\text{-}4)$$

Where the first term on the right hand side of the equation is the flow of electrical energy into or out of the film from an external power source as polymer is assumed to be a perfect insulator. The second term on the right is the conversion of electrical energy to *mechanical energy* or *work done*.

The actuation of dielectric elastomer involves two modes of energy conversion. The first mode is the actuator mode, which is the conversion of electrical energy into mechanical energy. In this mode of conversion because the area is increasing, the electrical energy is decreased due to separation of like charges on a single electrode.

The second mode of conversion is the generator mode, in which the conversion of mechanical energy into electrical energy takes place. In this mode the opposite charges on opposing electrodes come closer together, which results in decrease in area and an increase in electrical energy. These two modes of energy conversion are directly coupled, since elastomeric materials have Poisson's ratio of approximately 0.5 and therefore can change shape whilst maintaining a constant volume (O'Halloran et al., 2008, Pelrine et al., 1998, Carpi et al., 2008). Hence stretching in area is mechanically coupled to compression in thickness and vice versa:

$$Vol = Az = constant \quad (2\text{-}5)$$

In equation (2-5) A is the area, z is the thickness and Vol is the volume of elastomer. This equation shows a very good approximation that can be assumed for real elastomers. Considering incremental changes, this equation can be expressed as:

$$dVol = \frac{\partial V}{\partial A} dA + \frac{\partial V}{\partial z} dz = z dA + A dz = 0 \qquad (2\text{-}6)$$

which can be expressed as:

$$\left(\frac{1}{z}\right) dz = -\left(\frac{1}{A}\right) dA \qquad (2\text{-}7)$$

An important quantity in dielectric transduction is the incremental mechanical work done (dW) on the polymer by the electric field pressure which is also included in equation (2-4):

$$dW = -U_e \left\{ \left(\frac{1}{z}\right) dz - \left(\frac{1}{A}\right) dA \right\} \qquad (2\text{-}8)$$

For better understanding of change in electrical energy, it can be assumed that there is no charge flowing to or from the polymer film. Hence the change in electrical energy or work equation is:

$$dU_e = dW = \left(\frac{U_e}{z}\right) dz - \left(\frac{U_e}{A}\right) dA \qquad \text{(Constant charge)} \qquad (2\text{-}9)$$

According to equation (2-9) the two modes of conversion can be treated separately (compressive stress in the z-direction and tensile stress in the direction of the plane).

For example when considering a polymer that could only change in thickness with no change in area; then the second term on right hand side of the equation is zero, Hence, reduction in thickness due to electrostatic attraction between the opposite charges on the

electrodes results in a decrease in the electrical energy (Carpi et al., 2008, Pelrine et al., 2000).

Additionally, if the polymer could only change in area with no change in thickness, then the first term on the left hand side of the equation is zero. Hence an increase in area due to repulsion of like charges on one electrode reduces the electrical energy. Therefore both changes in thickness and area reduce electrical energy (Carpi et al., 2008).

Comparing dielectric elastomer actuators with air gap electrostatic actuators where rigid parallel plates are used, the resultant Maxwell stress in equation (2-1) is double the corresponding normal stress per unit area in a parallel plate capacitor device. This additional factor of 2 arises because DEs have a second coupled degree-of-freedom to convert electrical to mechanical energy in comparison to air-gap parallel plates. Also as mentioned in the previous paragraph both changes in thickness and area reduce electrical energy.

Although the two modes of conversion can be treated separately, it is better not to separate them, but to treat the two components as a single effective pressure or resultant Maxwell stress, which is twice the true normal stress. This is simply because the two modes are directly coupled via the constant volume condition in elastomers (Carpi et al., 2008).

2.2.2 DEA configurations

Although the basic functional element of dielectric elastomer actuation was described in the previous section, it is necessary to understand how the basic functional element can be incorporated into an actuator.

Dielectric elastomer actuators can be configured into many designs owing to their versatility. Basic dielectric elastomer actuators can use a range of geometries including stack, extender, bending beam, diaphragm and tube configurations (Figure 2.7).

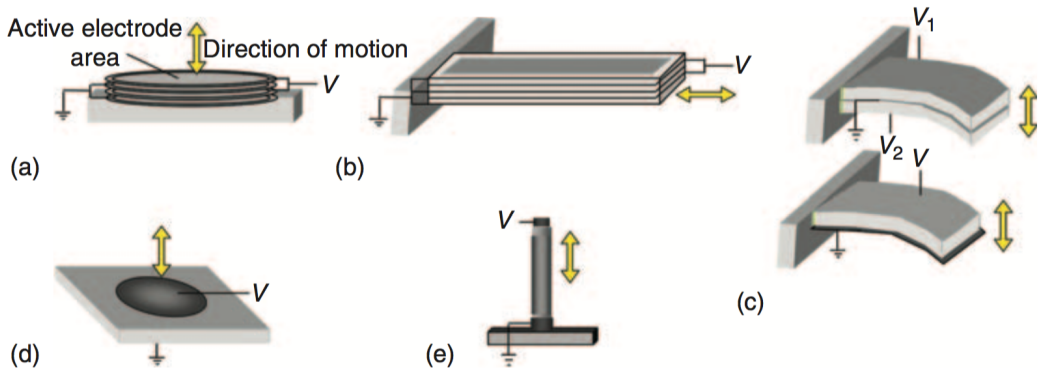

Figure 2.7- Basic DEA configurations, a) stack, (b) extender, (c) bimorph and unimorph bending beam, (d) diaphragm and (e) tube actuators (Carpi et al., 2008).

More sophisticated DEA configurations such as the bowtie and spider actuators couple two or more directions of planar expansion into a single direction of output. Rolled and framed actuator configurations offer flexibility and conformability (Pelrine et al., 1998, Carpi et al., 2008). Multi degree of freedom rolled actuators are a type of bending roll actuators that can extend in axial length and bend. Bow actuator and flexible frame saddle actuator configurations are used to maintain tension and prevent buckling (Kofod et al., 2006, Carpi et al., 2008). In these types of configurations, the frame that keeps the film in tension is not rigid (Figure 2.8).

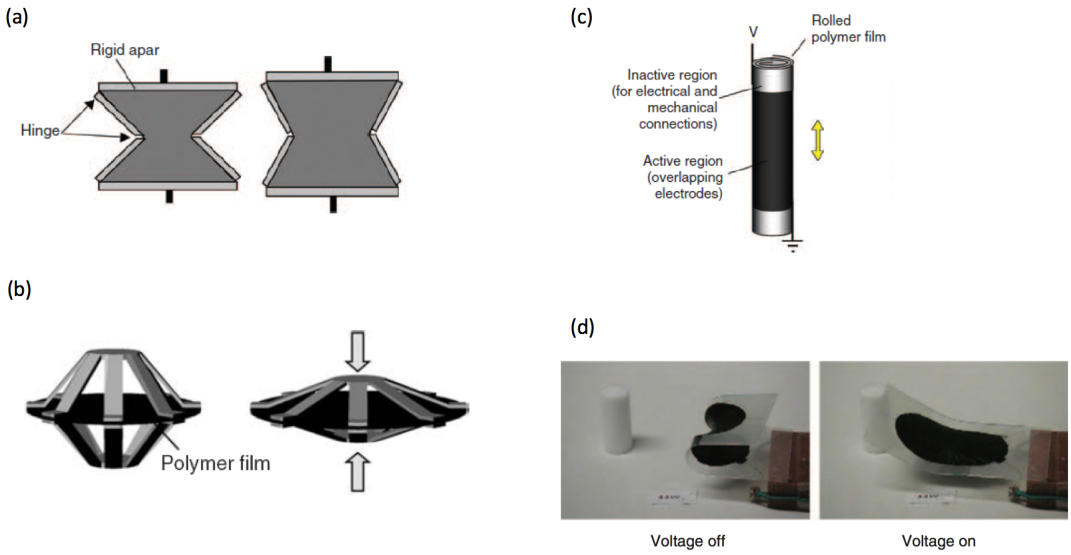

Figure 2.8- Enhanced DEA configurations, (a) bowtie, (b) spider, (c) rolled, and (c) flexible frame saddle actuator (Carpi et al., 2008).

All the above mentioned configurations operate using the planar deformation of the film Basic stack, helical and folded actuators use thickness mode of operation (Carpi and De Rossi, 2007). These actuators are used where a large amount of force is desired (Figure 2.9).

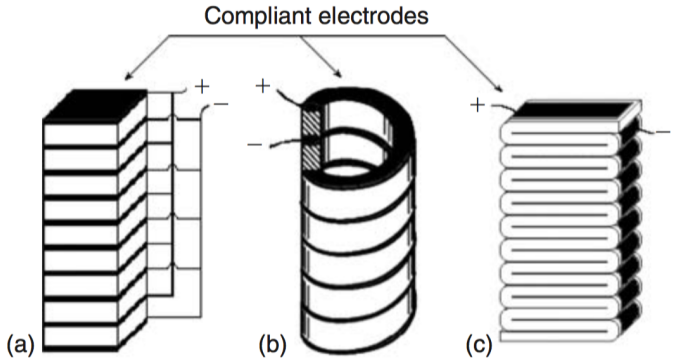

Figure 2.9- Thickness-mode actuators, (a) basic stack, (b) helical and (c) folded (Carpi et al., 2008).

In all the above examples, the coupling between the pre-stretched elastomer and either the rigid frame or any other substrate is a very important factor that needs to be considered while designing a DEA device as it can affect its overall performance.

The coupling between the prestretched elastomeric membrane and the frame can amplify or attenuate buckling and wrinkling behaviours in both passive and active states and hence modify the elastic strain energy within the DEA membrane from pre-stretch. In combination with the DEA's elastic strain energy, a mismatch between the DE membrane and any other attached substrate can cause bending or possibly cracking of substrate.

Moreover the presence of soft-rigid boundaries results in electro-mechanical non-linearities that generally are displayed as inhomogeneous active DEA strains across the membrane.

2.2.3 Breakdown Failure of DEAs

Although DEAs are a very promising technology for a variety of applications, they can experience high rates of failure as a result of dielectric breakdown. In a conventional DEA, dielectric breakdown occurs when the electrical field in the dielectric exceeds the maximal value tolerated by the material (Plante and Dubowsky, 2006). It is generally accepted that there are several possible causes and mechanisms responsible for the breakdown failure of dielectric elastomer actuators. The possible causes related to dielectric breakdown include presence of any contamination during fabrication, working conditions, processing methods, and environmental conditions (Carpi et al., 2008). The possible mechanisms which could initiate full dielectric breakdown include: electrical, electromechanical, thermal and partial discharge. The electrical breakdown of DEAs could happen due to the breakdown strength of the elastomer membrane being exceeded. The electromechanical breakdown is believed to happen where the electrostatic pressure overcomes the mechanical stresses in the membrane. In thermal breakdown the leakage

of charge through dielectric generates enough heat, which can damage the dielectric membrane. Finally, in the partial discharge breakdown, numerous partial discharges gradually weaken the dielectric to the point that full dielectric breakdown occurs (Dissado and Fothergill, 1992). The ultimate electrical breakdown of DEAs is unknown and there are several models which describe the breakdown behaviour that originates from the Stark-Garton model (Stark and Garton, 1955). The breakdown failure of DEAs may also be triggered by electromechanical instability (EMI) also known as pull-in instability (Koh et al., 2011). Pull-in instability is one of the most important of the DEA breakdown mechanisms. When the elastomer is subject to a voltage, it becomes thin. According to the equation (2-1), the Maxwell stress is proportional to the square of the electric field. When the elastomer is subject to the same voltage the Maxwell stress and electric field grow together as the elastomer becomes thinner (Anderson et al., 2012, Keplinger et al., 2010). Under certain conditions such as presence of impurities on the membrane or high electric field, if the Maxwell stress grows faster than the resisting elastic stress, there will be an unstable drop in the thickness of the elastomer. This causes a wrinkling pattern in the membrane leading to catastrophic failure from either the material or dielectric breakdown (Anderson et al., 2012, Carpi et al., 2008). Koh et al. (2011) found out that the pull-in instability severely limits the maximum actuation strain. However, when the pull-in instability has been supressed, then actuation strains greater than 100% may be achieved (Koh et al., 2011).

2.2.4 Pre-stretch

One method of avoiding this buckling type of pull in instability when using a thin film of a soft elastomeric material, is to apply a significant pre-tension in the plane of any applied stresses or strains. Therefore, for plane actuated DEAs, it is now conventional to apply a significant planar pre-stretch to the elastomeric membrane before it is bonded to the rigid

frame to avoid this buckling. However, some actuators are designed to operate in a buckling mode in which case a pre-stretch of the membrane is not required (Maffli, 2014, Carpi et al., 2008).

It is assumed that the elastomer is incompressible and has a Poisson's ratio of approximately 0.5 even at a high stretch. Pre-stretching of the elastomeric membrane in a DEA device has two advantages, one is that it enhances the breakdown strength and the second is that it suppresses the pull-in buckling instability. Both effects are seen to improve the performance of a device. Kofod et al. (2003) reported a significant increase in breakdown strength of a commercial acrylic membrane from 18 to 218 MV/m from a condition with no pre-stretch to a biaxial pre-stretch of 500% × 500% (Kofod et al., 2003). The main reason why the pre-stretch can reduce or remove the pull-in instability is that it modifies the stretch-voltage curve of the elastomeric membrane. Consequently, large actuation strains can be achieved, despite the significant membrane stiffening induced by its hyperelastic properties (Kofod et al., 2003, Maffli, 2014).

Akbari et al. (2013) investigated the optimum pre-stretch ratio required to both suppress the pull-in instability at large deformations whilst minimising the required actuation voltage in DEAs using castable PDMS elastomers. They found that to suppress any pull-in instability, the biaxial pre-stretch of 1.5 is required. Any further pre-stretching resulted in the stiffening of the membrane and increased the actuation voltage required to produce a given displacement. They also reported that uniaxial pre-stretch mode offered the highest actuation strain in the transverse direction as the elastomer became stiffer in the pre-stretched direction compared to biaxial pre-stretch mode (Akbari et al., 2013).

2.2.5 Elastomers

The desired material requirements for high performance dielectric elastomer transduction include high breakdown strength, low modulus, high permittivity and good elastic

properties. Since late 1990s, the performance of different types of polymers and elastomers such as polyurethane, silicone, polybutadiene, isoprene and acrylic have all been tested (Pelrine et al., 1998, Pelrine et al., 2000). Although many polymers show great performance (such as a large strain response of more than 10%), silicone and acrylic elastomers are the most promising materials as they have a better overall performance when compared to other polymers.

Commercially available acrylic elastomers (3M VHB 4910 and VHB 4905) are widely used in practice because they have many of the most promising properties including, a very high strain response of ~ 380% when pre-strained (initial loading condition) (Kornbluh et al., 2002). As is noted in the previous section this pre-strain can also significantly increase the electrical breakdown strength of an elastomer. However, pre-strained elastomer films may exhibit stress relaxation which can affect the actuation performance. Also high pre-strain requires that special structures or frames are used which complicates the actuator design and also increases the possibility of tearing. Acrylic elastomers have high theoretical energy density of ~ 3.4 MJ/m^3 and a high efficiency ~90% as well as having a large variation in temperature (Carpi et al., 2008, Brochu and Pei, 2010). One limitation of acrylic elastomers is that they have a slower response rate when compared to silicone elastomers as it has greater viscoelastic losses at room temperature, which influences the dynamic behaviour of acrylic elastomer actuators (O'Halloran et al., 2008, Carpi et al., 2008).

Silicone elastomers, which are based on a polydimethylsiloxane (PDMS) backbone, are advantageous over acrylic elastomers due to their lower glass transition temperature ~ - 120 °C and hence reduced viscoelastic energy dissipation at room temperature. Hence silicone elastomers have higher actuator efficiency and can operate at higher frequencies. Silicone elastomers also have a more stable stiffness performance over a wide range of

operating temperatures. One disadvantage though of silicone elastomers is the reduced strength of the material. Therefore even with a pre-strain a maximum strain of only about ~100% can be achieved which is lower than when compared to acrylic (Carpi et al., 2008, O'Halloran et al., 2008). They also have lower dielectric constant when compared to acrylic, which therefore requires the application of greater electric field to reach a similar level of actuation (Carpi et al., 2008). One advantage of the silicone elastomer is that both the electrical and mechanical properties can be altered by adding different volume fractions of hardener, filler or other materials.

2.2.6 Electrodes

In dielectric elastomer actuators, the electrodes play an important role in the performance of the DE device. Earlier is mentioned that the complaint electrodes must be conductive, and be able to sustain large cyclic deformations. In most studies carbon based electrodes are used which could be in a form of grease or a powder. In the following section, different types of electrodes are discussed.

Powder electrodes are loose powders typically made of carbon, which is deposited on the elastomeric membrane using a brush or spray. One of the advantages of electrode powder is that the weak binding force between the agglomerates, prevents them from contributing to the stiffness of the elastomeric membrane and therefore under deformation they can easily follow the hyper-elastic planar deformation of the film (Kovacs et al., 2009, Rosset and Shea, 2012). Powder electrodes are feasible particularly when applied to a sticky or adhesive film. This means that acrylic elastomers are a particularly useful material for working with these powder electrodes in addition for use in multilayer stack configurations (Kovacs et al., 2009). Carbon powders in comparison to metal powders are intrinsically less conductive. However, metal powders have tendency to form an insulating oxide on their surface and have larger particles, which are not as efficient at

forming a percolating (or electrically connecting) network. Therefore, better conductivity can be obtained using carbon powder electrodes (Rosset and Shea, 2012). The disadvantages of powder electrodes include: a high sensitivity to static charges: they are hard to handle and at large strains it is difficult to maintain full coverage.

Grease electrodes consist of powders such as carbon, that is dispersed into a viscous media such as grease or oil (Rosset and Shea, 2012). They can be used in variety of DEA configurations and are able to sustain large deformations whilst remaining conductive and are easier to handle compared to powder electrodes (O'Halloran et al., 2008). However, they are generally still quite messy to handle and are difficult to apply with a uniform thickness. Another difficulty is that they have long term stability issues. This is in part due to the evaporation of the lower molecular weight grease molecules or their diffusion into the dielectric elastomer membrane. This can even result in a short circuit or significant swelling of the elastomer membrane (Rosset and Shea, 2012). Also because it is a viscous material, it can flow which can limit the lifetime of the electrodes, especially with devices that are stored vertically (Rosset and Shea, 2012).

Rubber electrodes are formed by dispersing conductive particles such as carbon black into an elastomer, which is then crosslinked after the electrode has been applied onto the surface of the membrane (Rosset and Shea, 2012). These types of electrode that are bonded to the elastomeric membrane (polymer-carbon conductive composite) have a long lifetime as they are less prone to ablation or migration of the electrode material. Compared to carbon powder and carbon grease electrodes; the electrode does however make a significant contribution to the stiffness of the resulting device. Therefore these types of electrodes work well when the thickness of the electrode is small when compared to the thickness of the dielectric elastomer (Rosset and Shea, 2012, Pelrine et al., 1998). In order to avoid a significant reduction in the actuation performance, then the elastic modulus of

the rubber electrode must be closely matched to the modulus of the actuator (O'Halloran et al., 2008). In an elastomer-carbon black compound the stiffness of the composite depends very much on the amount of filler particles and the percolation threshold depends on the morphology and surface area of the filler as well as the matrix in which it is dispersed. The percolation threshold can vary between 1% - 24% volume fraction (Rosset and Shea, 2012).

Transparent electrodes are challenging for optical applications of DEAs such as diffraction gratings and optical lenses. For example, Son et al. (2012) introduced a transparent electromechanically driven variable-focus lens using a conductive polymer, poly 3,4-ethylenedioxythiophene (PEDOT) as a transparent electrode. Also partially transparent electrodes have been used based on thin layers of loose carbon black, carbon nanotubes and silver nanowires (Kovacs and During, 2009, Hu et al., 2009, Hu et al., 2012, Yun et al., 2012). In most cases the transmission of the electrode increases with increasing voltage and area strain and the amount of transmission of the electrodes is highly dependent on the conductive network formed on the surface and hence the quantity of conductive particles on the membrane (Rosset and Shea, 2012). The lower the amount of conductive particle on the surface, the better the optical transmission but this could then limit the actuation strain as the particles may lose their conductivity as the electrode is strained (Rosset and Shea, 2012). Another limitation of transparent electrodes based on conductive particles is the light scattering induced by the particles (Rosset and Shea, 2012). Hence in some optical applications, it is preferred to have opaque but active electrodes outside of the optical path (Carpi et al., 2011, Rosset and Shea, 2012).

Keplinger et al, (2013) introduced stretchable and transparent ionic conductors (STICs) that enabled the fabrication of a DEA device that was fully transparent to light over the visible spectrum. The transparent actuator was fabricated by sandwiching the dielectric

elastomer between two layers of electrolytic elastomer in which they were both transparent and stretchable and the electrodes were placed outside the area of the device. When the device is subject to voltage, the two layers of the electrolyte spread ions of the opposite charges on the two sides of the dielectric elastomer causing the elastomer to reduce in thickness and expand in area.

2.2.7 Optical applications of DEAs

Dielectric elastomer actuators are being studied for many applications (Carpi et al., 2008) (O'Halloran et al., 2008) such as soft robotics (Jordi et al., 2010), refreshable braille and haptic displays (Brochu and Pei, 2010, Carpi et al., 2012) and tuneable optics (Aschwanden et al., 2008, Carpi et al., 2011). They can be configured in many ways over wide range of dimensions to generate a variety of geometric changes. The following part of this review focuses on the optical applications of DEAs such as tuneable colour displays and variable focus lenses.

Dielectric elastomer actuators have been used in combination with soft materials to produce diffraction gratings that are based on reflection or transmission modes (Aschwanden et al., 2008). A tuneable grating was produced based on reflection mode by Ouyang et al. (2010) which uses conductive polymer PEDOT (poly 3,4-ethylenedioxythiophene): PSS (polystyrenesulfonate) as the top transparent electrode that allows light to pass through, gold is used as the bottom electrode, which is highly conductive and reflective, and viscoelastic PDMS (polydimethylsiloxane) as the transparent elastomer. By applying a voltage between the two electrodes the initial plane surface of polymer deforms into a sinusoidal grating, which acts as a phase grating with high diffraction orders. This modulator has achieved the response time of 250 μs with maximum 200 nm peak-to-peak relief depth on the PDMS surface (Ouyang et al., 2010).

Aschwanden et al. (2008) developed a tuneable grating based on transmission mode using pre-stretched acrylic elastomer film fixed on a circular plastic frame, carbon black ring electrodes and PDMS film with a moulded grating pattern (Figure 2.10). When a voltage of 4.5 kV was applied between the electrodes, the grating period changed from 2 µm to 1.87 µm, which corresponded to an in-plane biaxial strain of -7.5% of the membrane. This optical transmission grating operated with a high transmission that was greater than 90%, a good optical quality, a high optical damage threshold of 93 kW/cm^2 and was polarisation independent (Aschwanden et al., 2008).

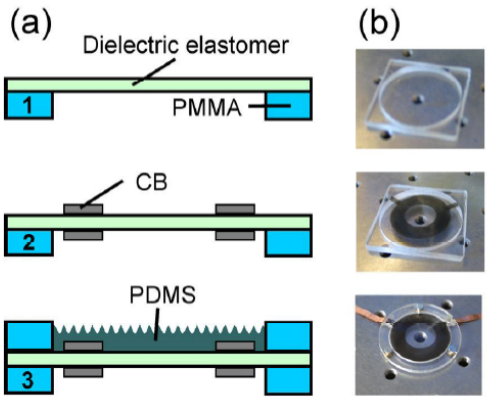

Figure 2.10- Transmission grating based on dielectric elastomer actuator, (a) schematic and (b) photographs of the fabrication process for shape changing transmissive optical elements (Aschwanden et al., 2008).

Using dielectric elastomer actuators, Fang et al. (2010) developed a technique to build dynamically tuneable optical devices. They used silicone rubber filled with functionalised graphene sheets (FGS/PDMS) as the patterned top electrode, pre-stretched acrylic film as the elastomer and carbon grease as the bottom electrode. In this device the electrode was illuminated with collimated white light from a halogen lamp and a CCD camera was used to observe the colour change from blue to green as the voltage was increased (Fang et al., 2010).

As mentioned earlier, optical lenses with electrically tuneable focus are desirable in many applications such as medical diagnostics and optical communications. Son et al. (2012) developed an electromechanically driven variable-focus lens based on transparent dielectric elastomer. In this study PEDOT was used as the transparent electrode and silicone as the elastomer. In this design, PEDOT-silicone rubber film is confined by the rigid frame boundaries. When the voltage is applied, the compressive force causes the material to expand. As a result, the film buckles and causes it to become either convex or concave, which results in a change in its optical focal length. This variable focus lens module has light transmittance of 70% with a maximum displacement up to 450 μm with a film thickness of 200 μm when at its maximum actuation (Son et al., 2012).

Carpi et al. (2011) used DE actuation in tuneable focus lenses inspired by the natural architecture of the crystalline lens and ciliary muscle of the human eye. Ciliary zonule (zonule of Zinn) is a series of fibres that connects the ciliary muscle to the crystalline lens, which has an asymmetrical biconvex structure (Figure 2.11). The ciliary muscle can change the shape of the crystalline lens by stretching and relaxing the zonule. The combined action of the muscle and zonule results in change in the radius of curvature of the lens and its focal length, which is known as its accommodation. This bioinspired tuneable lens was composed of a fluid-filled elastomeric lens that is surrounded by an annular DE actuator which works as an artificial muscle (Figure 2.11) (Carpi et al., 2011).

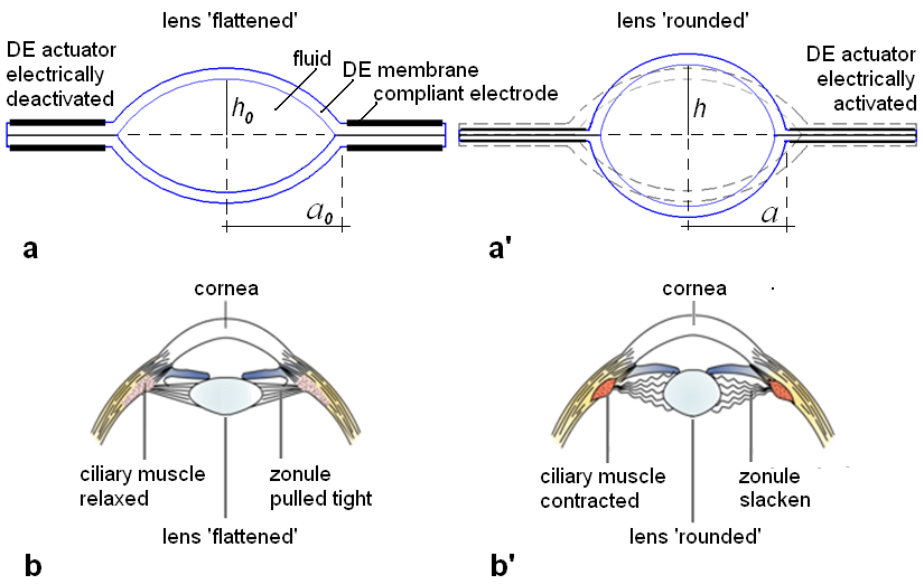

Figure 2.11- Schematic representation of sectional view of bioinspired lens and human lens. a,b) rest state. a',b') activation state (Carpi et al., 2011).

The lens consists of two optically transparent membranes (acrylic films) that are biaxially pre-stretched. The membranes are coupled together and fixed to a circular frame in order to obtain a symmetrical biconvex lens. A transparent fluid (silicone pre-polymer) is confined in the central region of the elastomers, which creates a closed chamber. The remaining part of the membrane is coated with carbon grease as the compliant electrodes. When the voltage is applied between the electrodes (using the aluminium connections attached to each membrane) the annular region of the membrane squeezes in thickness and expands in surface, which is due to its constant volume. This results in a change in lens diameter, the lens curvature and therefore its focal length.

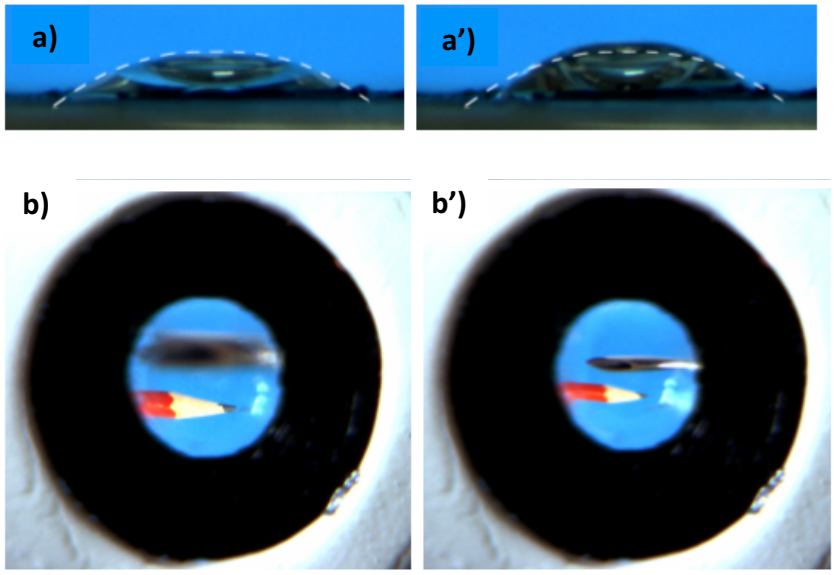

Figure 2.12- Bioinspired tuneable lens a,b) electrically at rest, a',b') electrically in action (Carpi et al., 2011, Suzumori et al., 2011).

Figure 2.12 a and a', are the lateral views of the lens, which show change in curvature when the voltage is applied. Figure 2.12 b and b' show electrically controlled focus change of a pencil and a syringe needle, located 10 and 3 cm respectively behind the lens. The device has a refractive index similar to the human lens and comparable relative variation of focal length. In addition, this simple and compact structure is lightweight, shock tolerant and silent, and shows fast response (60 ms) and low power consumption (160 mW) (Carpi et al., 2011).

Similar to the example above, Rossiter et al. (2012) have combined DEs with fluid, but for the purpose of active camouflage and active photovoltaics in compliant skins. This paper introduces artificial chromatophores, mimicking the radially orientated muscles found in natural chromatophores (Rossiter et al., 2012).

They demonstrated the pigment-based variable opacity in artificial chromatophores, using a contractile membrane actuator consisting of a passive central region surrounded by annular electrodes. A layer of soft gelatin gel mixed with small amount of methylene blue

was fabricated and deposited in the central region inside the electrode active region. By applying a voltage difference between the electrodes, the annular ring squeezes in thickness and causes a contraction of the pigmented gel (Figure 2.13). This increases the gel thickness and colour density and decreases the light intensity. Hence darker colouration of the soft gelatin gel is achieved.

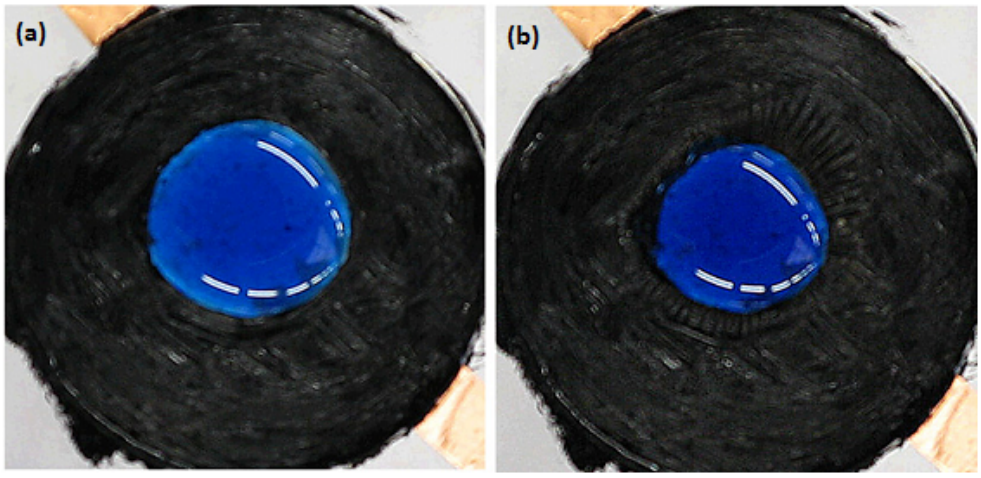

Figure 2.13- Fabricated contractile membrane actuator with the pigmented gel central spot showing 'off' (a) and 'on' (b) states (Rossiter et al., 2012).

They also developed an artificial ink-cell melanophore, mimicking the fluid translocation in zebrafish melanophores (Rossiter et al., 2012). The artificial melanophore consists of two dielectric elastomer pumps that are hydrostatically linked and translocate two immiscible liquids from one end of the ink cell to the other end.

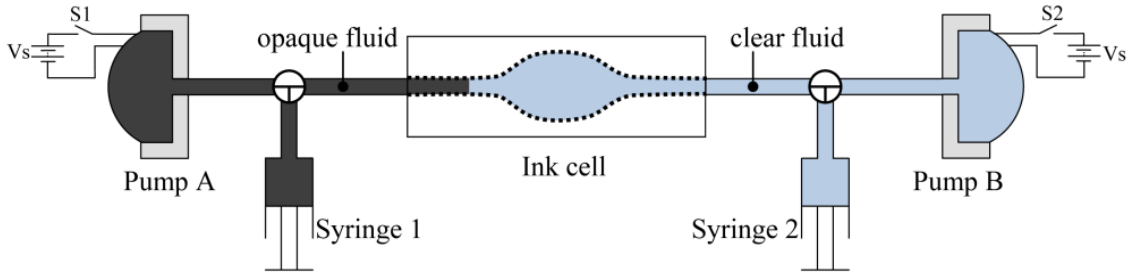

Figure 2.14- Experimental setup for the artificial melanophore (Rossiter et al., 2012).

As it shows in Figure 2.14 , the two syringes introduce hydraulic pre-load on the DEA membrane in the two pumps to balance the pressure of both pumps at rest. When voltage is applied to one DEA, its membrane relaxes and at the same time the other DEA membrane contracts in order to balance the pressure. This results in a sharp change in opacity as a result of liquid-liquid interface movement through the ink cell. Figure 2.15 represents the movement of fluid during activation at 3 seconds intervals.

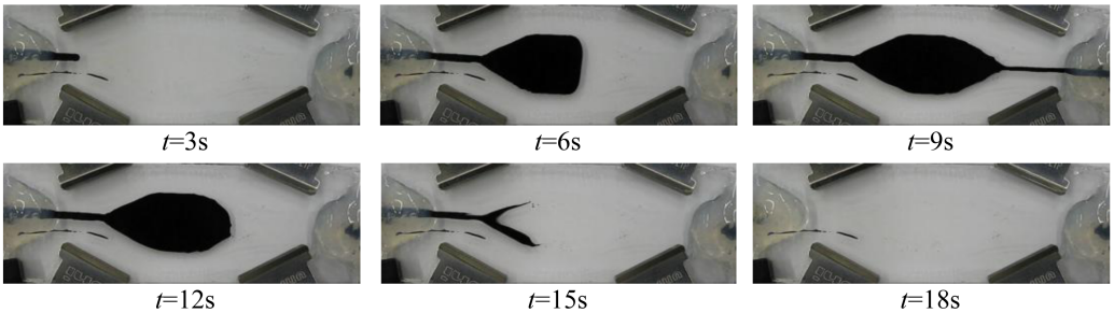

Figure 2.15- Ink cell chromatophore activated from transparent (t <3 s) to opaque (t = 9 s) to transparent (t > 16 s) (Rossiter et al., 2012).

Later on Rossiter et al. (2014) demonstrated a stacked multi-colour artificial chromatophore, inspired by the chromatophores in the skin of cephalopods to display a wider range of optical effects compared to their previous work on single-colour chromatophore (Rossiter et al., 2012). Three DEA elements for the three colour components (red, green and blue) were fabricated separately and were stacked together into a single multi-colour chromatophore. Ionic conduction approach was used to create the coloured electrodes shown in Figure 2.16. The colour range of the device was analysed and they showed how the colour can be shifted through colour space by changing the actuator strain. This allowed the chromatophore to generate a wide range of different colours. Figure 2.16 demonstrates the actuation of the RGB chromatophore through a cycle (Rossiter et al., 2014).

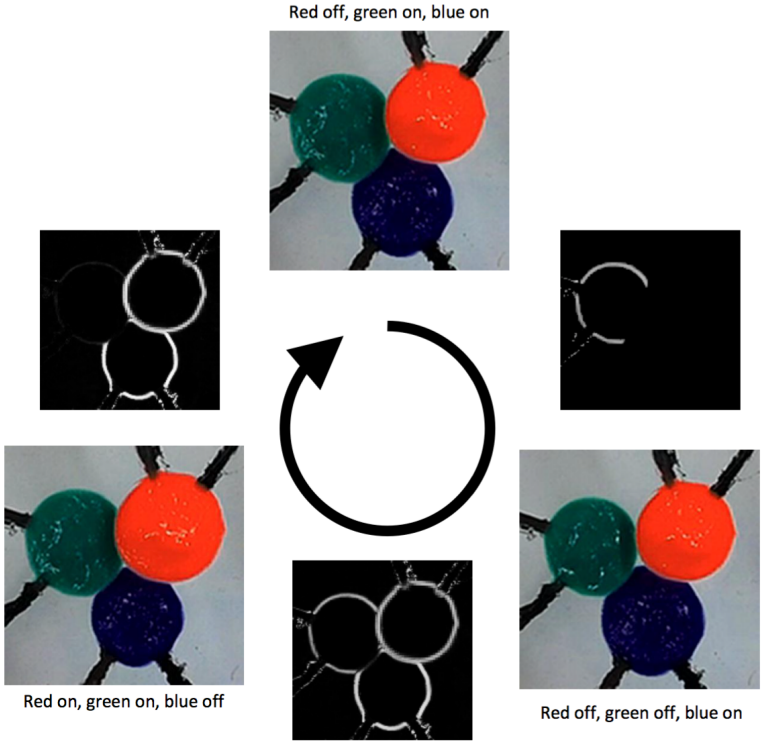

Figure 2.16- Actuation of three RGB elements, with monochrome images showing changes in actuator strain (Rossiter et al., 2014).

2.3 Liquid Crystals

Liquid crystalline state is a distinct phase of matter which shares properties normally associated with both liquids and crystalline solids. It was discovered at the end of 19th century (Finkelmann, 1987, Finkelmann, 1988, Oswald and Pieranski, 2005). It has been known that when certain compounds of low molecular weight are melted, they may not transform directly into an isotropic melt. These compounds however exist in a state which has a low viscosity rather like a liquid and display the physical anisotropic characteristics of crystalline solid when subjected to a certain threshold pressure and within a defined temperature range. These substances which form such phases are called liquid crystals (Finkelmann, 1987).

Liquid crystals (LCs) have different types of phases, also known as mesophases, which are based on the type of molecular ordering present (Oswald and Pieranski, 2005). In the solid crystalline phase molecules (*mesogens*) possess both positional and orientational order. With increasing temperature, solid phases turn into a liquid crystalline phase in which there is no positional order but some degree of orientational order remains. At higher temperatures an isotropic phase is achieved where the molecules have no positional or orientational order (Figure 2.17) (Collings and Hird, 1997).

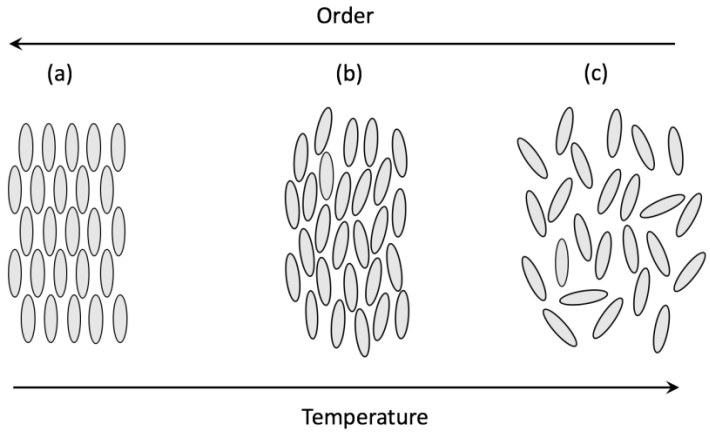

Figure 2.17- Schematic representation of (a) solid crystalline phase, (b) liquid crystalline phase and (c) isotropic phase.

Liquid crystal substances whose order and phase transitions are influenced by the temperature are called *thermotropic* liquid crystals. In some cases, liquid crystal order is influenced by the concentration of one component in another which is known as a *lyotropic* liquid crystal (Collings, 1990).

2.3.1 Liquid crystal phases

Depending on the degree of molecular ordering several liquid crystal mesophases are identified below:

Nematic Phase

The simplest and most common liquid crystal phase is known as the nematic phase. In the nematic phase the molecules maintain a preferred orientational order, meaning the mesogens are aligned in a uniform direction defined by the director ($\hat{n}$) with no positional order (Figure 2.18) (Oswald and Pieranski, 2005, Collings and Hird, 1997, Ohm et al., 2010). Nematic is a Greek word which means thread, since under polarised light nematic liquid crystals have a thread-like texture, which corresponds to the line defects in the orientational order (Collings and Hird, 1997, Oswald and Pieranski, 2005).

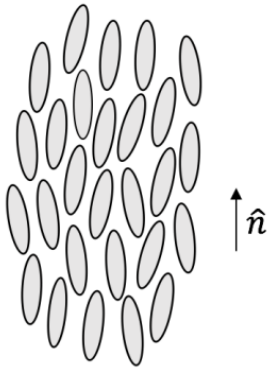

Figure 2.18- Schematic representation of the nematic phase.

Smectic phase

Smectic phases have number of classifications, in which smectic A and smectic C are the most well understood phases. In the smectic phase, molecules are arranged in layered structure hence they have both orientational order and positional order (Collings and Hird, 1997). In smectic A phase, the molecules are arranged in fluid layers where mesogens are parallel to the layer normal or in other words the director ($\hat{n}$) is perpendicular to the layers (Figure 2.19 a) (Collings and Hird, 1997, Oswald and Pieranski, 2005, Ohm et al., 2010). In smectic C the molecules are arranged in fluid layers but the mesogens are tilted towards the layer normal, or in other words the director makes

an angle other than 90° to these layers (Figure 2.19 b) (Collings and Hird, 1997, Oswald and Pieranski, 2005, Ohm et al., 2010).

Figure 6, represents schematic representation of smectic A and smectic C phases. In both phases there is no positional order within the layers and under polarised light they exhibit a focal conic texture (Collings and Hird, 1997, Oswald and Pieranski, 2005).

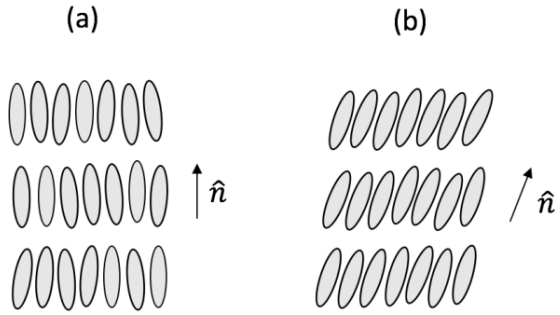

Figure 2.19- Schematic representation of (a) smectic A and (b) smectic C phase.

Cholesteric phase

Cholesteric phases are also known as a chiral nematic phase, in which the molecules organise themselves in layers. In each layer the director rotates in helical fashion about an axis (helical axis) perpendicular to the director (Figure 2.20). The centres of mass of each of the molecules are randomly distributed, meaning there is no positional order in each layer (Collings and Hird, 1997, Oswald and Pieranski, 2005). An important characteristic of chiral nematic phase is the pitch, which is the distance the director takes to complete a full rotation of 360° along the helix (Collings and Hird, 1997). Typically pitch value ranges from a few microns to hundredths of a nanometre.

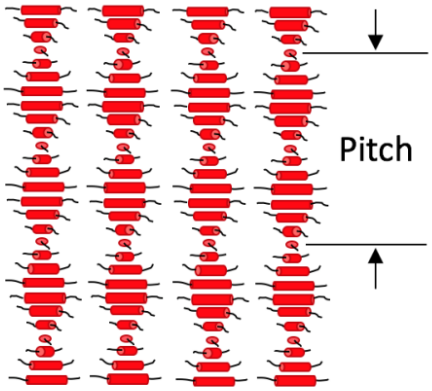

Figure 2.20- Schematic representation of cholesteric phase.

In a well orientated sample, when the wavelength of visible light in the liquid crystal is equal to the cholesteric pitch, *specular reflection* happens. This is the mirror like reflection, where the light from single incoming direction is reflected into a single outgoing direction. Cholesteric pitch can be changed by altering the pitch length of the cholesteric liquid crystals, which is done by changing the angle at which the director changes. Therefore a large angle reduces the pitch. This change in angle can be controlled by adding different concentrations of the chiral dopant when mixing the monomers (Alam et al., 2007):

$$P = (HTP \times C)^{-1} \qquad (2\text{-}10)$$

Where P is the pitch, HTP is the helical twisting power (i.e. 55 μm^{-1}) and C is the concentration of chiral dopant in weight percent. Therefore in the cholesteric liquid crystals, changing the chiral dopant concentration, changes the cholesteric pitch, which controls the wavelength of reflected light (Alam et al., 2007):

$$\lambda_0 = n.P \tag{2-11}$$

Where λ_0 is the wavelength of reflected light, P is the pitch and n is the average refractive index of cholesteric planes [$n = (n_o + n_e)/2$, where n_o is the ordinary index of refraction measured in a direction perpendicular to the local director and n_e is the extraordinary index of refraction which is measured in a direction parallel to the local director] (Mitov, 2012).

In cholesteric liquid crystals (CLCs), when the wavelength of light is equal to the cholesteric pitch, a specular effect happens. A cholesteric liquid crystal sample of the right orientation shows intense colours depending on viewing angle and can have a narrow or selective reflection band. Under oblique incidence with respect to the helical axis, the reflection band is given by Bragg's Law (St. John et al., 1995):

$$\lambda_0 = n.P \cos\ \theta \tag{2-12}$$

Where θ is the incident angle, the reflection band shifts towards the blue/violets part of the spectrum as the incident angle gets larger with respect to the helical axis.

2.4 Cholesteric Liquid Crystals

The orientation of molecules plays a crucial part in the optical properties of cholesteric liquid crystals which are also known as chiral nematic liquid crystals. There are three different organisations depending on the orientation of the cholesteric helix with respect to the surface of the film. The *Planar state* is achieved where the molecules or the director are aligned parallel to the substrate in each layer and the helical axis (helix) is perpendicular to the substrate or parallel to the incident light (Figure 2.21 a).

The *homeotropic state* is found where the molecules or the director are aligned perpendicular to the substrate in each layer and the helix is parallel to the substrate or perpendicular to the incident light (Figure 2.21 b). In the multi-domain organisation, the *focal conic state* is obtained where the helix is tilted randomly with respect to the surface (Figure 2.21 c).

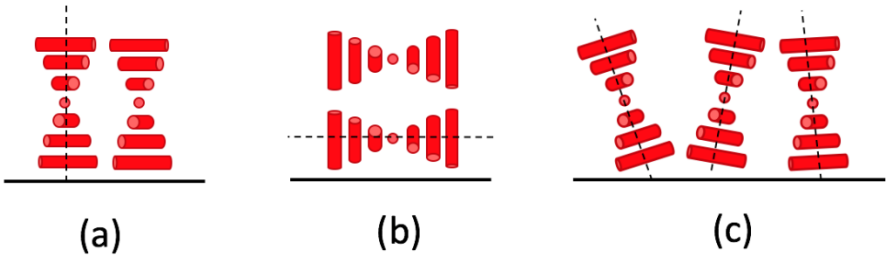

Figure 2.21- Cholesteric liquid crystals orientations: (a) planar (b) homeotropic and (c) focal conic. Black dashed line shows the direction of the helical axis (helix).

In planar orientation, when the light hits the CLC molecules, there is diffraction in the refractive index as the director axis in each layer changes. This is however not the case for homeotropic orientation and this is because the director axis is the same in each layer and therefore there is no diffraction in the refractive index. Hence in order to get reflection in cholesteric liquid crystals, the molecules must be aligned parallel to the substrate and the helix must be parallel to the incident light.

Usually there are three main ways of investigating the orientation of the CLC samples:

1. *Ultraviolet-visible* (*UV/Vis) spectroscopy*- if the shape of the curve at the selected wavelength of light (the peak) is flat, it is an indication of a planar alignment of the molecules (Figure 2.26). However, if the shape of the curve at the peak is not flat, it indicates lack of planar alignment of the molecules and hence the molecules are not aligned parallel to the substrate.

2. *Scanning Electron Microscopy (SEM)* - looking at cross-section of the CLC samples under SEM.
3. *Optical Microscopy*- under which, planar state has a uniform structure called an oily streak texture with colours depending on the pitch, homeotropic state which appears as a finger print texture and focal conic state that has a focal conic texture.

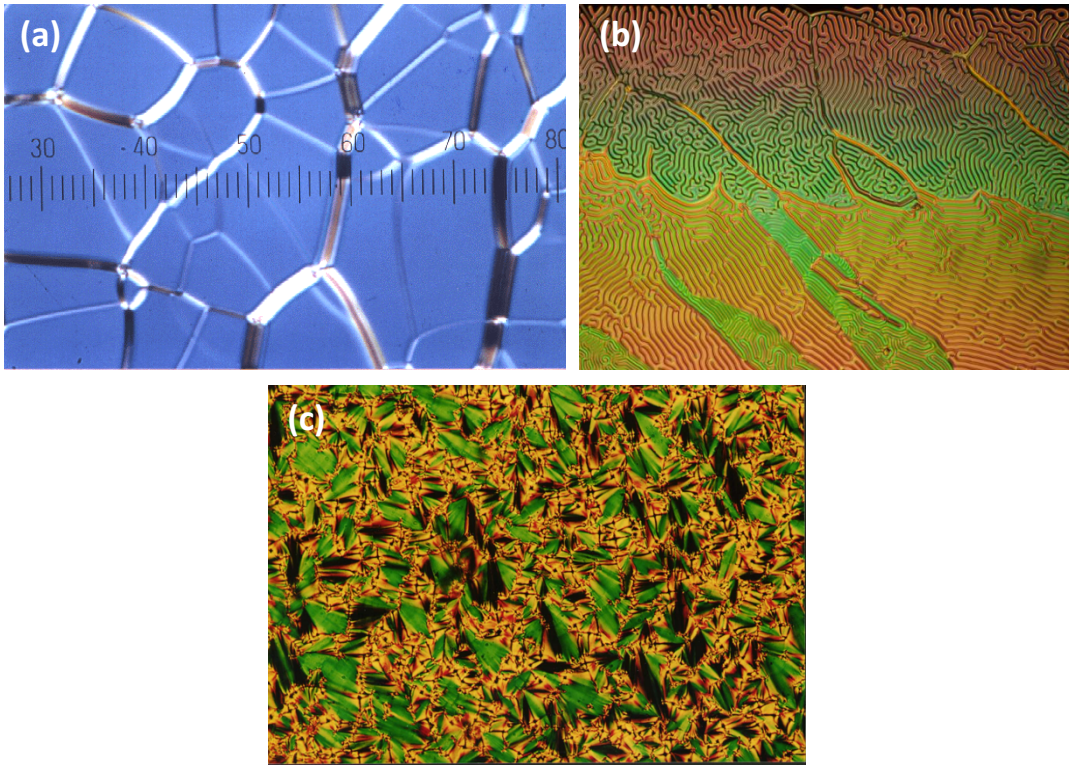

Figure 2.22- Cholesteric liquid crystal structure under a digital microscope: (a) oily streak texture (b) fingerprint texture (Dierking, 2003) and (c) focal conic texture in the CLCs (Park, 1999).

In Figure 2.22 a the irregularities in the CLC can provoke the appearance of defects called oily streaks.

2.5 Light and Liquid Crystals

2.5.1 Properties of light

Light is an electromagnetic wave with wavelength of 0.4-0.7 μm, which is visible to the human eye. Electromagnetic waves consists of propagating electrical and magnetic fields, in which a) both the electric field and the magnetic fields must be perpendicular to the direction of the propagation and b) the electric field must always be perpendicular to the magnetic field (Figure 2.23) (Collings and Hird, 1997).

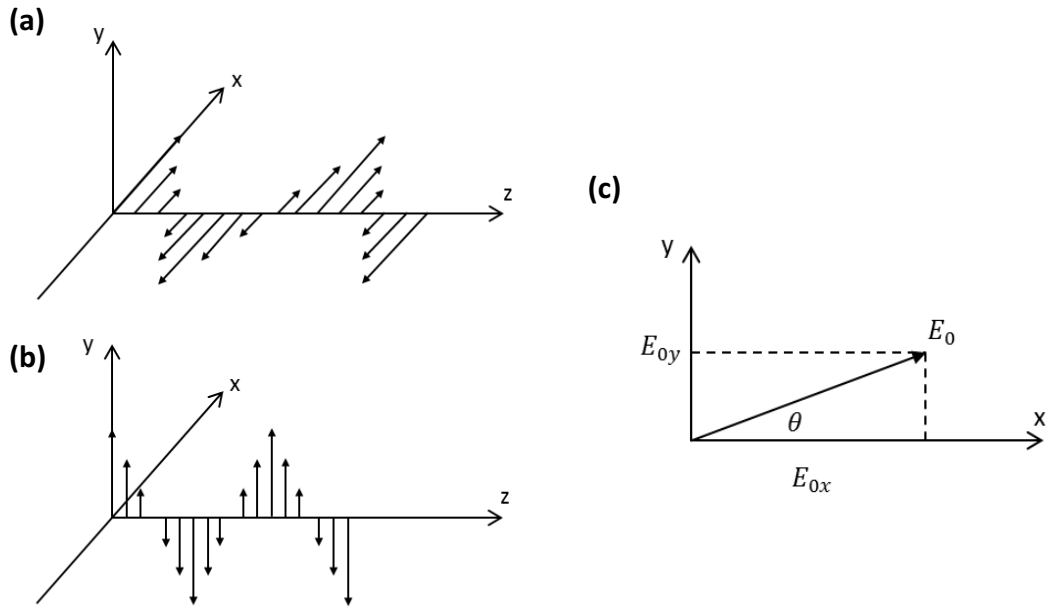

Figure 2.23- Schematic representation of an electromagnetic wave, (a) electric field, (b) magnetic field and (c) polarised in xy plane (Collings and Hird, 1997).

Figure 2.23 a, shows the electric field points along the x-axis and magnetic field points along the y-axis (Figure 2.23 b) and because the magnetic field is always perpendicular to the electric field, the orientation of the electric field is considered. Hence the wave in Figure 2.23 c is called a linearly polarised wave, where the x-axis is the only polarisation direction (Collings and Hird, 1997).

The polarisation of a wave is given by the ratio of the x and y components of the amplitude of the electric field, which are E_{0x} and E_{0y} respectively. This then gives the angle, θ, between the electric field and the x axis (Figure 2.23 c) (Collings and Hird, 1997):

$$\theta = tan^{-1}\left(\frac{E_{0y}}{E_{0x}}\right) \quad (2\text{-}13)$$

If the x and y components are 90° out of phase (where the electric field rotates around the z-axis in the xy plane) and x and y components of the electric field have the same amplitude (E_{0x}=E_{0y}), the wave is said to be circularly polarised.

If these waves were approaching to an observer looking back along the direction of propagation, its electric field vector would appear to be rotating counter clockwise, which is called a left handed circularly polarised light (LHCPL). If the electric field vector appeared to be rotating clockwise, it is called a right handed circularly polarised light (RHCPL) (Collings and Hird, 1997).

A polarising plate or polarising filter is usually used to change unpolarised light to linearly polarised light. The polariser has a transmission axis that only passes the components of electric field vectors that are parallel to its transmission axis. Vertical and horizontal linear polarisation can be achieved by changing the orientation of transmission axis vertically or horizontally. If two polarising plates are placed one after the other and their transmission axis is orthogonal, the polarisers are *crossed* and no light is transmitted.

2.5.2 Optical properties of chiral nematic liquid crystals

In chiral nematic liquid crystals, the helix could be either right handed or left handed. In the case of right handed helix, the right handed circularly polarised light is reflected and the left handed circularly polarised light is transmitted (Figure 2.24).

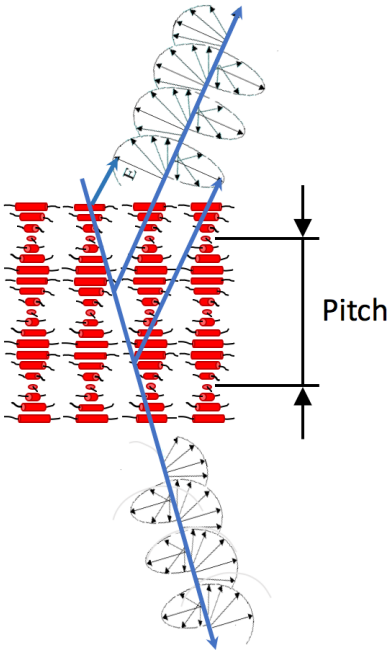

Figure 2.24- Schematic representation of reflection and transmission of circularly polarised light by the right handed helix in CLCs.

Figure 2.24 represents reflection of right handed circularly polarised light and transmission of left handed circularly polarised light in the right handed helix.

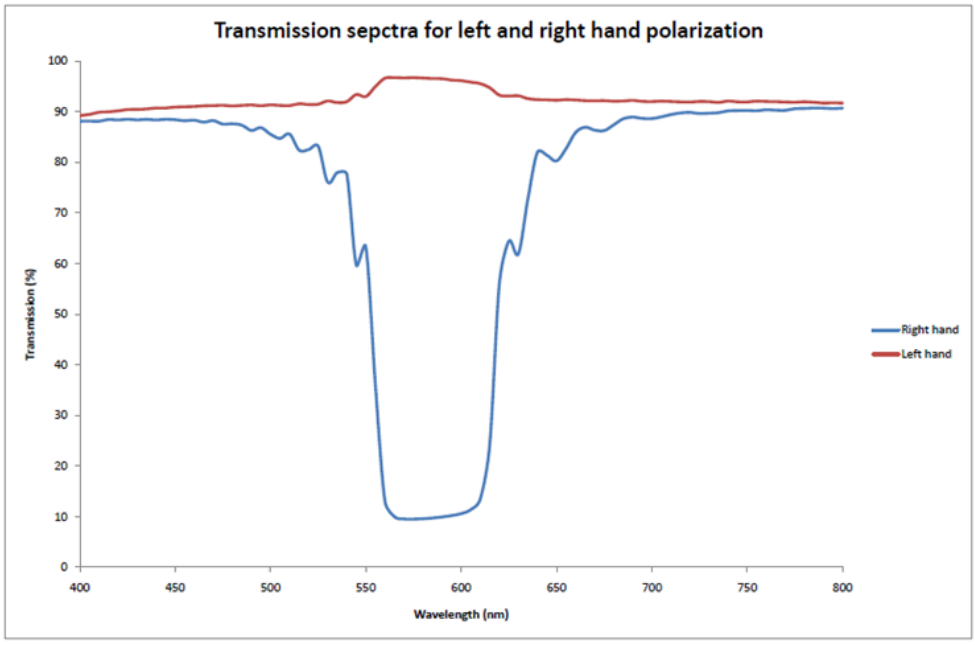

Figure 2.25- A graph of transmission spectra for left and right handed polarisation (Picot et al., 2012).

The reflected light is circularly polarised with the same handedness (RHCPL) and there is approximately 0% reflection in the circularly polarised light of opposite handedness (LHCPL). Hence the CLC structure constitutes the *polarisation-selectivity rule* that is only valid at normal incident light (Mitov, 2012).

By considering normal incident of unpolarised light, with planar orientation of CLCs, the reflected intensity is limited to 50% due to *polarisation-selectivity rule*. This reflected intensity increases with increasing film thickness and in correlation with the number of pitch lengths, which gives a flat topped peak (Mitov, 2012).

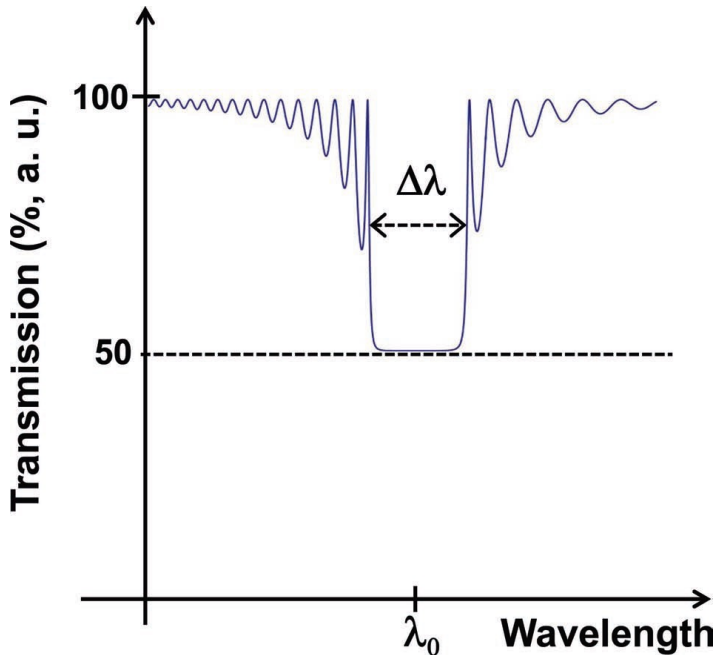

Figure 2.26- Theoretical transmittance spectrum of a cholesteric liquid crystal at normal incident of unpolarised light (Mitov, 2012).

As it shows in Figure 2.26, the negative peak is due to a band of reflection with the wavelength being specific to a range in the UV, visible or IR range of the light spectrum. λ_0 is the central wavelength that identifies the position of the band gap and is directly related to the helical pitch and $\Delta\lambda$ is the spectral bandwidth which is measured at the half-height of the peak (Mitov, 2012). Therefore chiral nematic liquid crystals can

have a selective reflection band, known as *selective reflection phenomena* where the maximum amount of selective reflection occurs at the wavelength λ_0 (Mitov, 2012).

Liquid crystals are anisotropic materials which means they have more than one index of refraction. When a beam of light containing both x and y polarised light is incident on an anisotropic material, the two polarisations have different indices of refraction and therefore travel along two different directions inside the material. This phenomenon is known as *birefringence.* Hence liquid crystal materials have two different refractive index values n_o (ordinary) and n_e (extraordinary) (Collings, 1990).

The spectral bandwidth Δλ, at normal incident is related to *birefringence* Δn, which is the difference between the two indices of refraction [$\Delta n = n_e - n_o$] and p [$\Delta\lambda = p\Delta n$] (Mitov, 2012, Collings and Hird, 1997). Therefore, any incident light with a wavelength λ out of Δλ is transmitted. Also because the birefringence is limited to 0.5, the Δλ is limited to few tens of nanometers in the visible spectrum (Mitov, 2012).

2.5.3 Polarised microscopy

As mentioned earlier optical microscopy and in particular polarisation microscopy is one of the main techniques of investigating the orientation of the nematic liquid crystals. Liquid crystals are uniaxially birefringent having higher extraordinary refractive index than the ordinary refractive index that is parallel to the nematic director (Drzaic, 1995).

In the polarised microscopy, crossed polarised light is a term that is used when two polarisers are inserted. The first one is called the *polariser* that is placed below the condenser at the bottom of the optical microscope, and the second one is called the *analyser* that is placed above the objective at the top of the optical microscope.

Any isotropic material that is placed between crossed polarisers, will appear dark as no light transmits. However, anisotropic materials such as nematic liquid crystals, will induce a phase shift in the light and the nematic will appear bright if the director makes

an angle with the polariser axes other than 0˚ or 90˚ (Figure 2.27). Conversely, no phase shift occurs when the local director field is parallel to either the polariser or analyser axes (Drzaic, 1995, Collings, 1990).

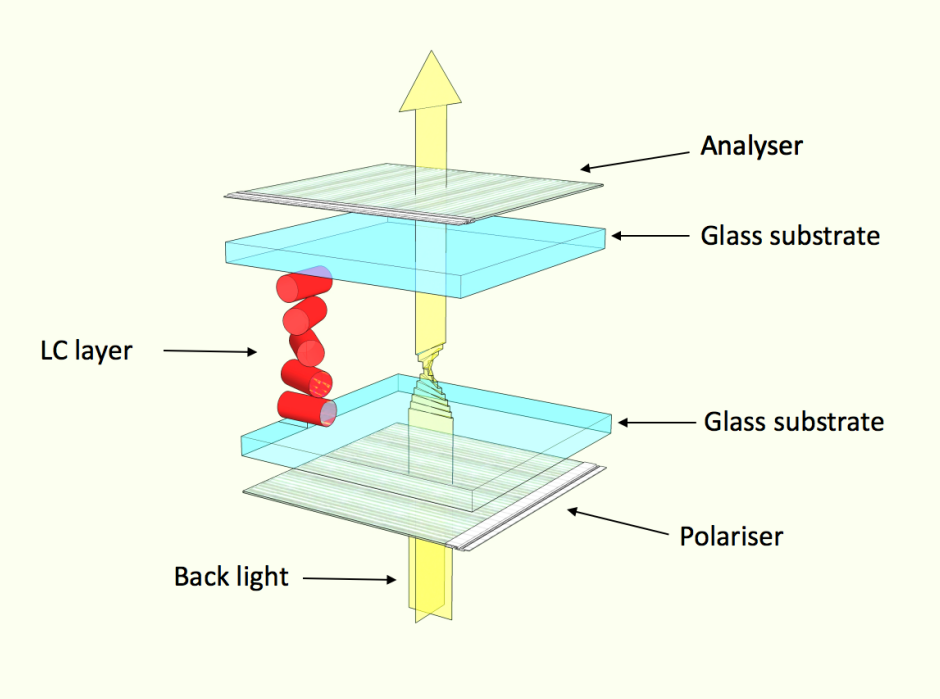

Figure 2.27- Principle of nematic liquid crystal cell in between crossed polarisers.

2.6 Alignment of Liquid Crystals

The molecules in the nematic liquid crystalline phase tend to align along a preferred direction. The materials are typically organised into poly-domains and usually there is a different orientation in each domain. However due to the strong dipole of the mesogens, the orientation of the director can be controlled by applying an external electric or magnetic field or induced surface alignment to get a more uniform mono-domain morphology in a liquid crystal film (Collings and Hird, 1997). Surface alignment can also be readily achieved for example by coating a substrate with polyvinylalcohol (PVA) or polyimide (PI) first, then applying a mechanical rubbing with a soft velvet cloth and then

casting a film on the prepared surface to obtain a homogenous alignment in the liquid crystal (Scharf, 2007).

Figure 2.28 shows different molecular organisations in the nematic liquid crystal film.

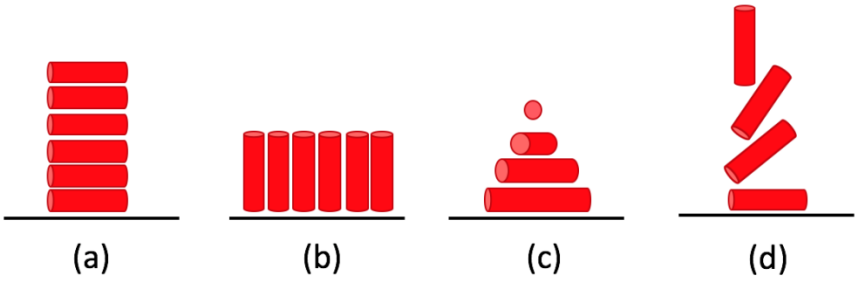

Figure 2.28- Schematic representation of different molecular organisations: (a) planar, (b) homeotropic, (c) twisted and (d) splay.

In the planar alignment the molecules or the director are aligned parallel to the substrate whereas in the homeotropic alignment the molecules or the director are aligned perpendicular to the substrate. In the twisted nematic (TN) alignment the director rotates 90° between the top and the bottom surface. The splay alignment is achieved when the molecular organisation is a mixture of both planar and homeotropic alignment (Picot, 2014).

2.6.1 Order parameter of the liquid crystal

To quantify the orientational order of the liquid crystal molecules, order parameter *S* is used and is defined using the following equation:

$$S = \langle (3cos^2\theta - 1) \rangle / 2 \qquad (2\text{-}14)$$

Where θ is the angle between the director and the long axes of each molecule. The brackets denote an average of one or many molecules at the same time. The order

parameter of isotropic liquid crystalline phase is equal to 0, whereas in a perfectly liquid crystalline phase S is equal to 1. The order parameter decreases with increasing temperature and typically S values are between 0.3 and 0.9 (Collings and Hird, 1997).

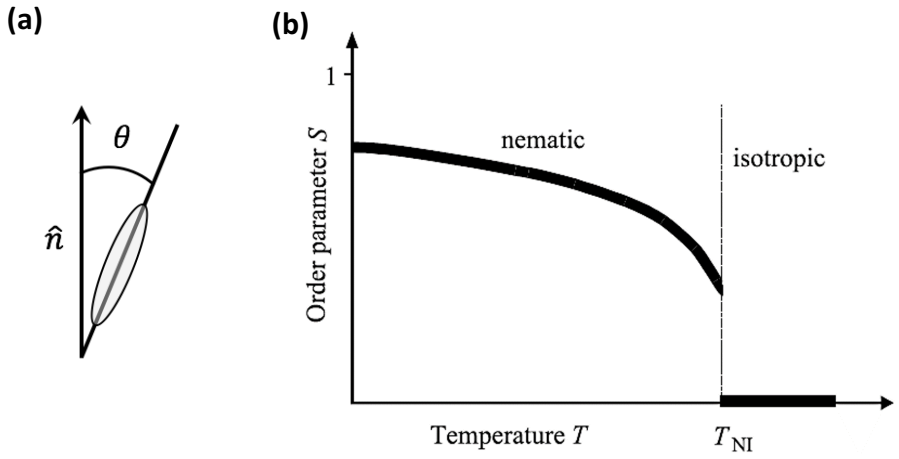

Figure 2.29- (a) schematic representation of angle θ, (b) Order parameter variation with temperature in the nematic liquid crystal phase. T_{NI} is the phase transition temperature from Nematic to Isotropic (Scharf., 2007).

2.7 Liquid Crystal Polymers

Liquid crystal polymers and elastomers have been used in various studies for different applications such as sensors, actuators, tuneable lasers and colour displays (Shibaev et al., 2010, Shibaev et al., 2008, Ohm et al., 2010, Winkler et al., 2010, Finkelmann, 1987, Doane et al., 1988).

A class of polymers that use low molecular weight liquid crystal molecules as monomer units are known as liquid crystal polymers. There are two types of polymers which give rise to liquid crystal phases (Figure 2.30). The first is called main chain liquid crystal polymer that is composed of rigid segments (mesogens) connected head to tail by flexible segments (polymer chains) (Scharf, 2007, Collings, 1990). Main chain liquid crystal polymers are stiff and have good heat resistance properties (Picot, 2014). The second type is called side chain liquid crystal polymer where the mesogens are connected as side

chains to the polymer backbone by short flexible segments called spacers (Scharf, 2007, Collings, 1990). Due to the freedom of liquid crystal molecules, this type of polymer liquid crystals can show mesogenic behaviour over a wide range of temperatures (Scharf, 2007).

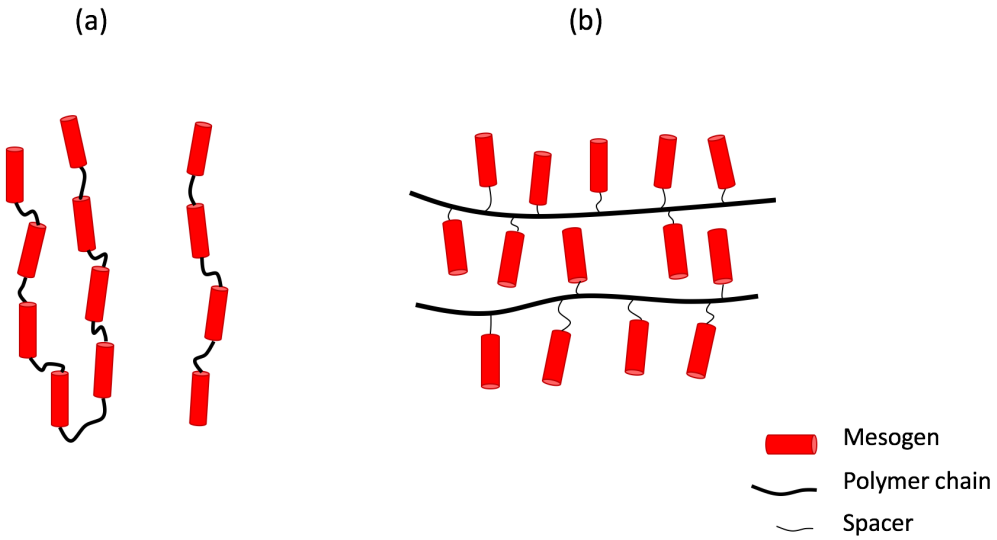

Figure 2.30- Schematic representation of liquid crystal polymers, (a) main chain and (b) side chain.

2.8 Liquid Crystal Networks

In liquid crystal networks monomers are connected on both sides to the polymer backbone and are produced by photo polymerisation of LC monomers. In this process the monomers are mixed with a photoinitiator that has a specific absorption wavelength. The amount of photoinitiator is usually very small (~1wt.%) that does not affect the transition temperature of the LC mixture. Then the whole mixture is exposed to that specific wavelength for polymerisation to take place (Liu and Broer, 2014, Picot, 2014, Broer et al., 1993). During the photopolymerisation process phase separation and phase transitions are kinetically suppressed as the process is very fast (Liu and Broer, 2014).

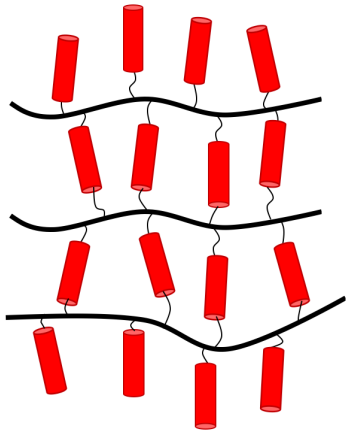

Figure 2.31- Schematic representation of a liquid crystal network.

Different types of alignment can be established in liquid crystal networks using surface alignment techniques and chiral additives followed by the polymerisation to lock in the molecular order. Films can be formed by processing from solution by producing a homogeneous mixture by dissolving all the components in a strong solvent that is subsequently evaporated. Also films can be formed by processing in the melt (Liu and Broer, 2014).

2.9 Polymer Dispersed Liquid Crystals (PDLCs)

Polymer dispersed liquid crystals (PDLCs) are nematic liquid crystal droplets of micron or sub-micron size embedded in a polymer matrix (Raina and Kumar, 2009, Parab et al., 2014). The orientation of the LC molecules varies from one droplet to another droplet and it depends on the anchoring force against the wall surface of the droplets (Drzaic, 1995).

2.9.1 Phase separation of PDLC films

In general, four different methods can be used to obtain PDLC films: Solvent Induced Phase Separation (SIPS), Thermally Induced Phase Separation (TIPS), Polymerisation

Induced Phase Separation (PIPS) and Microencapsulation (Drzaic, 1995, Malik and Raina, 2004).

Using the SIPS method, a polymer and liquid crystal are mixed with an organic solvent to form a homogenous mixture. Phase separation of the polymer and liquid crystalline phases is induced by the evaporation of the solvent (Drzaic, 1995).

Using the TIPS method, a thermoplastic polymer melt is mixed with liquid crystal at high temperature. When the mixture is cooled down, the liquid crystalline phase precipitates out from the polymer as the polymer solidifies (Drzaic, 1995).

Using the PIPS method, the liquid crystal is mixed with low molecular weight monomers that act as a solvent for the LC. This is then followed by polymerisation through the application of heat, light or radiation. During this process the polymer chains phase separate from the liquid crystals and form a matrix that surrounds liquid crystal domains (Drzaic, 1995, Malik and Raina, 2004).

Using the microencapsulation method, an emulsion of water-soluble polymer and water insoluble liquid crystals is prepared. The subsequent evaporation of the water results in a phase separation of the LC from the polymer as a result of insolubility of the liquid crystals in the aqueous media (Thakur and Kessler, 2015).

2.9.2 PDLC film transmittance

Liquid crystals within the micro-domain are found to be birefringent owing to their anisotropic nature and hence they have two different refractive index values n_o (ordinary) and n_e (extraordinary) (as an example for E7 n_o=1.52 and n_e=1.75) (Scharf, 2007). The polymer matrix has single refractive index n_p since it is optically isotropic (i.e. silicone n_p= 1.4-1.5). The matching and mismatching of the ordinary refractive index of LC and polymer matrix determines the overall transmittance of a PDLC sample. Since the orientation of the LC molecules within each droplet varies from one droplet to another or

in other words the symmetry axis of each droplet varies randomly from droplet to droplet, the light propagation normal to the film surface experiences a range of refractive indices between (n_o) and (n_e). Therefore, there is generally refractive index mismatch between the polymer matrix and the LC. This then produces light scattering and makes the PDLC film opaque (Isabel et al., 2012, Kim et al., 2015, Malik and Raina, 2004). However, the droplet symmetry axis in the PDLC film can be changed. For example, by applying a sufficient electric field across the PDLC film, the droplets symmetry axis is aligned with the field and each droplet possess a uniform refractive index at incident light parallel to the film. If the ordinary refractive index of the liquid crystal matches the polymer, the film can appear transparent (Kim et al., 2015, Drzaic, 1995).

2.10 Summary of the Literature Review

The literature review presented in this chapter is composed of three parts. The first part examines various existing colour changing technologies. It is observed that several of the underlying technologies are based on soft materials that produce colour with applied mechanical strain.

The second part of the literature review focuses on DEA based technologies as they are considered to be a highly promising way of creating actuation using highly stretchable materials that are low in weight, high in efficiency, low in cost and which offer the possibility of miniaturisation. The fundamental mechanism that produces actuation in DEAs is discussed and the upcoming challenges in this field are explored. The material requirements for high performance dielectric elastomer transduction are examined with a focus on commercially available acrylic and silicone elastomers. The different types of conductive compliant electrodes and a review of the state of the art in the area of optics are also discussed.

The third part of the literature describes the key concepts around polymeric liquid crystals such as the different liquid crystal phases that can exist and how their alignment might be controlled. There is also a discussion on the structure of a cholesteric liquid crystal and the resulting optical properties.

The final part of this survey explained different classes of materials containing liquid crystals such as liquid crystal polymers and PDLCs.

This review highlights that there are still many challenges to be overcome to make a soft material whose colour can be readily changed under the application of a strain. At the outset this investigation aims to develop a new approach to create a colour changing device using a dielectric elastomer actuator to generate the displacement field. To achieve this, a range of approaches are considered for detailed exploration including the development of a novel soft material that has some sort of structural organisation that can produce spectral colour and which is compatible with elastomer substrate materials used in a DEA. For the proposed soft material predominantly liquid crystals are investigated as they are considered to be a good candidate owing to their dynamic colour changing behaviour.

Chapter 3: Two Colour Switching DEA Positioner and Mask Device

3.1 Introduction

Materials' capable of adapting their colour are becoming an increasingly attractive prospect in many research fields and applications, such as; communication, display devices and structural designs. One potential technology to achieve this might be to adopt Dielectric Elastomer Actuators (DEAs), which have been the subject of great interest since their development by researchers from the Stanford Research Institute (SRI) (Pelrine et al., 2000). They are a highly promising new technology for optical applications, including tuneable transmission gratings and variable diffraction grating (Aschwanden et al., 2008, Fang et al., 2010) tuneable focus optical lenses (Son et al., 2012, Carpi et al., 2011) and active camouflage (Rossiter et al., 2012). Developing a DEA application that

can change colour would be very beneficial due to the material's robustness, light weight, high energy efficiency and low cost whilst there is also the potential for miniaturisation. This chapter presents a novel approach to create a colour changing device using a Dielectric Elastomer Actuator. The proposed concept relies on the use of a simple planar DEA coated with two different coloured spots that are masked by a frame with a single viewing hole. The hole is aligned with one coloured spot, such that when a voltage is applied between the electrodes, the coloured spots move, becoming visible or hidden through the hole of the mask. Thus, the device behaves as a positioner of coloured spots behind the mask and which then serves to make them visible on demand. The resulting effect is that the whole device can be used to switch from one colour to another.

3.2 Experimental

3.2.1 Configuration and materials

Figure 3.1 shows the schematic diagram of the first configuration of the proposed device demonstrating a single pixel colour change. An elastomeric membrane (acrylic double-sided tape VHB 4905 3M with a thickness of 0.5mm) was bi-axially pre-stretched 250% and fixed to a rectangular plastic frame. Carbon grease was used for both top and bottom electrodes and was applied only half way through the membrane forming a region called the active zone. Aluminium foil strips were used as electrical leads. Two different coloured paper spots were placed directly at the centre of the elastomeric membrane called the passive zone. The dimensions of each coloured paper spot was roughly 2 × 2 mm. A mask was made out of a black cardboard by making a square hole of the same size as a single coloured spot. The mask was placed on the frame of the actuator where only the yellow coloured spot was visible by the eye from the top view at a fixed angle. When a voltage difference of 4000 Volts was applied between the electrodes, the active, actuated

zone of the device was squeezed in thickness and stretched in area, causing the passive zone to contract in area due to the pre-stretch. Hence the spots on the surface were displaced, causing the yellow coloured spot to position below the mask and pink coloured spot to position below the hole on the mask giving appearance of a colour change from yellow to pink.

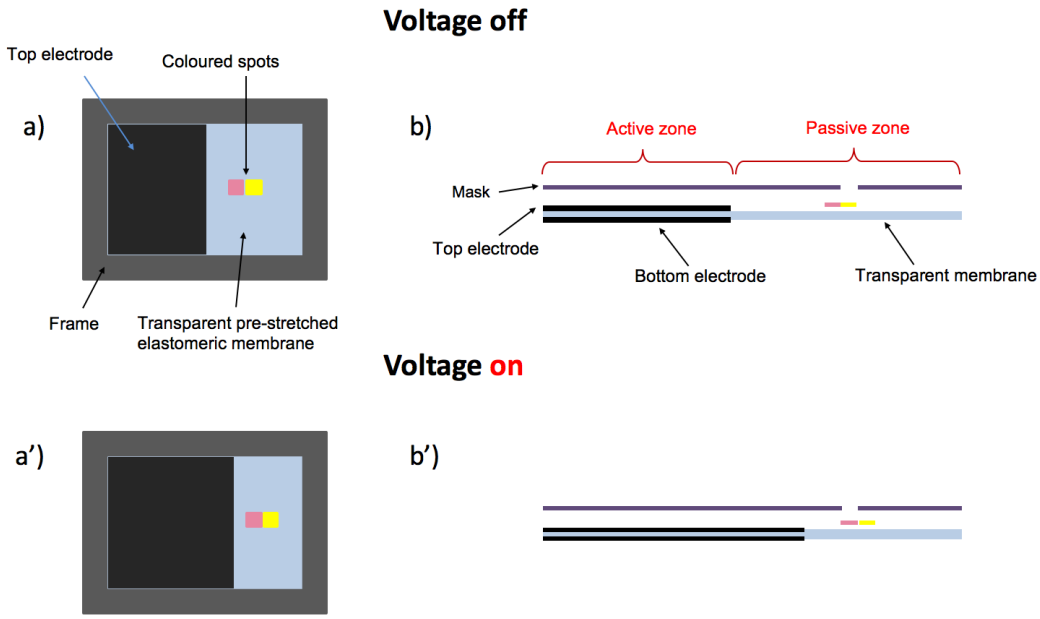

Figure 3.1- Schematic diagram of the proposed device (configuration 1). a, b) device at electrical rest, a',b') device under electrical activation, a, a') top views of the device and b, b') lateral views of the device with the mask.

As it is shown in Figure 3.2 at 4000 Volts, the device changes colour from yellow to pink. However, in this prototype device more than 99% of the device is covered by the mask and the colour change is dominated by the appearance of the mask.

Figure 3.2- DEA device (configuration 1), (a) at rest and (b) at 4000 Volts.

To increase the coloured areas, another device with an array of coloured spots that was masked by a frame with an array of viewing holes was proposed. Figure 3.3 shows the schematic diagram of the proposed configuration, demonstrating multi pixel colour change. An elastomeric membrane (acrylic double-sided tape VHB 4905 3M with a thickness of 0.5mm) was bi-axially pre-stretched 250% and fixed to a rectangular plastic frame. The top electrode (again made from carbon grease) was applied to the entire membrane whilst the bottom electrode was applied only to one half of the membrane (in what is now termed the active zone). The coloured paper spots were placed on the central axis of the device on the top electrode, where the maximum displacement was observed as they are furthest away from the frame. When a voltage difference was applied between the electrodes, the active, actuated zone of the device was squeezed in thickness and

stretched in area, causing the passive zone to contract in area due to the pre-stretch. Hence the spots on the surface were displaced into positions below the holes on the mask, giving the appearance of a colour change, Figure 3.3.

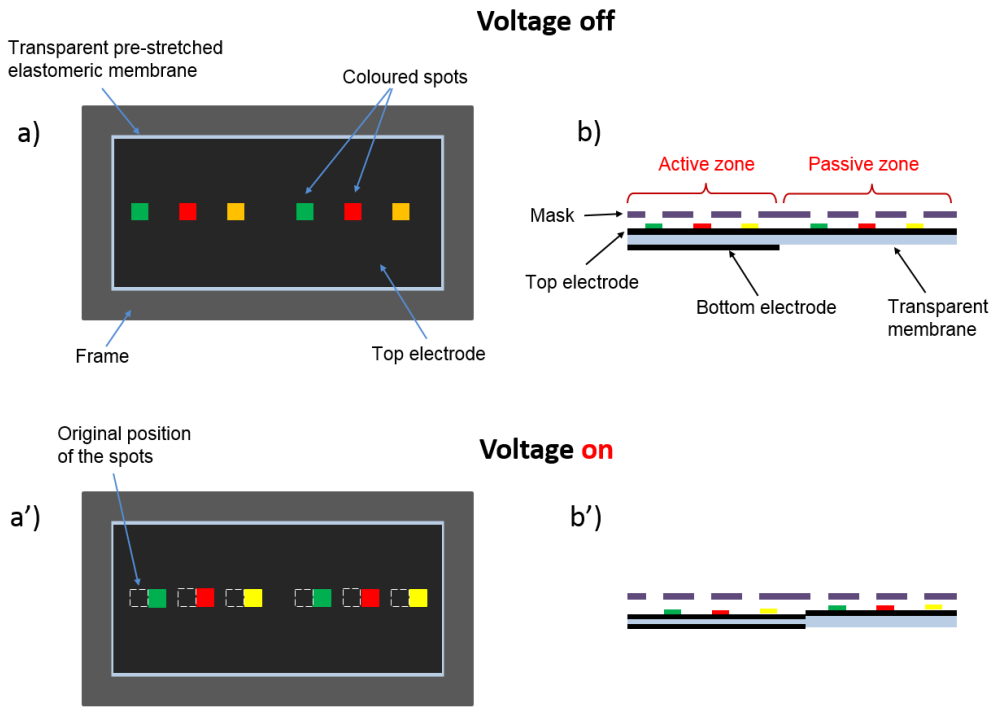

Figure 3.3- Schematic diagram of the proposed device (configuration 2). a, b) device at electrical rest, a',b') device under electrical activation, a, a') top views of the device and b, b') lateral views of the device with the mask.

The movement of the spots is actuated by the application of a voltage between the electrodes. The amount of the displacement of each spot then depends on their position on the membrane relative to the rigid frame and the proximity to the actuating electrodes. To understand how the device behaves, a MATLAB algorithm was used to detect and monitor the position of spots at different parts of the membrane at different applied voltages.

3.2.2 Data processing

A digital camera was used to capture the position of each spot on the membrane at different voltages. The camera was placed at a fixed angle facing the coloured spots and the images acquired were then processed using a MATLAB algorithm which is described in the following section. This algorithm is based on the colour contrast between two areas: the coloured spots and the electrode. Initial experiments using a simple transparent rubber in the passive region resulted in too little colour contrast. To improve the contrast the back electrode was again extended over the entire back of the rubber sheet. This allowed a very clear colour contrast that can be easily measured between the coloured paper spots and the black electrode background. The MATLAB code starts with the function below for the name of each image and storing all the (x,y) coordinates of the spots:

```
names = dir('Image_*.bmp');
ps = zeros(length(names)*2,63);
    xs=0;
    ys=0;
```

Followed by the function that specifies the number of spots in each row:

```
tablerange = [3,3,3,18,18,18]
```

Then a loop starts from this point when the original picture is loaded (Figure 3.4):

```
I = imread([names(k).name]);
```

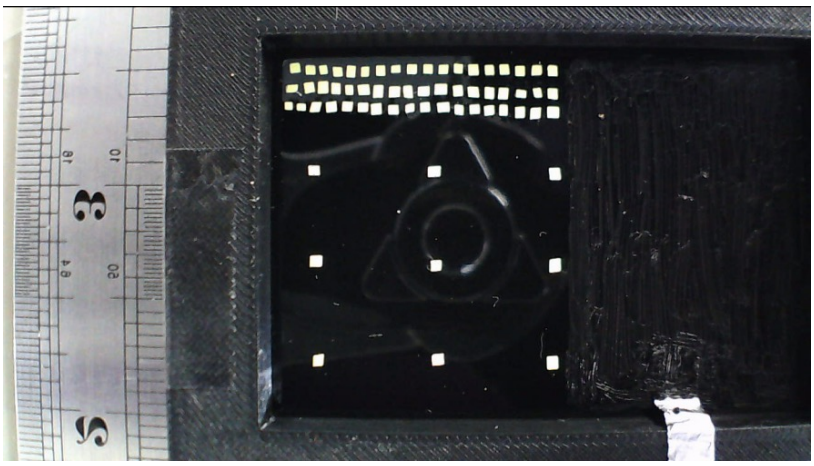

Figure 3.4- Original image captured by the digital camera.

Then the original image is transferred to black and white image (Figure 3.5) and is displayed using function below:

```
I = rgb2gray(I)
imshow(I)
```

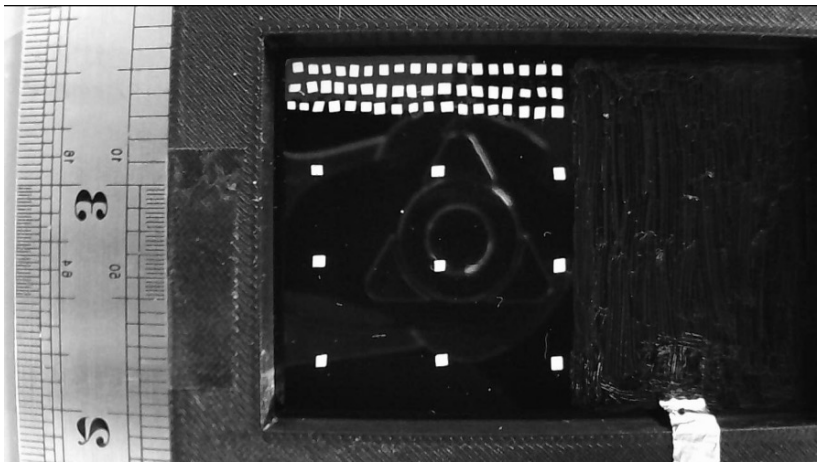

Figure 3.5- Original image is converted to a black and white image.

The area of interest can be selected by creating a rectangular area based on two points that are defined by the mouse and the rest of the image is cropped (Figure 3.6):

```
if (k==1)
[xs,ys] = getpts(fig);
end
rect = [xs(1),ys(1),[xs(2),ys(2)]-[xs(1),ys(1)]];
```

```
rectangle('Position',rect);
```

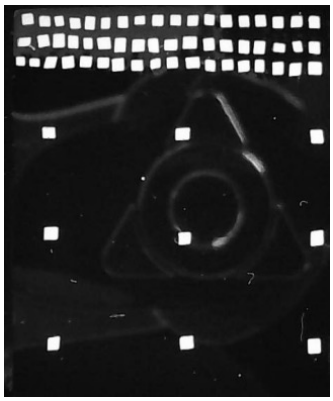

Figure 3.6- Cropped black and white image.

Most of the noise is filtered out using the threshold1 (180) which is for black and white image (Figure 3.7):

```
bw = Icrop>threshold1;
```

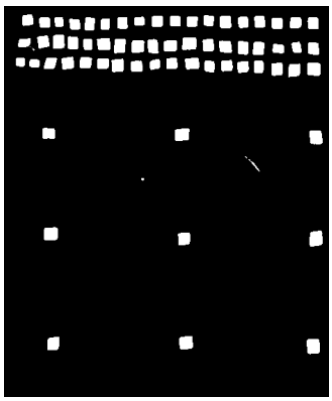

Figure 3.7- Cropped black and white image with the applied threshold including the noise particles.

A function is used to find all the possible white objects including small noise particles. The centre of each object is then detected and the (x, y) coordinated are picked (Figure 3.9). For filtering out the small noise particles threshold2 is used (Figure 3.8). Therefore, each object that contains more than 50 pixels is counted as a spot, and less than 50 pixels is counted as a noise particle:

```
CC = bwconncomp(bw);
S = regionprops(CC,'Centroid');
pls = CC.PixelIdxList;
poneimg = [];
m = 1;
for k2 = 1:length(S
    if (length(pls{k2})>threshold2)
            x = S(k2).Centroid(1)+xs(1);
            y = S(k2).Centroid(2)+ys(1);
```

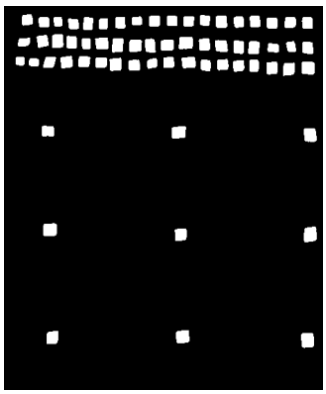

Figure 3.8- Cropped back and white image after removal of noise particles.

The recognition path for the spots is shown in Figure 3.9, where a red line goes through the centre of each spot. The (x,y) coordinates of the centre of each spot is the output in a table in csv format.

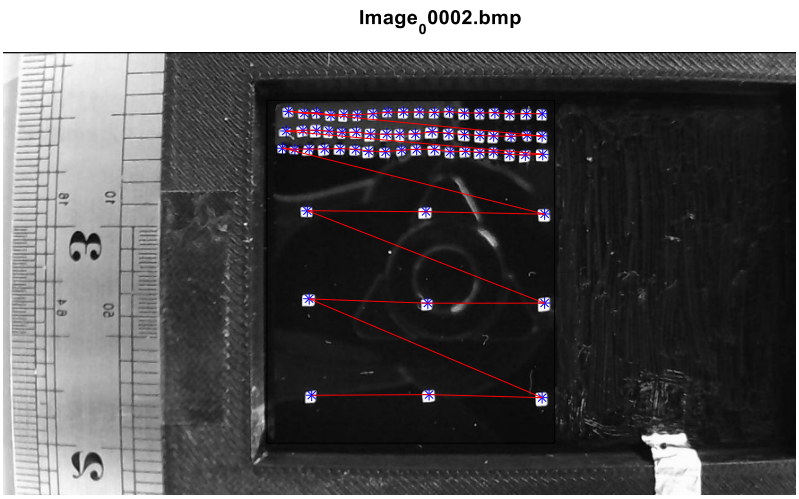

Figure 3.9- Processed image of the device where the position of the spots are recognised by placing (*) at the centre of each spot followed by a red line across the centre of each spot to show the recognition path.

This process was repeated for each captured image and the results are processed to derive the motion in pixels of each point for a given applied voltage.

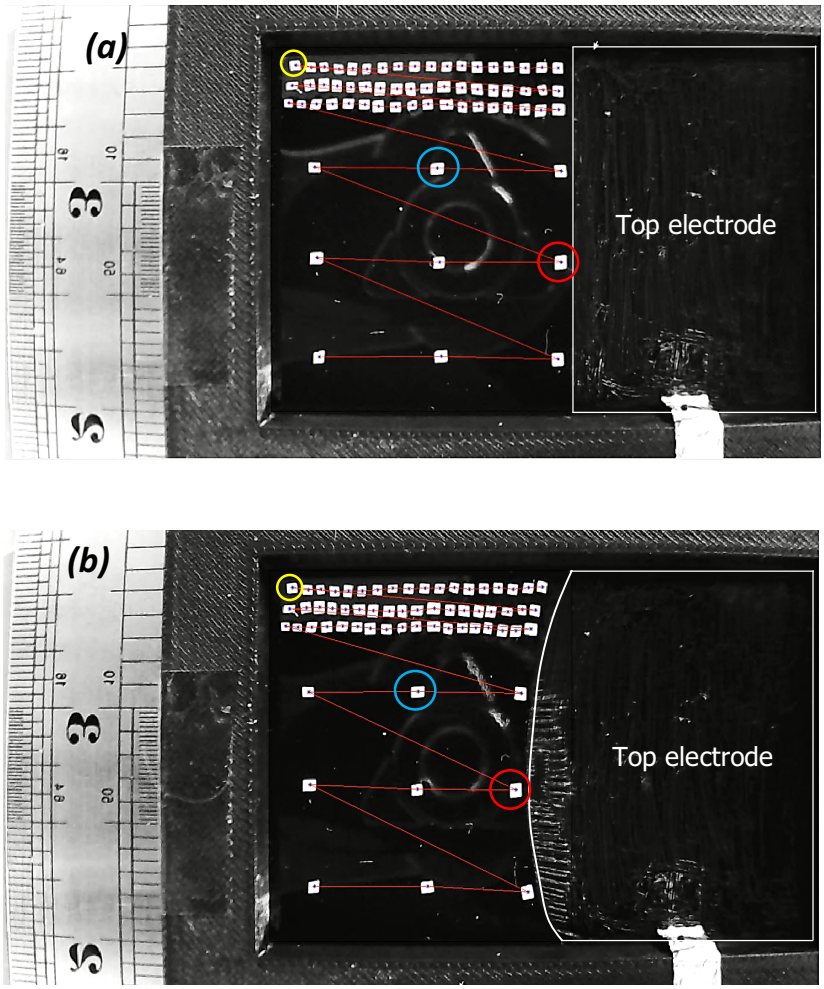

Figure 3.10- Processed images (a) device at rest and (b) device at 3000 Volts.

Figure 3.10 a and b show the processed images of DEA device at rest and at 3000 Volts respectively.

3.3 Results and Discussion

The relative movement of the spots at different parts of the membrane under voltages ranging from 0 to 3000 Volts is shown in Figure 3.11.

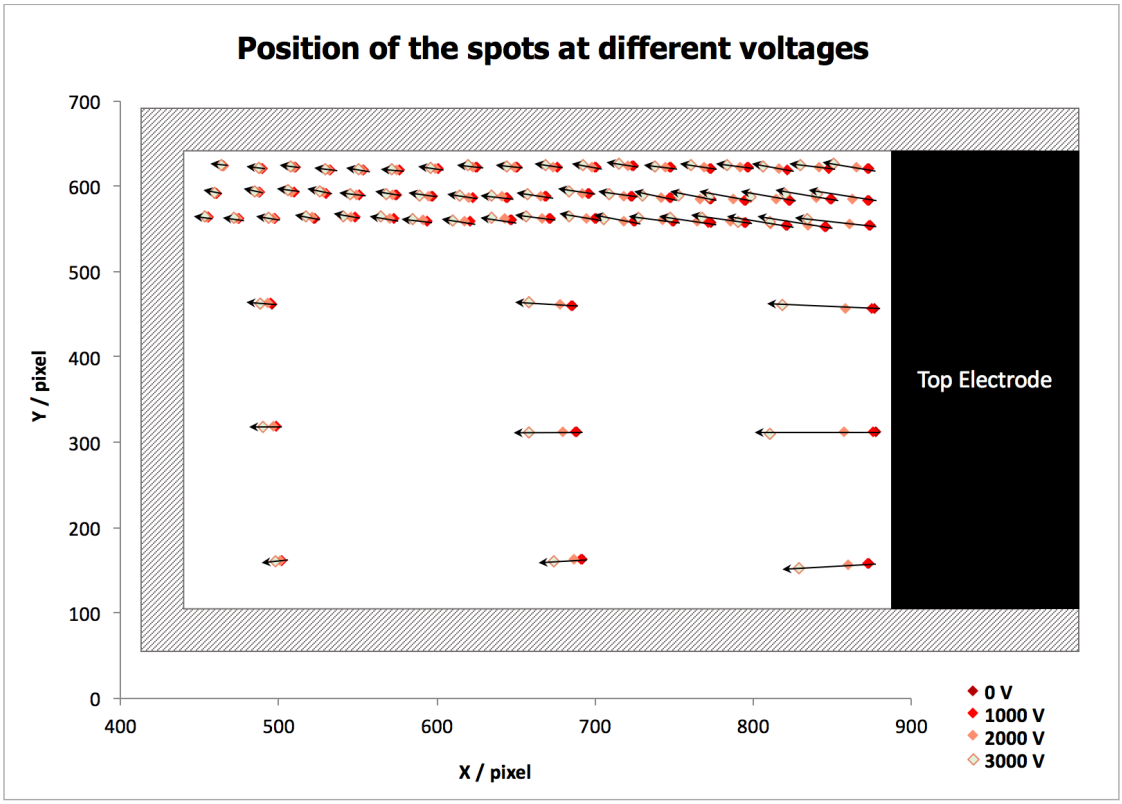

Figure 3.11- A graph showing the (x,y) coordinates of the centre of each spot on the membrane (in pixel) at different voltages. Each pixel is equivalent to 0.07 mm.

As highlighted in Figure 3.11, the maximum displacement is observed at the spots that are furthest away from the frame and closest to the electrode. Furthermore, spots placed on the central region of the membrane have negligible displacement in the direction orthogonal to the main axis of motion. The single spot highlighted in red circle in Figure 3.10 is displaced 65 pixels from 0 to 3000 Volts in the direction of the main axis of the motion. This displacement is equivalent to 4.58 mm. The displacement of each spot is measured as a function of the applied voltage. A graph of displacement against voltage is plotted for three spots at different positions on the actuator. These three spots are highlighted by different coloured circles in Figure 3.10.

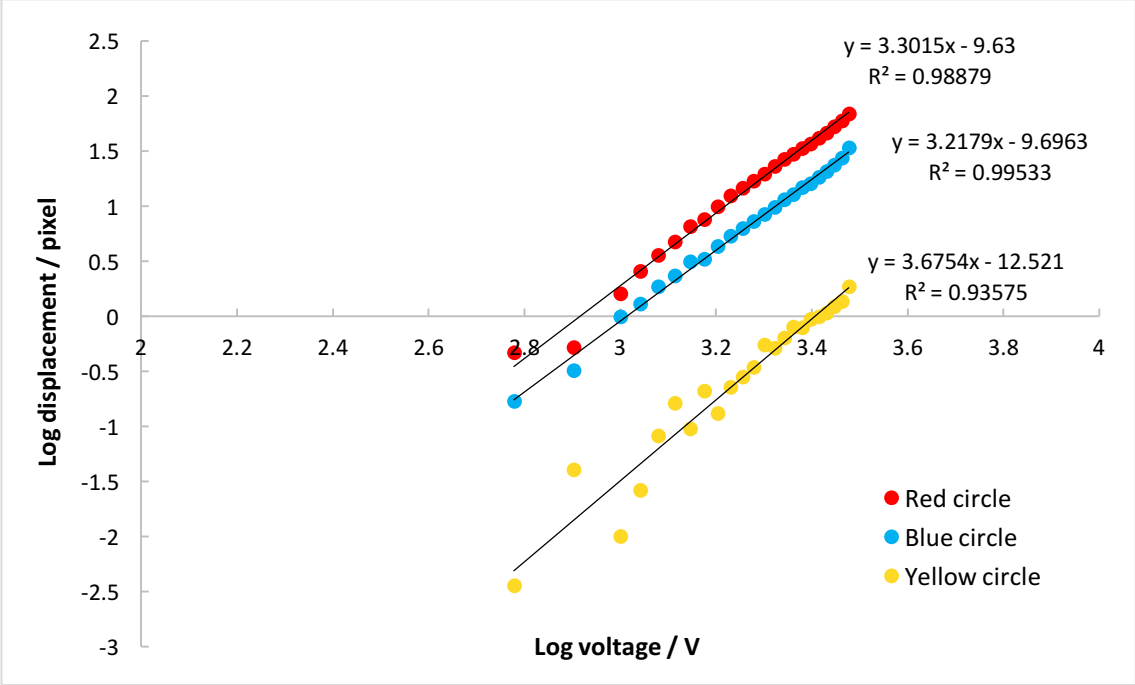

Figure 3.12- A graph showing the log of displacement against the log of voltage for three different spots on the membrane.

The electrostatic pressure generated in a DEA is proportional to the square of the applied electric field (equation (2-1). However, as is shown in Figure 3.12 the power relationship between the displacement and the applied voltage for all three positions on the passive surface is around 3. Clearly the displacements of the points are modified by the edge constraints. As it shows in Figure 3.11 the further the position of the spot from the electrode and the closer to the frame results in the smallest displacement of the spots with the applied voltage. The same effect can also be seen from the plot in Figure 3.12 as the spot highlighted with the yellow circle displays a much smaller displacement from 0 to 3000 Volts (0.13 mm) in comparison to the spot highlighted with the red circle. Hence these two boundary conditions influence the homogenous active strain of the membrane and therefore affect the displacement of the points at different parts of the membrane. In order to achieve the optimum configuration, the electromechanical behaviour of the device would need to be modelled. The total device could be characterised by measuring

the displacement of every point as a function of applied voltage, as well as their relative movements and separation. Moreover, it is important to consider different parameters such as the extent of the biaxial pre-stretch of the film prior to clamping in the frame as it can alter the relationship between the displacement at specific locations as a function of the applied voltage. Other features might include investigating how different geometric features of the frame might alter the voltage displacement response. Each of these features would need to be optimised to enhance the electromechanical response of the device.

3.4 Conclusion

In conclusion a new approach to create a simple device capable of switching between two or more colours using a DEAs was demonstrated. The movement of the spots on the actuator was analysed and the results showed that in the central region, where the displacement was highest, the movement of the spots was mostly unidirectional. Spots further away from the electrode displaced significantly less than their central equivalents whilst the spots closest to the frame exhibited the smallest displacement as the frame restricted their movement. This new approach was capable of producing a subtle colour change by masking certain areas of the material and repositioning coloured spot into view through the application of an applied voltage. A large portion of the device was covered by the mask and only a small portion showed colour and the colour change was dominated by the mask. To produce a large overall colour change using this approach a much more complex design involving an array of many devices would be required. After having a discussion with the sponsor of this project, it was decided to consider an alternative approach to produce a more significant colour changing device using DEAs.

Chapter 4: Polymer Dispersed Liquid Crystals (PDLCs)

4.1 Introduction

Polymer dispersed liquid crystals (PDLCs) can be produced with nematic liquid crystal droplets of approximately micron or sub-micron size embedded in a polymer matrix. The orientation of the LC molecules varies from one droplet to another droplet depending on the anchoring force against the wall surface of the droplets (Drzaic, 1995).

PDLCs have been widely studied and used in a range of optical applications such as switchable windows and optical display devices owing to their great electro-optic properties (Drzaic, 1995, Park and Hong, 2009). Electro-optical properties of the PDLC films are controlled by the director configuration of the dispersed liquid-crystal droplets. For example, applied electric field normal to the surface of the PDLC film can change the

director configuration of the dispersed liquid crystals as the director tends to align in the direction of the applied field (Drzaic, 1995).

Malik and Reina (2004) investigated the electro-optical and the thermo-optical properties of the PDLC composite films. They found that the electric field strongly influences the droplet orientation and the optical transmission and threshold voltage increases with increasing temperature due to the reduction in effective voltage drop across the LC droplet (Malik and Raina, 2004).

Amimori et al. (2003) performed an opto-mechanical analysis on the PDLC film in which they found that polymer chain orientation during stretching of the PDLC matrix, influences not only the droplet shape anisotropy but also the liquid crystal alignment within the droplets (Amimori et al., 2003).

Zou and Fang (2011) investigated adhesive PDLC films with low cohesive strength developed using solvent- and polymerisation-induced phase separation. A simple method was introduced that allowed printing of a thin PDLC film into structural and orientational patterns on substrates, which can be used as a composite material for sensor applications (Zou and Fang, 2011).

In this chapter PDLC films were produced by mixing a nematic liquid crystal with a reactive silicone resin by solvent induced phase separation. The immiscibility of these compounds resulted in a dispersion of the liquid crystal droplets in the silicone matrix. The aspiration being to create a thin PDLC film whose optical properties can be changed by the application of a strain to the film. To create a suitable film, the alignment of the different dispersed liquid crystal droplets was verified using LCs with different molecular chemistries. The best films were then subjected to a mechanical deformation and in order to make a suitable device the effect of layering the films onto different elastomeric substrates was also investigated.

4.2 Experimental

4.2.1 Materials

PDLC film was prepared with silicone ESSIL291 (Axon Technologies) and commercially available nematic liquid crystal E7 (SYNTHON Chemicals). E7 is made of four different components: 51% 4-cyano-4'-n-pentyl-biphenyl (5CB), 25% 4-cyano-4'-n-heptyl-biphenyl (7CB), 16% 4-cyano-4'-n-oxyoctyl-biphenyl (8OCB), 8% 4-cyano-4"-n-pentyl-p-terphenyl (5CT). P-Xylene anhydrous, ⩾99% (Sigma Aldrich) was used as a suitable solvent.

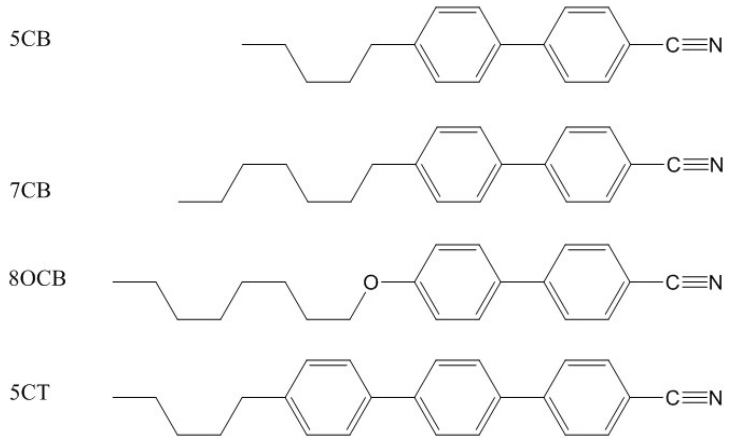

Figure 4.1- Chemical structure of E7 mixture.

The mixing ratio between silicone and xylene was varied in order to establish the optimum weight ratio required to create homogeneous evaporated film containing well dispersed E7 phase droplets of an appropriate size. The total amount of xylene was split in two parts and was mixed with E7 and silicone separately. Initially, E7 at different concentrations was mixed with xylene in the isotropic phase in a bottle. Then silicone part A (resin) and part B (catalyst) were mixed at 10:1 weight ratio and xylene was added

to the mixture and this was stirred thoroughly to ensure effective mixing. Following this, the liquid crystal and the silicone mixtures were mixed together by shaking action until a transparent homogenous blend was produced.

4.2.2 Measuring the viscosity of the different solvent volume fractions

The xylene solvent significantly reduced the viscosity of silicone, which made it easier to create a thin film using the spin coating process. As the resulting viscosity of the solution is an important processing parameter, a TA Instruments AR 2000 Rheometer was used to measure the viscosity of the silicone/xylene mixture over a range of shear rates for a range of different ratios of silicone rubber to xylene. For the rheology measurements, shear strain rates between 0.01-100 per second were used. The measurement was taken at room temperature and a 40 mm head was used. Silicone parts A and B were mixed for 2 minutes by hand before being placed in the vacuum oven for 25 minutes to extract any entrapped air bubbles. Prior to testing xylene was then added to the mixture in a wide range of ratios and this was then carefully mixed to avoid the inclusion of additional air bubbles as far is practical.

4.2.3 Spin coating

The homogenous mixture was spin coated (SCS 6800 Spin Coater Series) on a microscopic glass slide at two different spin coating rates 500 and 2500 rpm for 30 seconds. When a PDLC film was produced the initial film was transparent, but as the xylene was evaporated from the film the PDLC film transformed into an opaque film as a consequence of the phase separation of the LC droplets. The PDLC film was left on glass slide in the fume hood to be cured at room temperature for 48 hours.

4.2.4 Characterisation

The director configuration of the dispersed liquid crystal droplets in PDLC films was characterised with an Olympus BX60 microscope with crossed polarisers. Transmission measurements were performed using a Perkin Elmer Lambda 950 UV/VIS spectrophotometer, integrating sphere. Tensile mechanical analysis was performed on an Instron testing machine. Thermodynamic phase transitions such as the resulting glass transition of the PDLC films were measured using differential scanning calorimetry (DSC) PerkinElmer DSC 4000 with a heating and cooling rate of 10 °C per minute.

4.3 Results and Discussion

4.3.1 Rheology measurement results

The rheology measurement was performed on pure silicone (parts A and B) without the incorporation of any liquid crystal using five different volume fractions of xylene in silicone. A plot of viscosity against shear rate is shown in Figure 4.2.

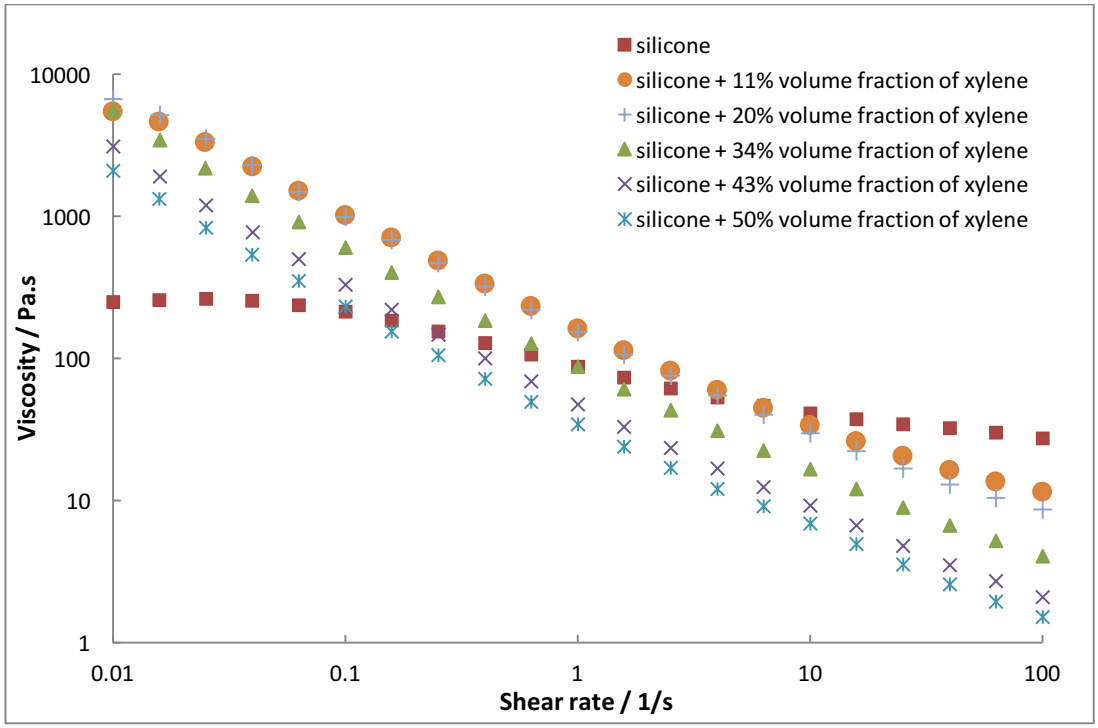

Figure 4.2- Rheology data for pure silicone and silicone mixed with five different volume fractions of xylene.

The results shown in Figure 4.2 were somewhat unexpected as the viscosity of silicone increases dramatically at low shear rates from around 250 Pa.s for the pure silicone to 5450 Pa.s even when as little as 11% volume fraction of xylene was added to the silicone. At low shear rates the viscosity appears to reduce with a further increase in the volume fraction of the xylene. This increase in the viscosity at low shear rates could be due to the xylene somehow accelerating the cure chemistry when silicone parts A and B are mixed together. It is then interesting to note that at the much higher strain rates there is a monotonic decrease in viscosity with volume fraction of xylene as was anticipated prior to the testing. It is plausible that at these higher rates of shear that any new crosslinks are being broken. The increase in viscosity at low shear strain rates could result from some other complex interaction between the xylene and either silicone part A, part B or a combination of both.

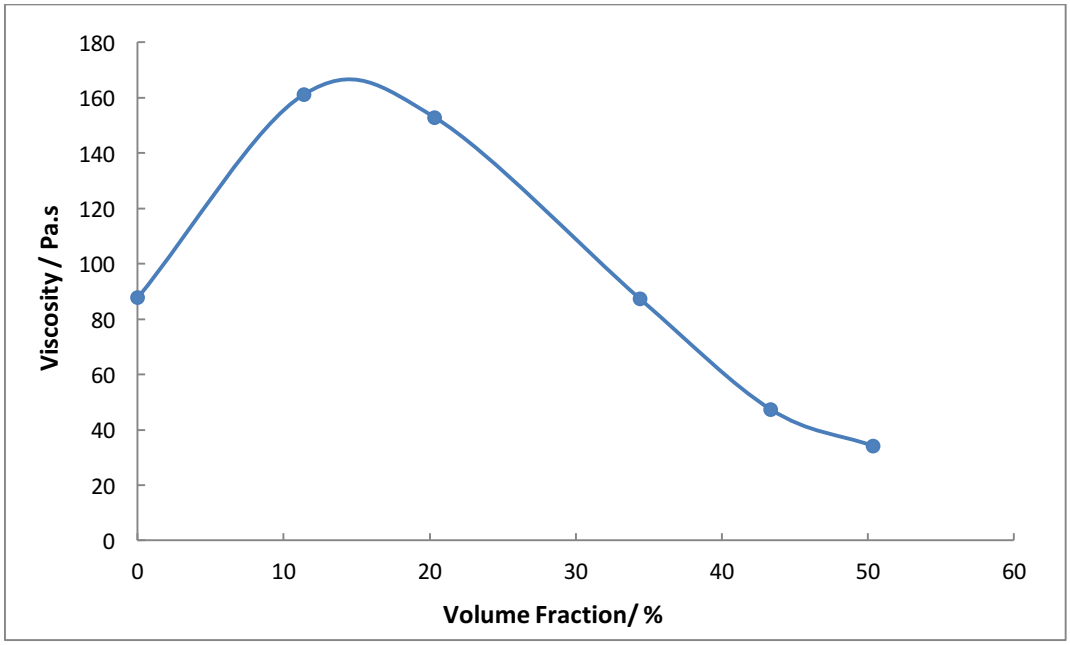

Figure 4.3- A graph showing silicone viscosity at different volume fractions of xylene at 1/s shear rate.

Using the rheological data shown in Figure 4.2 it is simple to extract a graph of how the viscosity varies against volume fraction of the solvent at a specific shear rate. The 1/s shear rate data is shown in Figure 4.3 . It indicates that the viscosity of silicone increases as soon as it is mixed with the xylene. The viscosity increases significantly where the volume fraction of the xylene is low and it then decreases with increasing volume fraction of xylene. A 50% volume fraction of xylene tested at a 1/s shear rate reduces the viscosity of the silicone to 34 Pa.s. This being approximately the upper threshold required to perform the spin coating. However, this fraction was too low to allow the manufacture of a PDLC film from a suitable initially homogeneous mixture of the nematic liquid crystal (E7) in the silicone rubber. Therefore, a greater volume fraction of xylene was chosen from a trial and error approach to the spin casting process. For this case the best mixing ratio between the silicone and the xylene was 1:2 by weight as this resulted in a homogenous PDLC mixture with low viscosity for the spin coating.

4.3.2 Liquid crystal concentration

Different liquid crystal concentrations of 5, 20, 30 and 40 wt.% were added to the silicone. The final PDLC films were observed using an optical microscope in transmission with and without crossed polarisers.

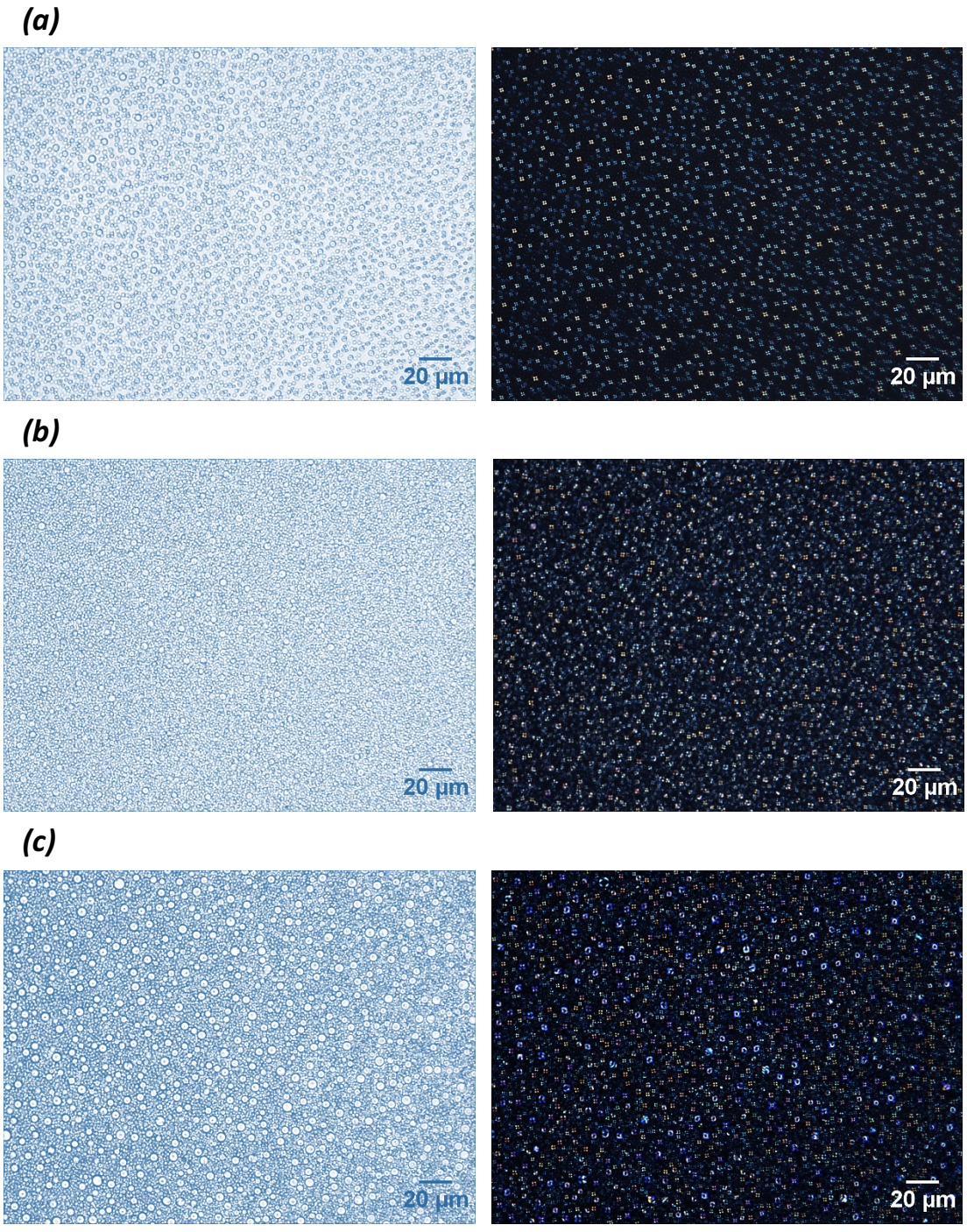

Figure 4.4- Optical microscopy images of PDLC film spin coated at 2500 rpm at different liquid crystal concentrations (a) 5 wt.%, (b) 20 wt.%, (c) 30 wt.%, transmission images are shown for non-polarised light on the left and crossed polarised light on the right.

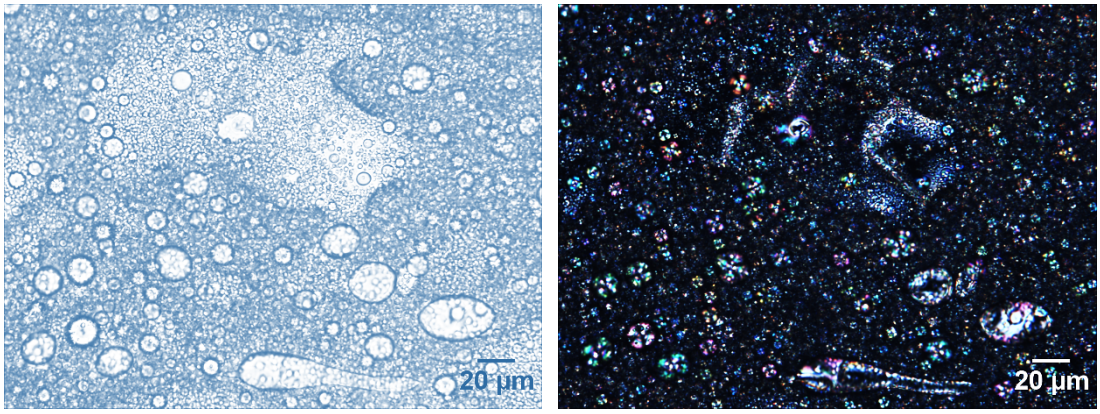

Figure 4.5- Optical microscopy images of PDLC film spin coated at 2500 rpm at 40 wt.%, transmission images taken using non-polarised light on the left and crossed polarised light on the right.

At 40 wt.%, large areas of E7 can be seen which shows that E7 was not fully phase separated in small droplets as the threshold of dispersing E7 in the silicone was reached (Figure 4.5). At 5, 20 and 30 wt.% the individual dispersed LC droplets show a spherical shape in the polymer matrix and they produce a Maltese cross pattern when viewed using the crossed polarisers. This pattern indicates a radial director configuration in the LC droplet with perpendicular anchoring at the E7- polymer interface (Figure 4.4 and Figure 4.6) (Drzaic, 1995). Droplet configuration is determined by the preferred alignment of the nematic liquid crystal molecules at the surface of the polymer binder (Drzaic, 1995). This preferred alignment is enforced by a balance between the surface anchoring energy and the elastic forces within the liquid crystal droplets (Zou and Fang, 2011, Drzaic, 1995).

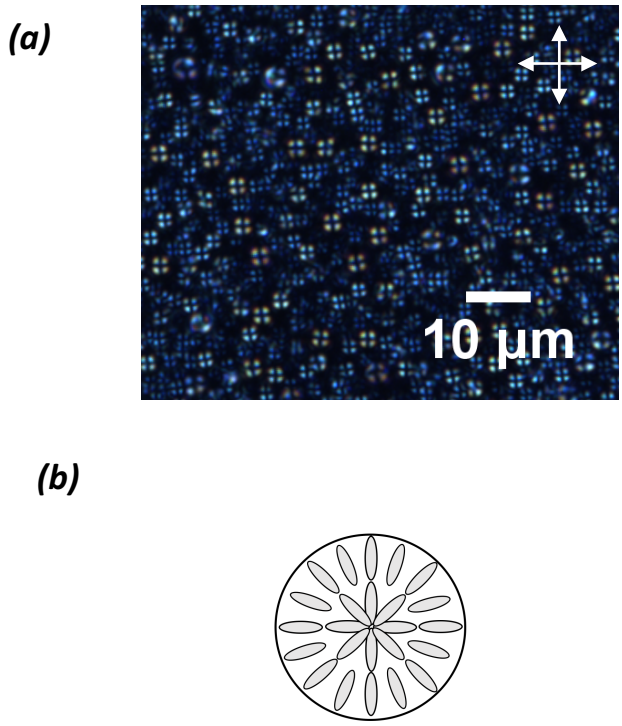

Figure 4.6- (a) close up image of the spherical LC droplets in the PDLC film at 20 wt.% concentration and spin coating rate of 2500 rpm. The direction of the polariser and analyser is indicated by white arrows, (b) schematic structure of radial director configuration.

Since E7 is amphiphilic, the polar head of the molecules point away from the surface as silicone is hydrophobic and this results in the radial configuration of the droplets that is shown in Figure 4.6 b.

The individual LC droplet size for the 5, 20 and 30 wt.% fractions were measured using ImageJ software by measuring the average diameter of 20 randomly selected droplets at two different spin coating rates.

Table 4.1- A table of average diameter of LC droplets and the number of droplets at different concentrations for different spin coating rates of 500 and 2500 rpm.

LC concentration/ wt.%	500 rpm		2500 rpm	
	Average diameter/ µm	Number of droplets in 1 cm^3 of volume	Average diameter/ µm	Number of droplets in 1 cm^3 of volume
5	3 ± 0.22	2.9×10^9	2.5 ± 0.28	5.1×10^9
20	3.4 ± 0.29	8.3×10^9	2.9 ± 0.37	13.4×10^9
30	4.3 ± 0.33	6.3×10^9	3.8 ± 0.39	9.2×10^9

It is seen that at both spin coating speeds the liquid crystal droplet size was smaller and more uniformly distributed in the lower LC concentration films (Table 4.1). The number of droplets in 1 cm^3 volume increased from 5 wt.% to 20 wt.% and then decreased slightly from 20 wt.% to 30 wt.% at both spin coating speeds.

UV/vis spectroscopy was performed to measure the transmittance of the PDLC films at different concentrations. The measurement was taken in transmission (400− 700 nm) with non-polarised light at normal incidence.

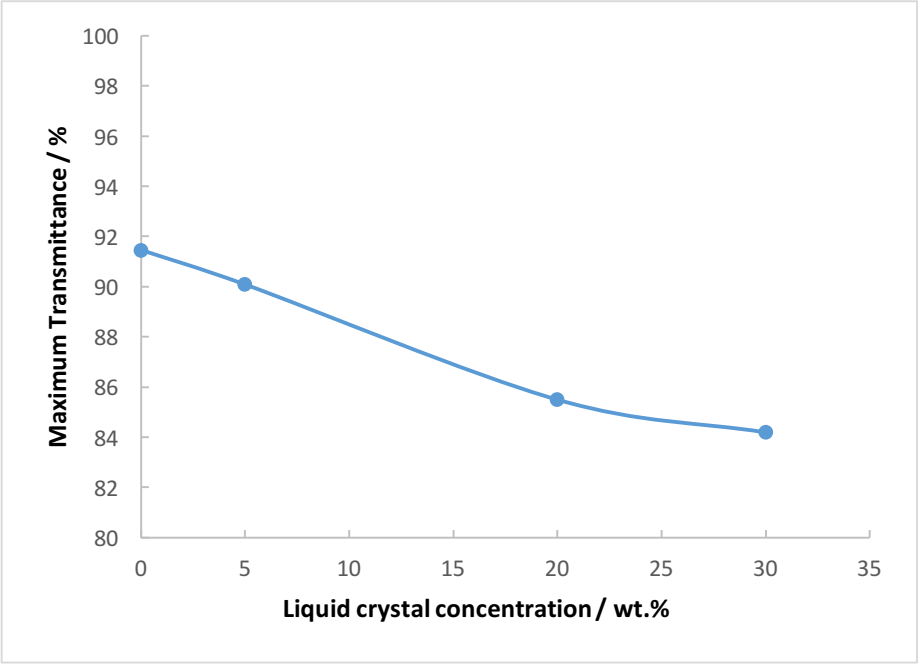

Figure 4.7- Transmission spectra of different LC concentrations at 550 nm wavelength.

As shown in Figure 4.7, the transmittance decreased with increasing LC concentration from 5 wt.% to 20 wt.%. Since the size of the LC droplets are one order of magnitude larger than the wavelength of the incident light, more forward scattering is observed which is known as the *Rayleigh-Debye scattering*, as there are larger number of droplets at 20 wt.% (Bleile, 1997). Also with larger number of droplets, there was a greater number of interfaces in a given volume which can produce a greater amount of light scattering resulting in the PDLC that was more opaque. However, at 30 wt.% the larger droplet size resulted in fewer droplets per unit volume (Table 4.1). Therefore, the resulting fewer interfaces made the transmission decrease only slightly from 20 wt.% to 30 wt.% (Figure 4.7).

4.3.3 Effect of chemistry on the LC alignment

To investigate the effect of LC chemistry on the LC alignment in the droplets, fluorinated liquid crystal monomers were used as fluoro substituent compounds are likely to be more stable for longer term applications when compared to the E7 compound owing to the increased strength of C-F bond in their structure (Broer et al., 1991). To produce a nematic phase at room temperature, a mixture of two different fluorinated LC monomers ST04229 (3,4,5-trifluoro-4`-(4-propyl-cyclohexyl)biphenyl) and ST04230 (3,4,5-trifluoro-4`-(4-pentyl-cyclohexyl)biphenyl) (SYNTHON Chemicals) was prepared in a 1:1 weight ratio (Figure 4.8). The same recipe was used to mix 20 wt.% fluorinated LC with silicone and the sample was left to cure at room temperature for 48 hours.

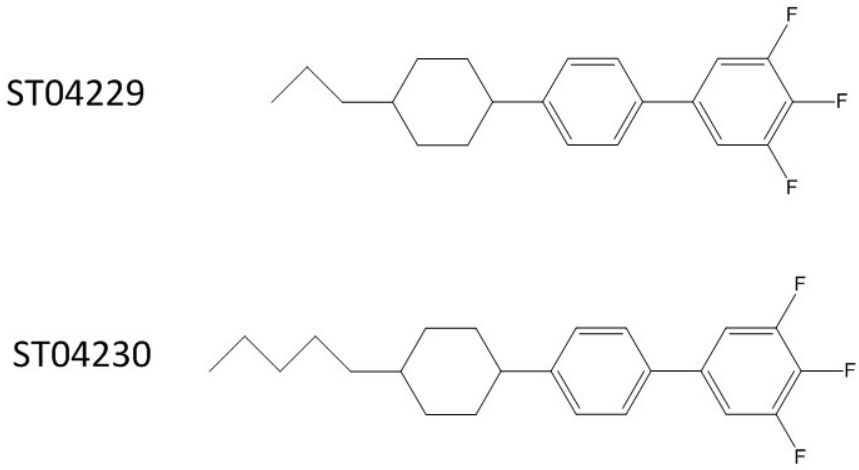

Figure 4.8- Molecular structure of the fluorinated monomers.

The configuration and size of the droplets were observed using a simple optical microscope in transmission with and without crossed polarisers.

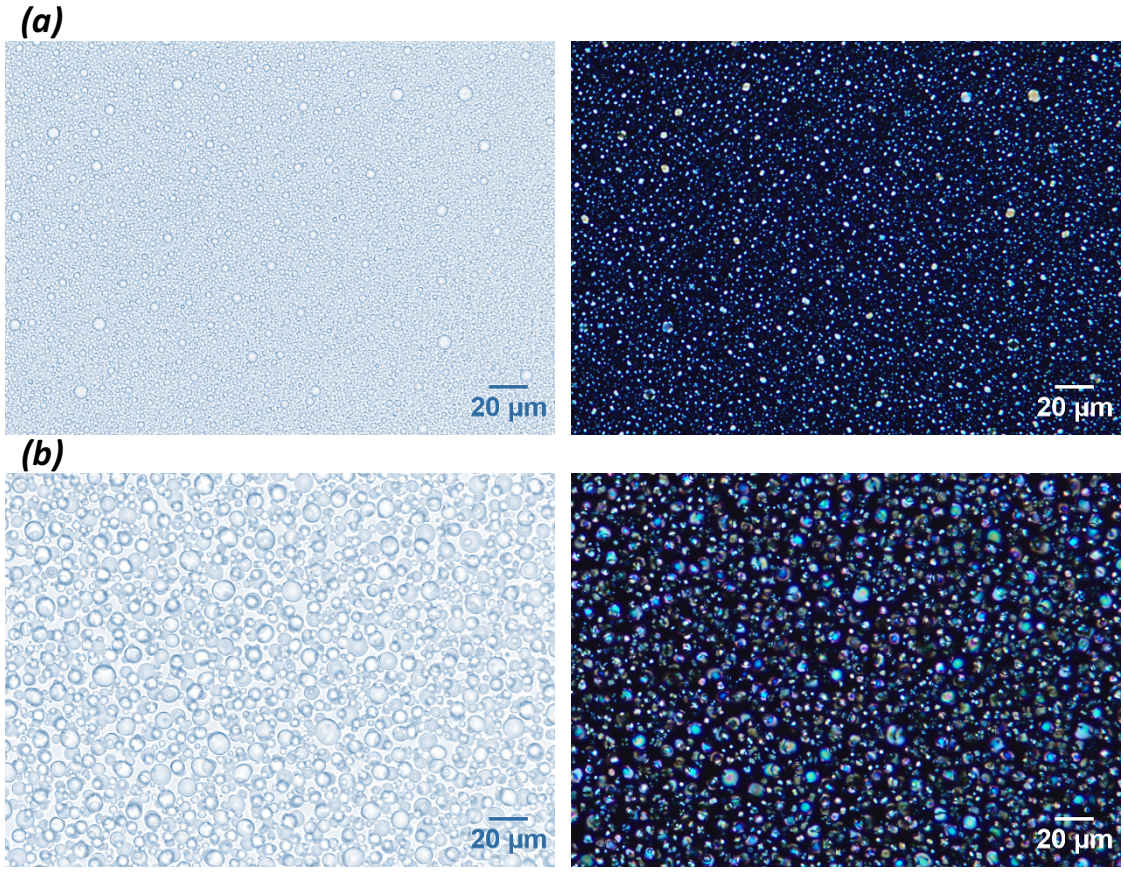

Figure 4.9- 20 wt.% fluorinated PDLC film spin coated at (a) 2500 rpm, (b) 500 rpm, shown in transmission using non-polarised light on the left and crossed polarised light on the right.

The dispersed LC droplets that were formed are clearly visible on the left hand side images of Figure 4.9. The images taken using the crossed polarised light highlight that the resulting LC bipolar axes in the droplets were randomly distributed in the polymer matrix. A close up view of this is shown in (Figure 4.10 a). The resulting image shows that a spherical bipolar configuration with parallel wall alignment was formed.

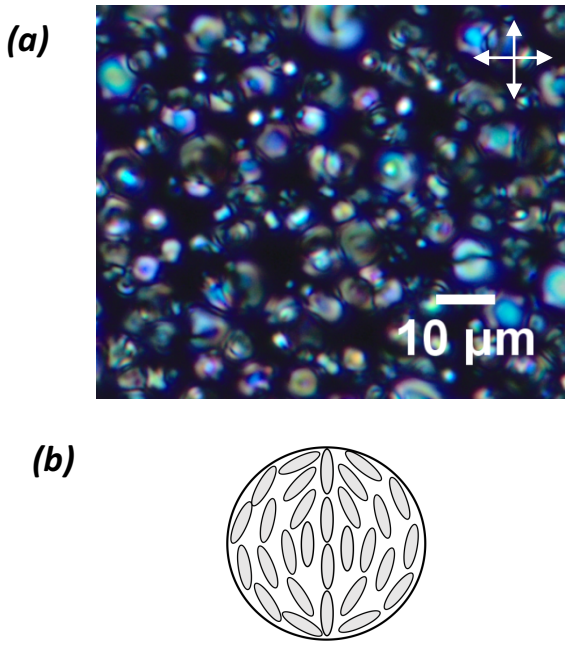

Figure 4.10- (a) close up image of the spherical LC droplets in the PDLC film at 20 wt.% concentration and spin coating rate of 500 rpm. The direction of the polariser and analyser is indicated by white arrows (b) schematic structure of bipolar director configuration.

Since fluorinated LC is hydrophobic, the molecules align on the surface of silicone and this results in the bipolar configuration of the droplets that is shown in Figure 4.10 b. Again the resulting droplet size was measured using ImageJ software to measure the average diameter of 20 random droplets.

Table 4.2- A table showing range of diameter and average diameter of fluorinated LC droplets at 20 wt.%.

500 rpm	2500 rpm
Average diameter/ µm	Average diameter/ µm
6.5 ± 0.46	3.1 ± 0.43

Clearly, the higher spin coating speed formed droplets that were smaller in size. There was a significant size distribution for both speeds. The size of fluorinated LC droplets in comparison to the E7 droplets were larger and less uniformly distributed at both spin coating speeds.

4.3.4 Effect of mechanical deformation on the LC alignment

For tensile measurement, both pure silicone and PDLC film made from E7 liquid crystal were drop cast on a glass petridish and left on a flat surface to cure for 48 hours and later were cut into dumbell shape. The Young's modulus of the free sanding PDLC film was calculated from the linear region of the stress-strain curve (Table 4.3) and was compared to similar free standing silicone rubber film.

Table 4.3- A table showing Young's modulus values of silicone and PDLC films.

Sample	Young's modulus upto 10% strain / MPa	Strain to break (%)
Silicone	0.99-1.00	250
PDLC (E7)	0.21-0.24	270

As shown in Table 4.3, the Young's modulus of the PDLC film was significantly lower than the silicone rubber with slightly higher elongation to break. It is obvious that the LC phase separated droplets in the elastomer results in a large reduction in the resulting modulus of the resulting film. E7 is a nematic liquid crystal that acts as a Newtonian fluid.

Consequently, the Young's modulus of E7 is essentially zero and the decrease in the PDLC modulus can perhaps completely be explained by this. Also the presence of additional reactions can affect the crosslinking of the PDLC film that may result in a drop in modulus of the PDLC film compared to silicone. To see if the rubber phase of the PDLC film was being altered by the incorporation of the E7 liquid crystal phase additional DSC measurements were performed on pure silicone film and PDLC film in order to measure the glass transition temperature of the rubber phase. The results are shown in Table 4.4.

Table 4.4- A table showing glass transition temperature of silicone and PDLC films.

Sample	Glass transition temperature (Tg) / °C
Silicone	-43.4
PDLC (E7)	-45.1

The glass transition of the PDLC film is slightly lower than pure silicone film by around 1.7 °C. From the results in Table 4.3 and Table 4.4 it can also be presumed that either a small amount of xylene remained in solution in the PDLC film during testing or to a small extent some of the E7 remains soluble in the silicone rubber. Either of these options would result in a plasticising effect on the rubber, reducing slightly both the glass transition temperature and the modulus of the rubber phase when tested at room temperature. The effect of a plasticiser being to increase the chain mobility and reduce the intermolecular forces along the polymer chains.

To investigate the effect of polymer chain alignment on the liquid crystal structure and droplet shape anisotropy, both pure silicone and the PDLC films were uniaxially stretched and were observed under an optical microscope in a conventional transmission mode and again using crossed polarising light.

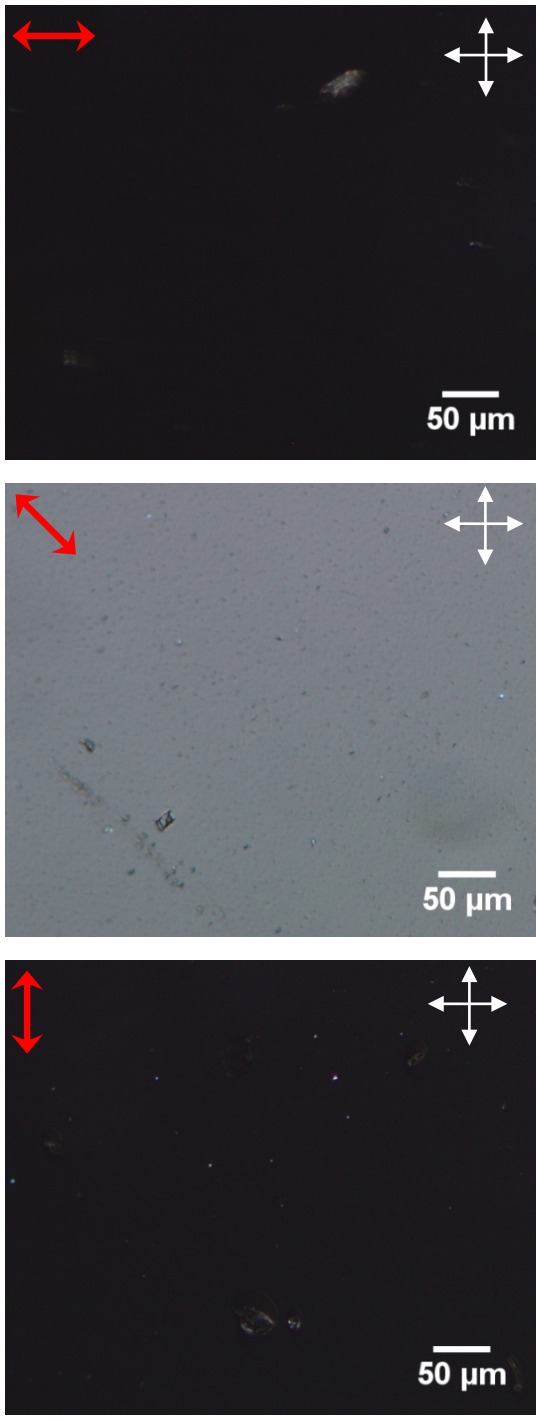

Figure 4.11- Cross polariser transmission optical microscopy images of free standing silicone film produced through drop casting at 50% strain . The white arrows indicate the orientation of the optical axis for the polariser and analyser. The red arrow indicates the stretch direction of the film.

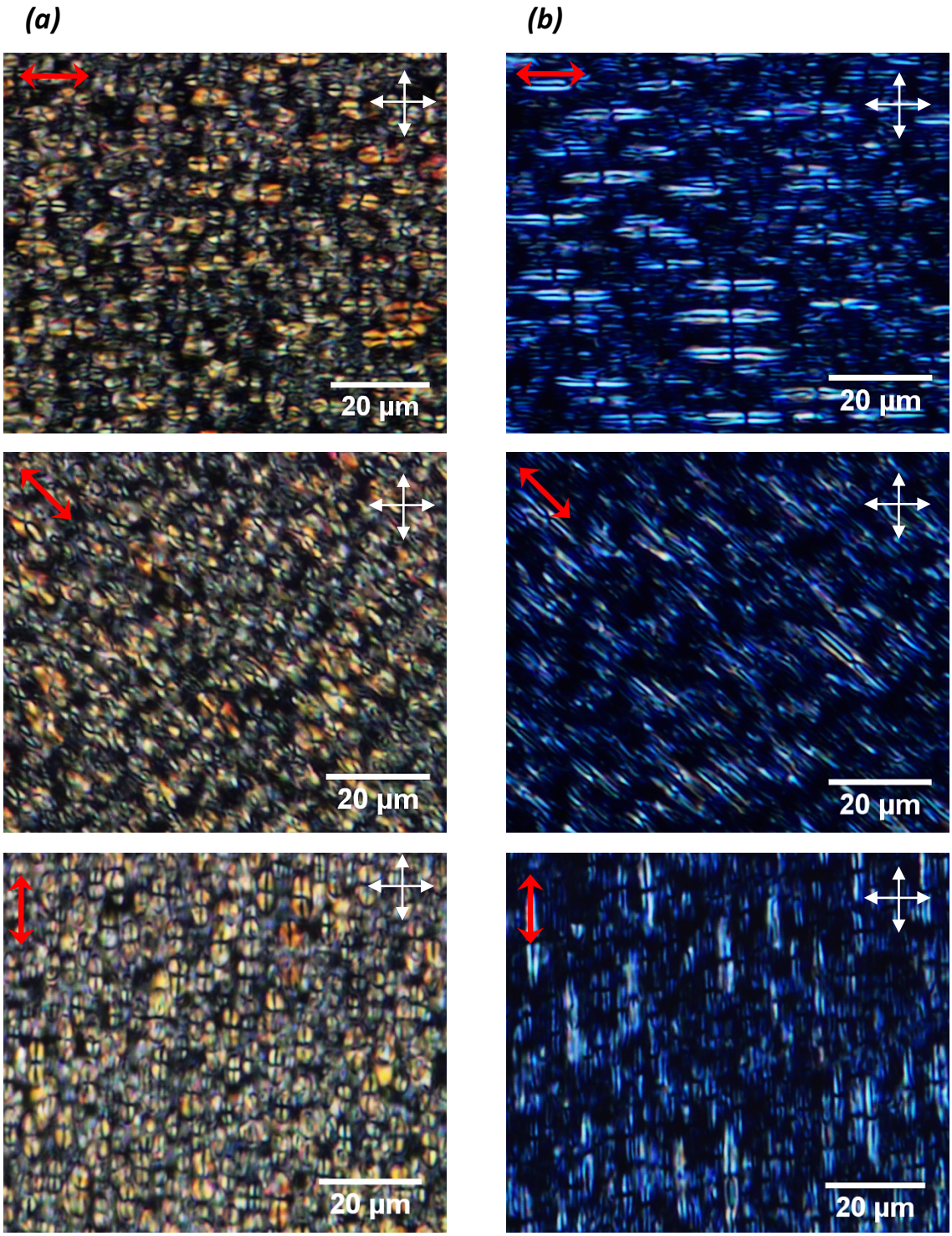

Figure 4.12- Cross polariser transmission optical microscopy images of free standing PDLC film at 20 wt.% concentration spin coated at 2500 rpm at (a) 50% strain, (b) 170% strain. The white arrows indicate the orientation of the optical axis for the polariser and analyser. The red arrow indicates the stretch direction of the film.

As shown in Figure 4.11, a pure silicone film became anisotropic at 50% strain and appeared bright at 45° to the analyser and the polariser. As mentioned in section 2.5.3, any isotropic material that is placed between crossed polarisers, will appear dark as no light transmits. However, with the applied mechanical strain to the elastomer, the polymer chains align in the direction of the mechanical stretch and become anisotropic. Therefore, when an anisotropic stretched elastomeric film is placed under crossed polarisers parallel to either the polariser or analyser axes, the film appears dark as no light transmits. However, when the stretched film is placed at 45° to the polariser and analyser axes, the film appears bright, showing the film has become birefringent.

The dispersed LC droplets in the PDLC film at 50% strain in Figure 4.12 a changed shape from spherical to elliptical with their long axes aligned in the direction of stretch. However, the LC molecules inside the droplets did not change their alignment in response to the applied uniaxial strain and hence the configuration of the LC droplets remained bipolar and produced the characteristic Maltese cross pattern. Surprisingly the silicone matrix also did not become anisotropic in the PDLC film at 50% strain unlike in the pure silicone film. Even when a greater strain of 170% was applied to the PDLC film, the alignment of the LC droplets and the polymer chains in the silicone matrix did not change (Figure 4.12 b). When the loading was released at both strains, the elliptical LC droplets reverted back to their initial spherical shape. Since the major contribution to the strain is from the LC droplets, it would appear that the polymer chains in the matrix did not align themselves along the direction of the applied mechanical stretch, LC orientation within the droplets also did not change. The reasons for this effect are not clear and are not well understood from the literature.

Zou and Fang (2011) investigated adhesive PDLC films with low cohesive strength by solvent- and polymerisation-induced phase separation. A simple method was introduced

that allowed printing of a thin PDLC film into structural and oriented patterns on substrates, which can be used as a composite material for sensor applications. They used a two part silicone rubber which were diluted with toluene and liquid crystal 4-cyano-4'-n-pentyl-biphenyl (5CB). They also reported that the elliptical 5CB droplets remained in the radial configuration with the characteristic Maltese cross pattern when the free standing PDLC film was under a large 300% extension (Zou and Fang, 2011).

4.3.5 Effect of substrate on the LC alignment

In practice the free standing films that were produced so far were not robust enough to be used in any real colour changing application. Therefore, it was necessary to consider what sort of flexible substrate might be suitable for use in real devices. To examine this free standing PDLC films were placed on three different substrates glass, nylon 6 and acrylic elastomer. Observations of the free standing PDLC film on acrylic substrate under optical microscopy showed that the dispersed LC droplets were sensitive to the substrate in contact with the freestanding PDLC film. Both crossed polarised and non-polarised light were used to monitor any changes in the configuration and the persistence of the droplets over time when the PDLC film was placed on all three substrates.

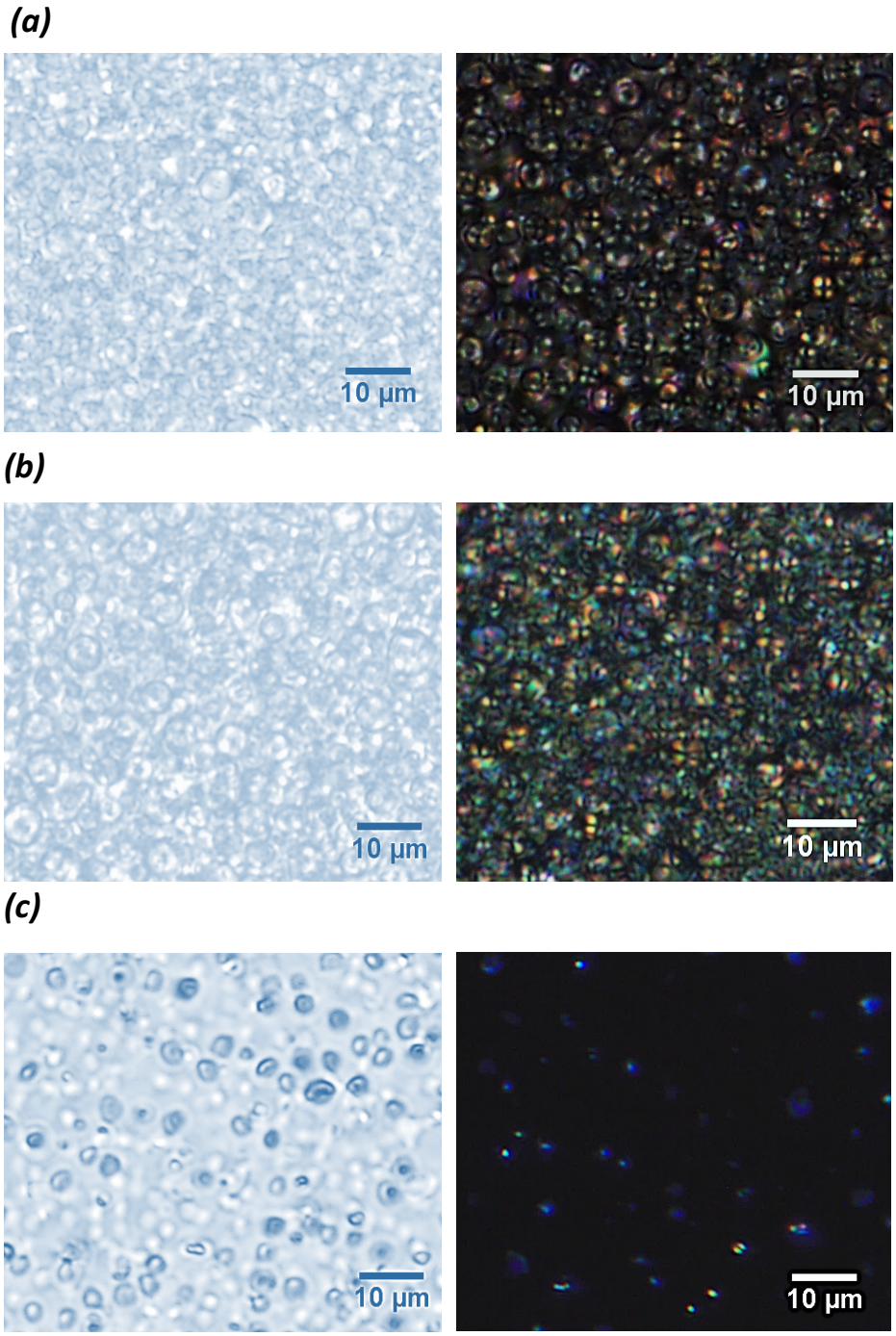

Figure 4.13- Free standing PDLC film spin coated at 500 rpm observed in transmission using non-polarised light on the left and cross polarised light on the right after 30 minutes on (a) glass substrate, (b) nylon 6 substrate and (c) acrylic rubber substrate.

Optical microscopy images showed no change in droplet configuration when PDLC film was placed onto either glass or nylon 6 substrates after 30 minutes being in contact (Figure 4.13 a and b). However as soon as the PDLC film was placed on the acrylic elastomer,

the droplets started to disappear as viewed under the crossed polarised light and after 30 minutes being in contact most of the droplets had disappeared showing little transmitted light through the cross polarised image of the PDLC film and PDLC film's morphology had significantly changed in the non-polarised light image (Figure 4.13 c). To further investigate the reason why the PDLC droplets were disappearing when positioned onto the acrylic substrate, the effect of a solvent on the PDLC film was monitored. A drop of xylene was placed on the PDLC film for 30 minutes. Then the surface was cleaned by tissue to ensure any remaining xylene was removed from the surface of the film. The film was observed under the optical microscope with and without crossed polarisers.

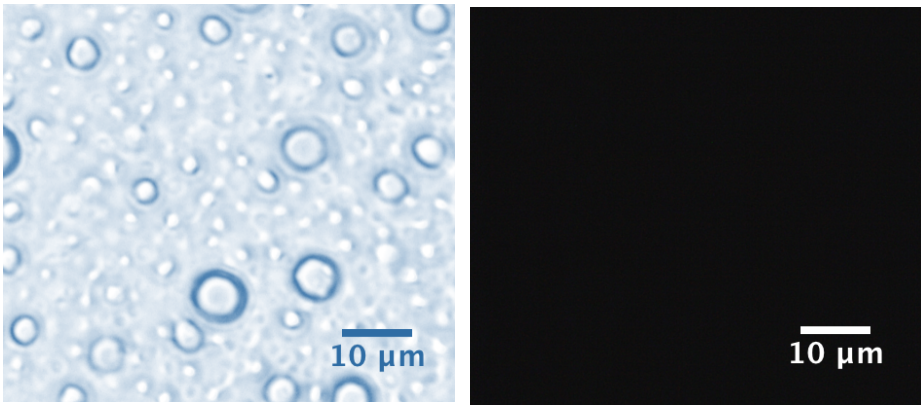

Figure 4.14- PDLC free standing film after 30 minutes being exposed to xylene.

After 30 minutes the PDLC film was exposed to xylene, the droplets under the crossed polarised light (on the right) disappeared and the morphology of the film under non-polarised light (on the left) changed (Figure 4.14). This shows that the xylene swelled into the PDLC film, causing the liquid crystals to change from nematic to isotropic phase and hence no light was observed at all directions under the crossed polarisers. This was similar to the behaviour to what was observed when the PDLC film was placed on acrylic substrate in Figure 4.13 c.

A DSC measurement was performed to determine the liquid crystal transition temperatures of PDLC film and PDLC film 30 minutes after being in contact with acrylic substrate.

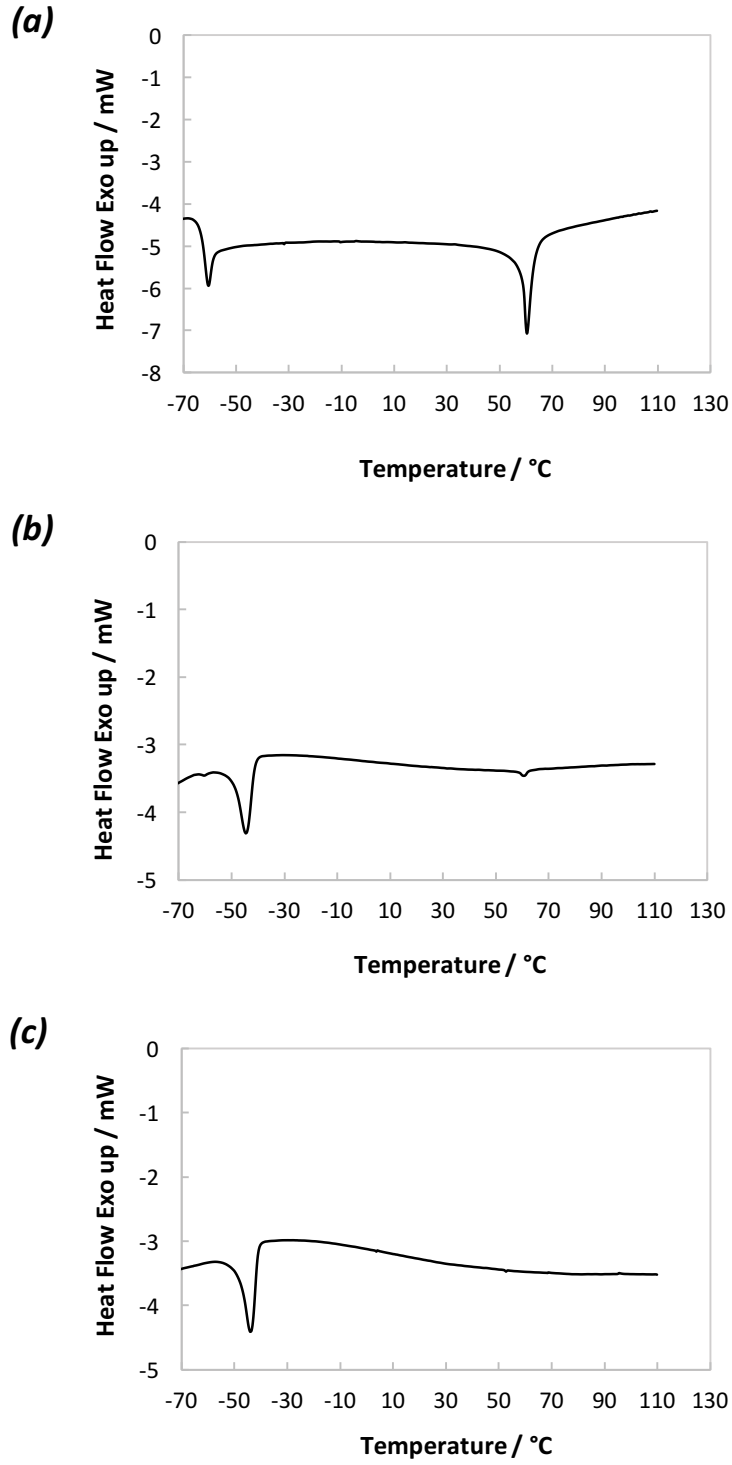

Figure 4.15- DSC thermogram of (a) E7, (b) PDLC film, (c) PDLC film 30 minutes after removed from acrylic substrate.

As shown in Figure 4.15 a, upon heating, E7 mixture shows nematic to isotropic transition at 60 °C. The DSC thermogram of PDLC film also shows a similar nematic to isotropic transition temperature (Figure 4.15 b) albeit of a much smaller magnitude. However, the PDLC film that was in contact with acrylic substrate shows no nematic to isotropic transition peak, which indicates that the PDLC droplets were now all in an isotropic phase. From the optical microscopy results in Figure 4.13 and Figure 4.14 and the DSC thermogram results in Figure 4.15, it was concluded that when the PDLC film was in contact with acrylic substrate the volatile compounds in the acrylic, required for its adhesive properties are likely to be affecting the LC state. It is suggested that these mobile molecules diffuse into the PDLC film inducing a nematic to isotropic transition of the LC molecules in the droplets, resulting in the loss of their orientational and positional order. Hence they are no longer birefringent and the droplets are not bright in any direction under the crossed polarised light. volatile compounds in VHB 4905, required for its adhesive properties, are likely to be affecting the LCs.

The change in the state of the droplets within the PDLC film with time was also visible by the eye, after the film was in contact with acrylic substrate for 30 minutes.

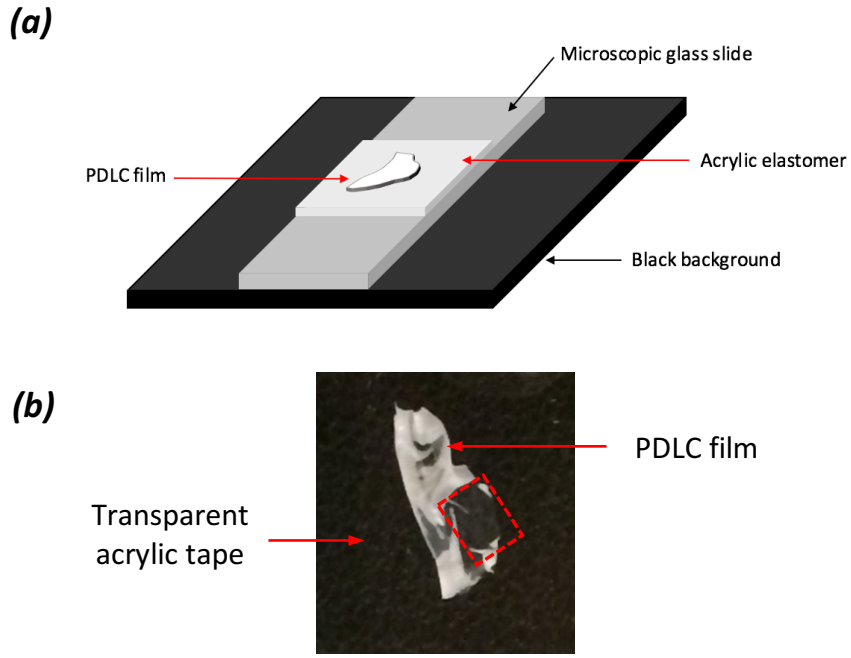

Figure 4.16- a) schematic representation of the PDLC film on acrylic substrate, b) top view image of the PDLC film on acrylic substrate on a black background after 30 minutes.

From Figure 4.16 b, the red dotted rectangle shows the contact area between the PDLC film and the acrylic elastomer. In this area the PDLC film becomes less opaque and scatters less light as a result of change in the state of the LC droplets from nematic to isotropic. Consequently, the isotropic LC droplets have refractive index that is closer to the refractive index of silicone and hence the film looks transparent. The rest of the film appears mostly opaque. Under closer examination this highlighted the regions where there was a lack of contact between the PDLC thin film and the acrylic rubber substrate.

After 30 minutes contact between the two films, the PDLC film was removed and was placed onto a glass substrate to see if the change in the state of LC droplets is reversible with time.

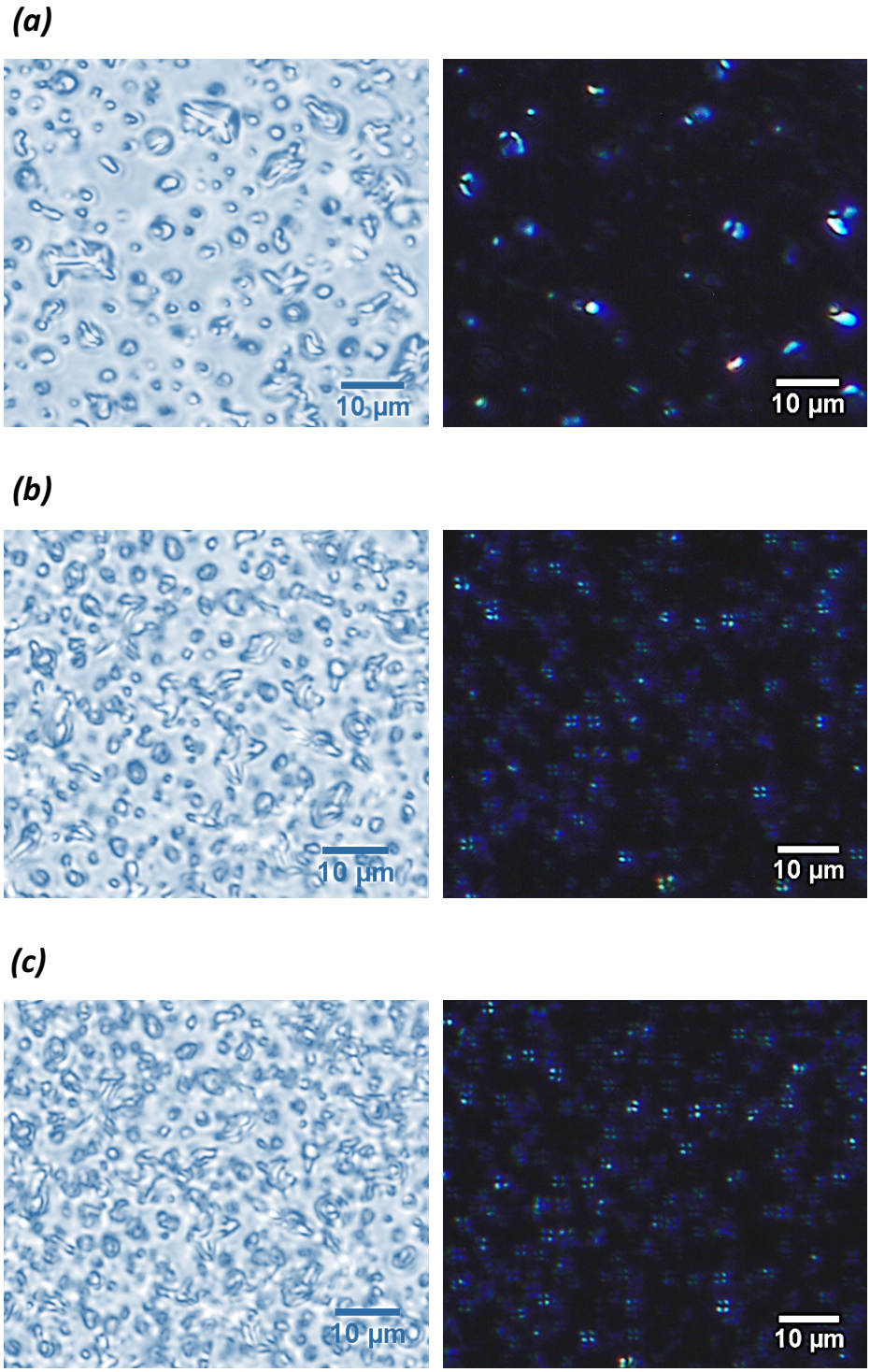

Figure 4.17- Free standing PDLC film spin coated at 500 rpm a) 30 minutes after removed from acrylic on glass substrate, b) 24 hours after removed from acrylic on glass substrate, (c) 72 hours after removed from acrylic on glass substrate.

In Figure 4.17 a, optical microscopy image of PDLC film under crossed polarised light looks brighter after 30 minutes being removed from the acrylic substrate compared to when the PDLC film was in contact with acrylic (Figure 4.13 c). Also there are a few droplets showing a bipolar configuration. After 24 hours and 72 hours there was even more light transmitting through the PDLC film and under crossed polarised light LC droplets show a return of the characteristic Maltese cross pattern (Figure 4.17 b and c). Thus over time droplets change from bipolar to radial configuration and it seems that some of the LC molecules inside the droplets go back to nematic state when PDLC film was removed from acrylic; assuming the molecules on the surface of acrylic that diffused into the PDLC film and resulted in the initial change in state of the LC droplets are diffusing out from the PDLC film and evaporating with time. Nevertheless, the state of LC molecules is not fully reversible to the initial nematic state.

UV/vis spectroscopy was also used to measure the change in transmission of the PDLC film before and after it was placed on the acrylic substrate and the results are shown in Table 4.5.

Table 4.5- Transmission measurement results at 550 nm wavelength.

Sample description	Transmission at 550 nm / %
PDLC	66.77
PDLC on acrylic after 30 mins	93.00
PDLC on glass 2 hours after removal	80.95

As shown in Table 4.5 the transmission spectra at 550 nm is increased by around 26% when the film was in contact with acrylic substrate for 30 minutes. This supports the conclusion drawn from the optical microscopy observations seen in Figure 4.13 c, that the state of liquid crystals has changed from a nematic to an isotropic state. This results in an increase in the transmission of the PDLC film as the refractive index of the LC molecules inside the droplets are closer to the refractive index of the silicone when they

are in isotropic state. To further investigate the reversibility of the state of the LC molecules inside the droplets, the PDLC film was removed from the acrylic substrate and was placed on a glass slide for 2 hours and then the transmission spectra of the film was measured. The transmittance of the PDLC film did recover somewhat to its initial state but not fully. Therefore, it can be concluded that the state of the LC molecules inside the droplets was not fully reversible to the initial nematic state after the film was removed from acrylic substrate.

4.4 Conclusion

In this chapter an approach to try and create a thin flexible film that contains phase separated micron sized LC droplets in a silicone elastomer is described. It was hoped that this film would change refractive index reversibly when subjected to a large deformation. A simple PDLC thin film was eventually created that contained liquid crystal droplets of the desired shape, polymer morphology and size. To create this system a wide range of processing parameters such as the ideal concentration for the various components and the solvents, were explored. The different spin coating speeds produced films with different liquid crystal droplet sizes and distributions. The presence of the LC droplets in the material also served to significantly reduce the transmittance of the PDLC film compared to the properties of the silicone rubber. The transmittance was decreased by increasing the LC concentration. From 5 wt.% to 20 wt.% the decrease in transmittance was found to be dominated by increase in the number of droplets in the film resulting in more light scattering as there are more interfaces at 20 wt.% LC concentration. However, at 30 wt.%, the larger size of the droplets resulted in fewer droplets inside the film and less interfaces. Therefore, the reduction in transmittance from 20 wt.% to 30 wt.% was not as significant. The alignment of the dispersed liquid crystal droplets was investigated using two chemically different liquid crystal molecules incorporated with a cured two part silicone

rubber. Different alignment configurations were found which was resulted from chemical nature of each of the LC molecules and their anchoring force against the wall surface of the droplets. It was found that the PDLC film has a much lower Young's modulus and a slightly lower glass transition temperature value when compared to the pure silicone elastomer. Since E7 is a nematic liquid crystal that acts as a Newtonian fluid, its Young's modulus is essentially zero. Thus this large reduction in the Young's modulus of the PDLC film was explained by this. Also it is presumed that either residual xylene or a small amount of LC molecules within the elastomer phase act as a plasticiser, reducing slightly the Tg and modulus of the rubber phase.

The effect of a mechanical deformation on the alignment of the molecules inside the droplets was examined. Intriguingly, the silicone matrix did not become significantly anisotropic along the direction of the applied deformation and this rather disappointingly resulted in no change in the director configuration of the liquid crystal dispersed droplets. However, the shape of the droplets changed from spherical to elliptical with the applied deformation and upon unloading their spherical shape was restored.

The state of the molecules inside the droplets was found to be influenced when the PDLC film was in contact with a soft substrate such as commercial acrylic materials that is commonly used in dielectrically actuated elastomer systems. From the results it is concluded that the volatile compounds in the acrylic, required for its adhesive properties diffused into the PDLC film causing it to change the state of the LC molecules inside the droplets from a nematic to an isotropic phase. This resulted in the PDLC film becoming transparent as the refractive index of the isotropic LC molecules inside the droplets was closer to the refractive index of the silicone matrix and hence less light was scattered. Due to these complications it was decided to attempt to create a colour changing elastomer

film using an alternative approach and the idea of using a phase separated PDLC film was abandoned for the rest of this thesis.

Chapter 5: Reflective Dielectric Elastomers Adopting Cholesteric Liquid Crystal Coatings

5.1 Introduction

Current significant research effort is being dedicated towards mimicking the structural colour often found in nature. The aim being to replace the conventional methods of producing colour using dyes and pigments. These conventional methods are based on absorption or scattering of visible light. The adoption of structural colour is taking off in a wide variety of applications related to vision (Kinoshita and Yoshioka, 2005, Mitov, 2012). Cholesteric Liquid Crystals (CLCs) have attracted a significant interest amongst scientists since they can produce very bright and intense colours due to their ability to selectively reflect light of specific wavelengths as a consequence of the pitch of their

helical structure (Mitov, 2012, Collings, 1990). CLC coatings are being developed for use in the field of textiles for both fashion and sensing applications (Picot et al., 2013b, Mulder et al., 2014). Picot et al. (2013a) demonstrated an optical strain sensor consisting of a crosslinked cholesteric liquid crystal layer spray coated on a uniaxially oriented polyamide 6 substrate. By applying uniaxial extension to the substrate a 40 nm shift in the reflection band at 13% strain was observed. The change in the reflection band was attributed to the decrease in the pitch length of the cholesteric helix due to change in the thickness of the CLC layer. The colour response from orange to green was found to be entirely dependent on the mechanical behaviour of the polymer substrate. Upon unloading the colour shift was reversed and a residual shift of 3 nm in the wavelength was related to the residual plastic strain in the substrate (Picot et al., 2013a).

This chapter explores the potential of applying a CLC coatings onto an elastomeric substrate using spray deposition technique. The aim being to make a large strain reversible colour changing device or sensor. To achieve a cholesteric structure, diacrylate monomers and a reactive chiral dopant are used in the monomer mixture. Commercially available double sided VHB acrylic tape was used as the elastomeric substrate and polyvinylalcohol (PVA) aligned substrate is used as a reference substrate. In this study the reference substrate is used because the alignment of the LC molecules on this substrate is well understood and therefore this can be used to find how well liquid crystals align themselves on an elastomeric substrate. The alignment and structure of the CLC coating is characterised and the optical properties of the coating is evaluated.

5.2 Experimental

5.2.1 Materials

Cholesteric mixture was prepared using diacrylate liquid crystalline monomers RM 257 (C3M) and RM 82 (C6M) (Merck), which were mixed in a 1:4 weight ratio. 4.8 wt.% Palicolor LC756 (BASF) was used as the chiral dopant to obtain an orange reflection. 1 wt.% hydroxycyclohexyl-phenylketone, 99% (Sigma Aldrich) was used as the phonotinitiator in the mixture. The monomers and the phonoinitiator were dissolved in p-xylene (Sigma Aldrich) (1:2.5 solute to solvent ratio) in a UV protected bottle to ensure thorough mixing. The solution was stirred on a hot plate at 80 °C for 15 minutes until it was completely transparent. This ensures that the material is in an isotropic phase.

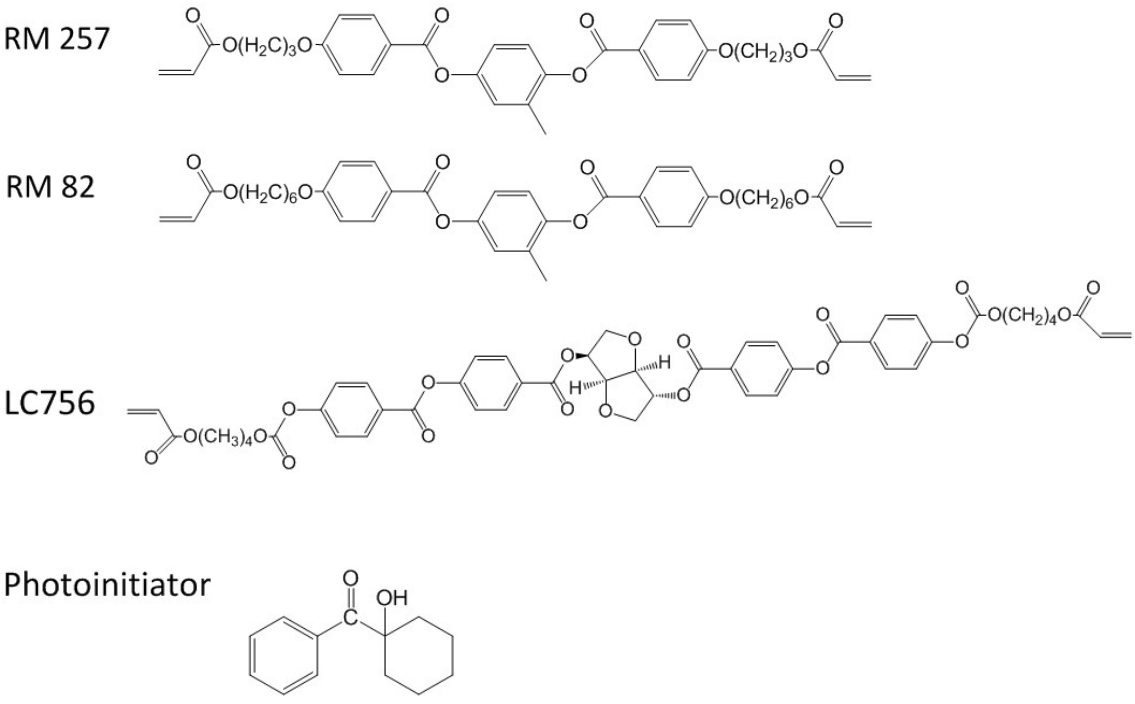

Figure 5.1- Molecular structure of the monomers and the photoinitiator.

The elastomeric membrane was commercially available acrylic elastomer double-sided tape (VHB 4910 3M) with an unstrained initial thickness of approximately 1mm.

For the reference substrate, 5 wt.% polyvinylalcohol (PVA) was dissolved in de-ionised (DI) water under vigorous stirring at 90 °C. PVA used has molecular weight Mw= 85,000-124,000 99+% hydrolysed (Sigma Aldrich). PVA solution was then spin coated (SCS spin coat G3P-8) on a microscopic glass slide at 1000 rpm for 30 seconds and was cured in an oven at 80 °C for 30 minutes.

5.2.2 CLC coating sprayed on acrylic and PVA substrates

Acrylic elastomer and PVA substrates were surface treated by rubbing their surface ten times along a velvet cloth smoothly in one direction prior to the application of the CLC coating to achieve planar alignment of CLC molecules.

The CLC coating was applied through spray coating of CLC monomer mixture on the substrates. The spray gun used was an Iwata- HP-CP, and the air compressor was an Iwata smart jet pro. The spraying pressure used for this experiment was around 280 kPa. The spray nozzle on the spray gun was 3 (medium opening) and the spraying distance was approximately 10 cm. The substrates were put in an oven for 30 seconds every 3-4 layers of spraying to ensure the solvent was evaporated completely and then cooled to room temperature. The CLC coating was photopolymerised using a mercury lamp (EXFO Omnicure S2000 λ= 350-450 nm) under nitrogen at room temperature for 200 seconds.

5.2.3 CLC coating transfer print on acrylic elastomer

CLC coating was prepared by spraying 7 layers of CLC solution on PVA aligned substrates and the sample was photopolymerised using UV exposure for 200 seconds. The PVA layer was used as sacrificial layer, which was then dissolved by putting the

samples in DI water for few days. The free standing CLC films were then transfer printed on acrylic elastomer Figure 5.6.

5.2.4 Characterisation

Ultraviolet-visible (UV/Vis) spectroscopy was used to check the optical properties of the samples. The measurements were taken in transmission mode using Perkin Elmer Lambda 950 UV/Vis spectrometer, integrating sphere. The wavelength being measured was set to 400-700 nm. Optical images were taken using Olympus BX60 microscope. Scanning Electron Microscopy (SEM) images were taken using a FEI Inspect with secondary electron detector. Photographs of the samples were taken using a digital camera.

5.3 Results and Discussion

5.3.1 CLC coating sprayed on acrylic and PVA substrates

CLC spray coated on acrylic substrate resulted in some de-wetting effect, which was then solved by plasma treating the surface prior to the spray coating. The surface of the elastomer was treated by oxygen plasma using Corona Treater BD-20 High Frequency Generators that provide a high voltage, high frequency spark at the tip of an electrode.

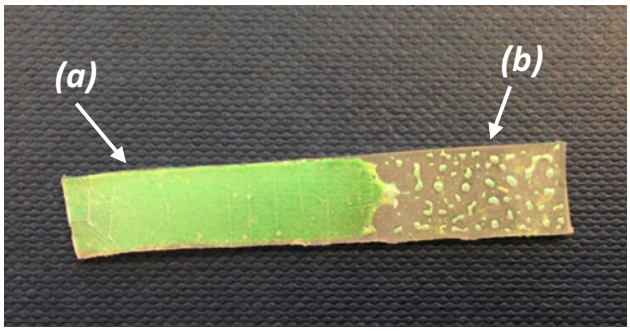

Figure 5.2- Image of acrylic elastomer spray coated with CLC solution (7 layers), (a) Plasma treated area showing good wettability, (b) area without plasma treatment showing de-wetting effect.

As it shows in Figure 5.2 a, plasma treated area, which showed good wettability, displayed a green visible reflection band instead of the anticipated orange reflection band. Spray coating onto the PVA, which was the reference substrate showed good wettability and displayed orange reflection band (Figure 5.3).

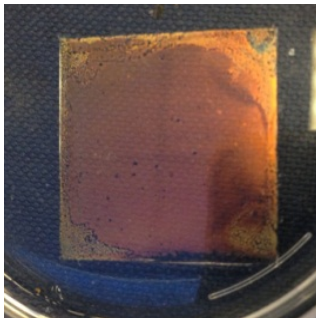

Figure 5.3- Image of PVA substrate spray coated with CLC solution (7 layers).

Optical microscopy images of both substrates in reflection mode without polarisers were taken.

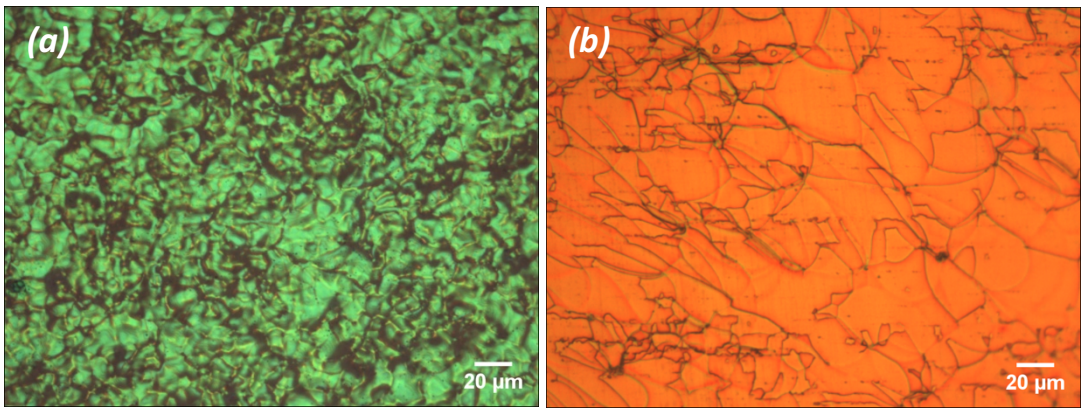

Figure 5.4- Optical microscopy image of (a) acrylic elastomer and (b) PVA substrate spray coated with CLC solution in reflection mode without polariser.

Examination of each of the coatings showed there was a lack of planar alignment of CLC molecules on the acrylic substrate producing an unexpected green reflection band (Figure 5.4 a). However, the PVA substrate showed the characteristic oily streak morphology, typical of a planar CLC alignment with the anticipated orange reflection band (Figure 5.4 b).

UV/vis spectroscopy was performed to measure reflective properties of both substrates. The measurements were taken in transmission (400− 700 nm) with non-polarised light at normal incidence.

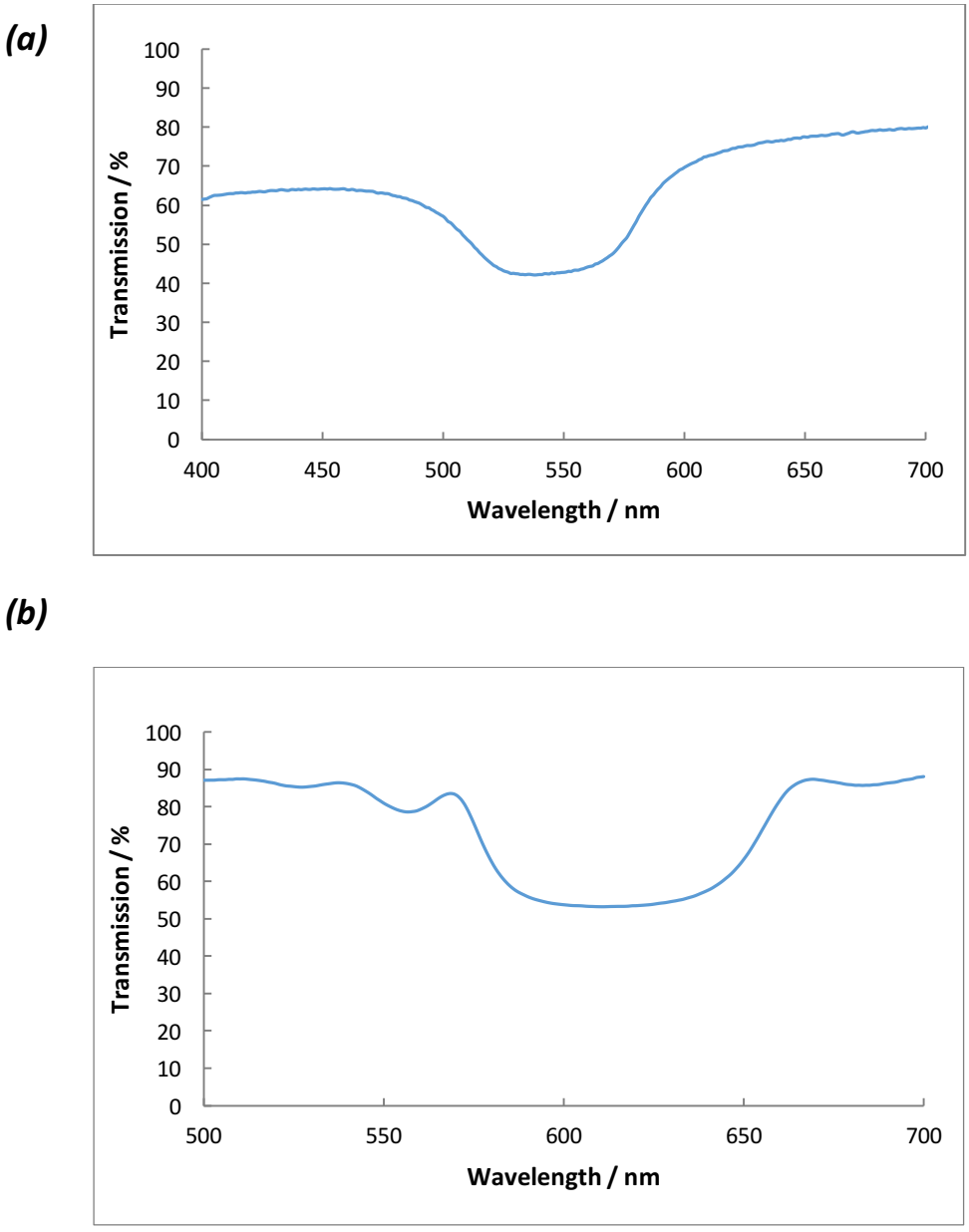

Figure 5.5- Transmission spectra of (a) acrylic and (b) PVA substrates with CLC coating for non-polarised light.

From the spectrum shown in Figure 5.5 a, CLC coated acrylic showed reflectivity of around 35% with central reflection band at λ_0 = 542 nm (green) and a width $\Delta\lambda$ = 67 nm. Comparing this with the spectra in Figure 5.5 b, CLC coated PVA substrate shows a reflection band of around 35% with central reflection band at λ_0= 615 nm (orange) and a width $\Delta\lambda$ = 79 nm with a higher baseline. The green reflection band shown by the acrylic substrate might be related to xylene, which is a volatile organic solvent that is dissolving/swelling the acrylic elastomer and hence causing the small liquid crystal molecules (RM 257) to diffuse into acrylic during spray deposition before the curing process. This causes the concentration of chiral dopant to increase in the mixture and this results in the reflected wavelength being at lower part of the visible spectrum.

5.3.2 CLC coating transfer print on acrylic elastomer

PVA substrate with CLC coating of 7 layers that was placed in water for several days for the PVA layer (sacrificial layer) to be dissolved completely. After the PVA was dissolved completely, it was very difficult to remove the coating from the glass slide since the coating was too thin. Consequently, a transfer print technique was used to adhere the CLC coating to the acrylic elastomer. The backing paper of acrylic elastomer was removed from one side and the sticky side of the tape was placed on the CLC coating and was pressed firmly by fingers to ensure adhesion between the two layers (Figure 5.6 a). Then

the tape was removed in one direction which automatically peeled off the CLC film from the glass slide (Figure 5.6 b).

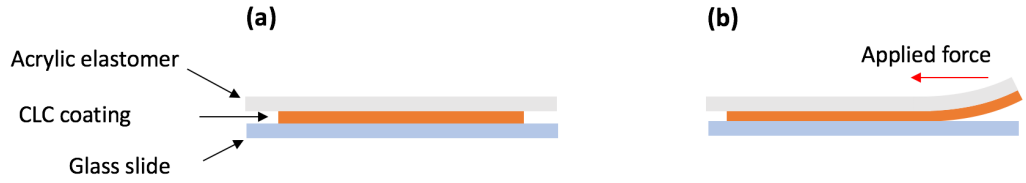

Figure 5.6- Schematic representation of transfer print technique.

Transmission spectrum of the CLC coating transfer printed on acrylic was obtained for non-polarised light at normal incidence using UV/Vis spectroscopy.

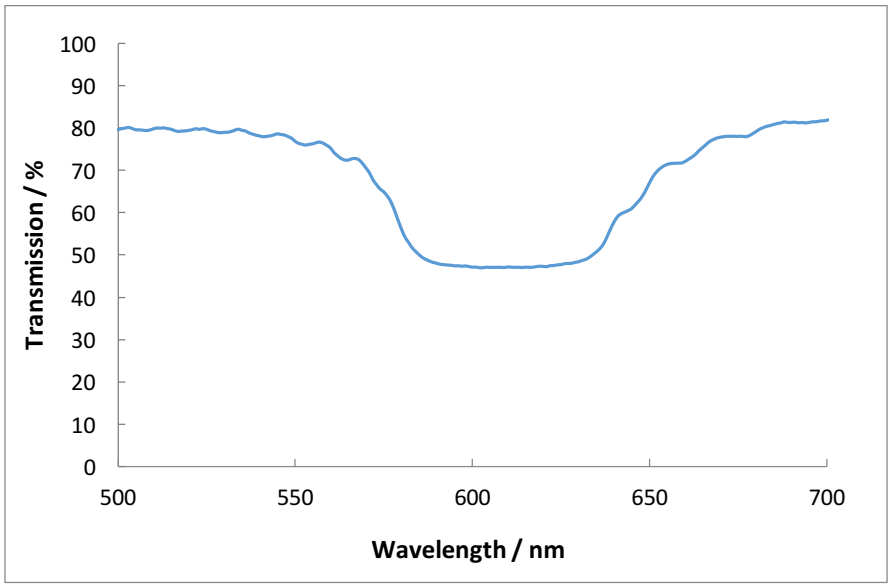

Figure 5.7- Transmission spectrum of CLC coating on acrylic elastomer.

As shown in Figure 5.7, reflectivity of around 35% with central reflection band being at λ_0= 612 nm (orange) nm and a width $\Delta\lambda$ = 72 nm was detected. The spectrum is very similar to the spectrum of the CLC coating on PVA substrate shown in Figure 5.5 b.

Scanning Electron Microscopy (SEM) was used in order to look at the cross-section of the free standing CLC coating. The film was snapped into small pieces and was placed between two conductive stands and gold coated and was observed under SEM.

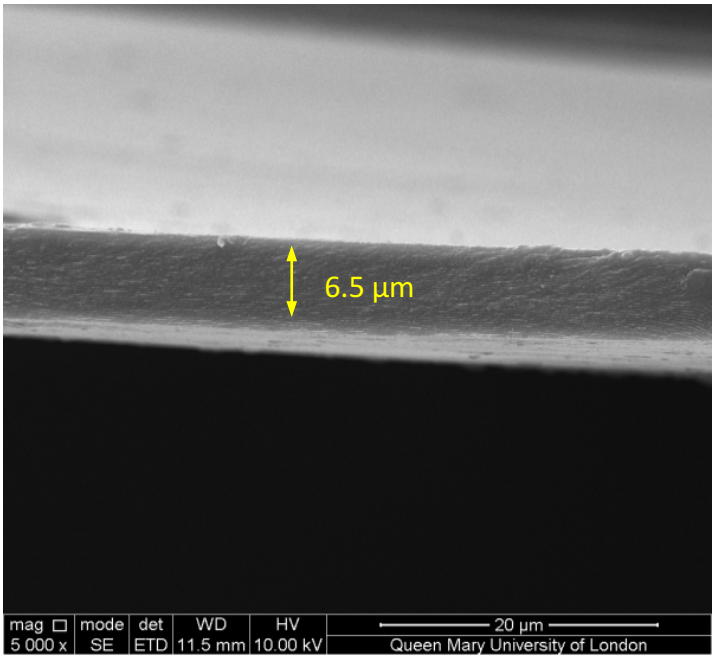

Figure 5.8- SEM image of the thickness of the CLC coating of 7 layers.

As it shows in Figure 5.8, the thickness of the film of 7 layers CLC is calculated to be approximately 6.5 µm at low magnification. An average of 5 readings was taken because the film was slightly curved.

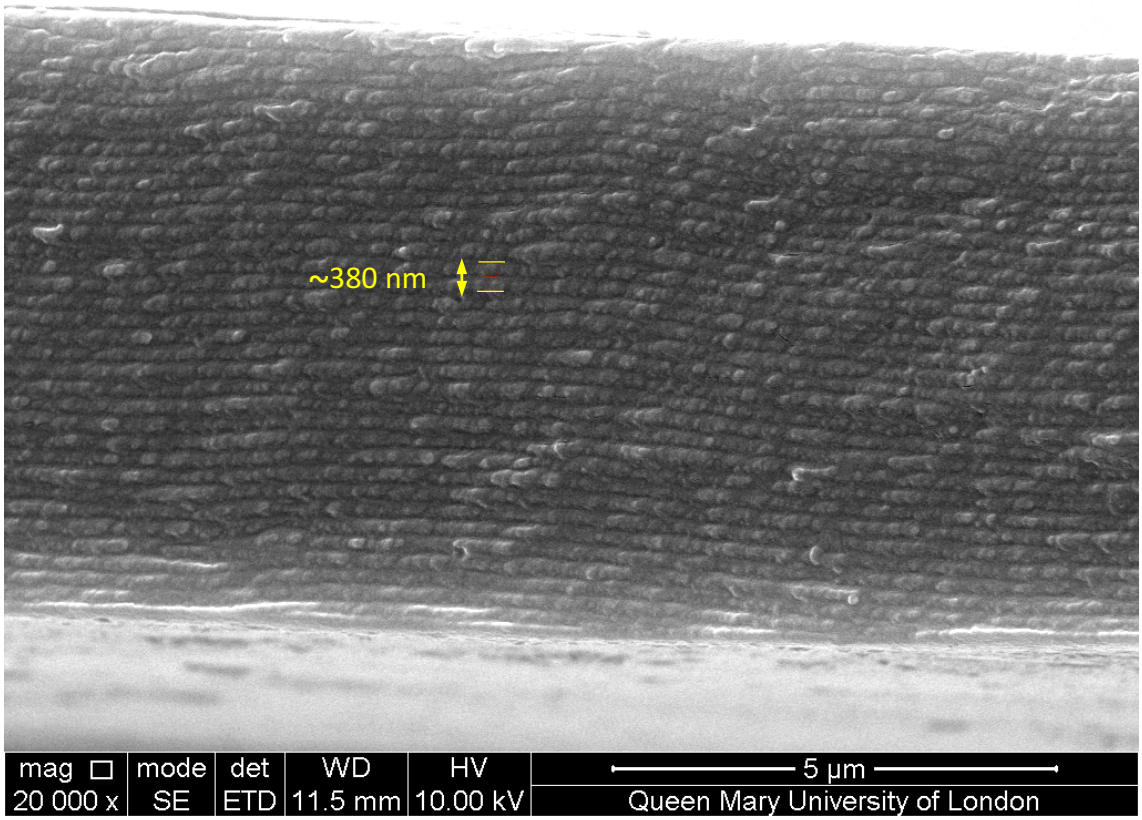

Figure 5.9- SEM image of CLC film, showing the alignment and helical structure of CLCs.

Figure 5.9, is the SEM image of 7 layers sample at high magnification, which reveals the CLC molecules have a planar orientation. The distance between two neighbouring dark stripes corresponds to layers thickness p/2 (the distance from a yellow line to the red line). The distance between the two yellow lines represents 1 pitch, measured to be around 380 nm. Knowing the thickness of the film, the number of pitch calculated is 17, which can also be found by just counting the number of layers from the SEM image. Using equation ($\lambda_0 = n.p$), knowing the pitch and average refractive index of the liquid crystalline polymer (1.6), the calculated central wavelength is approximately 608 nm. This values is very close to the value λ_0= 615 nm that was calculated from the transmission curve in Figure 5.5b. The error (~1%) could be related to the pitch length measured from the SEM image.

An initial observation of a shift in the reflection band of the sample was done under a manually applied uniaxially strain as shown in Figure 5.10.

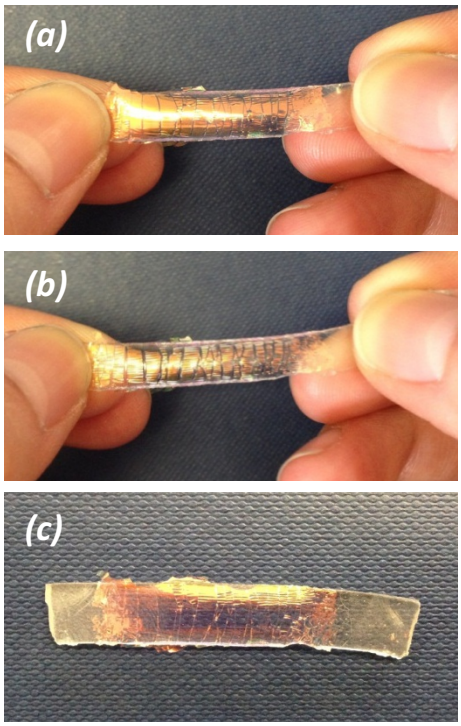

Figure 5.10- Images of CLC coating transfer print on acrylic elastomer, (a) & (b) under uniaxial strain, (c) released state.

As is shown in Figure 5.10 a and b, when a modest (greater than 10%) uniaxial strain is applied then cracks form on the CLC coating. The cracks remain even after the film is released as shown in Figure 5.10 c. The presence of cracks could be due to the mismatch of the modulus of CLC coating and the acrylic elastomer or could be that the uniaxial strain exceeded the strain limit of the CLC coating.

5.4 Conclusion

A mixture of monomer was spray coated on PVA and acrylic aligned substrates followed by photopolymerisation. A planar alignment was obtained for PVA substrate and the visible reflected light was cantered in the orange region of the visible spectrum. The acrylic substrate showed no planar alignment. Potentially this was due to the swelling of

the elastomer with the xylene and hence this caused the small molecules in the mixture to diffuse into the elastomer before curing and this changed the concentration of the chiral dopant in the CLC mixture.

Free standing CLC film was transfer print on acrylic substrate which showed similar optical properties as the PVA substrate. The substrate was stretched uniaxially which caused the CLC layer to crack either because of the mismatch of modulus of the two layers or that the strain exceeded the strain limit of the CLC layer.

Chapter 6: Liquid Crystal Elastomers

6.1 Introduction

Liquid Crystal Elastomers (LCEs) known as artificial muscles were first proposed by de Genne (de Gennes, 1997) and have been the subject of several publications and review articles (Xie and Zhang, 2005, Kupfer and Finkelmann, 1991, Davis, 1993, Ohm et al., 2010). LCEs are crosslinked liquid crystal polymers that combine the orientational order in the liquid crystals with the shape changing properties of polymer networks (Warner and Terentjev, 2003, Ohm et al., 2010, Li and Keller, 2006).

Liquid Single Crystal Elastomers (LSCEs) are monodomain structures where the optical axis of the polymer molecule is macroscopically and uniformly aligned making them very

promising for use in the application of colour changing large strain capable materials (Finkelmann et al., 2001, Kupfer and Finkelmann, 1991, Xie and Zhang, 2005).

LCEs have also been studied in the field of actuators and sensors due to their shape changing properties (Ohm et al., 2010).

This chapter demonstrates lightly crosslinked networks that when supported on a substrate can be stretched and hence demonstrate a reversible colour change with the applied strain. A mixture of two types of monomers (Diacrylates and Monoacrylate) are used in which the mechanical properties of the anisotropic network can be tailored by altering the ratio of the two molecules in the monomer mixture. In the mixture diacrylate molecules act as crosslinkers, binding together the long polymer chains formed by the monoacrylates (Elias et al., 2006). To achieve a cholesteric structure in which the director rotates around an axis throughout a sample, a reactive chiral dopant is added to the monomer mixture. To allow polymerisation of the LC films at room temperature, a nematic mixture was also added to broaden the temperature range of the nematic phase (Sawa et al., 2011).

LC mixture was characterised using Differential Scanning Calorimetry (DSC), which helped indicating the transition temperatures of the mixtures together with optical microscopy and thermal analysis using a heating stage. UV/Vis spectroscopy was used to measure the optical response of the various LCE materials developed under the application of a uniaxial strain.

6.2 Experimental

6.2.1 Materials

For the cholesteric mixtures monoacrylate liquid crystalline monomer RM105 (Merck) and diacrylate liquid crystalline monomers RM82 (Merck) and Palicolor LC756 (BASF)

were used. Commercially available nematic liquid crystal E7 (SYNTHON Chemicals) was used as the nematic mixture which is made of four different components: 51% 4-cyano-4'-n-pentyl-biphenyl (5CB), 25% 4-cyano-4'-n-heptyl-biphenyl (7CB), 16% 4-cyano-4'-n-oxyoctyl-biphenyl (8OCB), 8% 4-cyano-4"-n-pentyl-p-terphenyl (5CT). Hydroxycyclohexyl-phenylketone, 99% (Sigma Aldrich) was used as the phonotinitiator. P-xylene anhydrous, ⩾99% (Sigma Aldrich) was used as the solvent to mix the monomers and the photoinitiator. The elastomeric membrane used as a substrate was a commercially available acrylic elastomer double-sided tape (VHB 4905 3M) with a thickness of 0.5 mm.

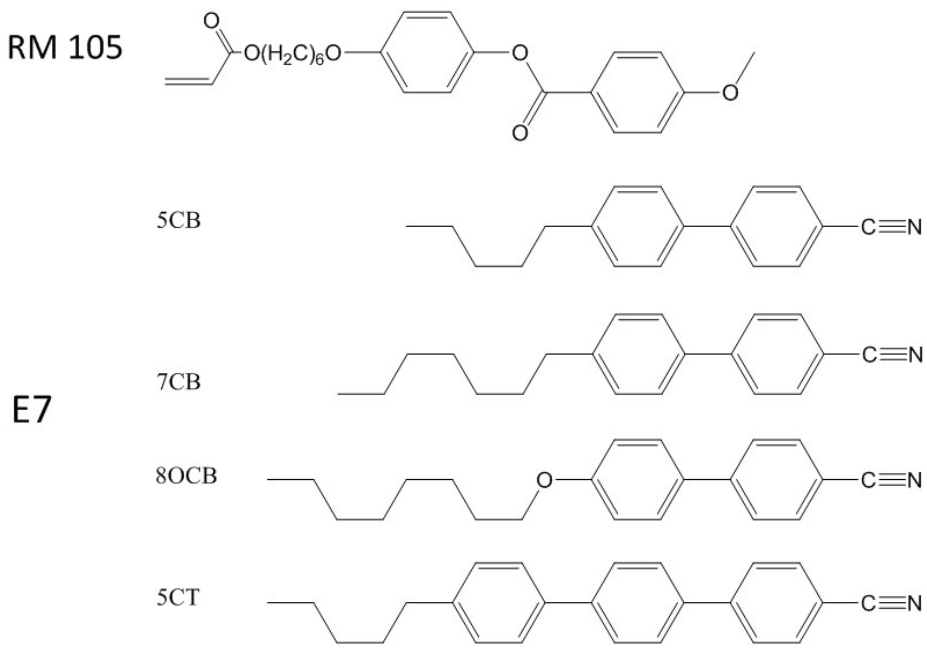

Figure 6.1- Chemical structure of RM105 monomer and E7 mixture.

Mixture 1

To achieve a cholesteric structure RM105 liquid crystalline monomer was mixed with 5 wt.% LC756 by placing the mixture on a hot plate at 90 °C (isotropic phase) under vigorous stirring for 2 hours.

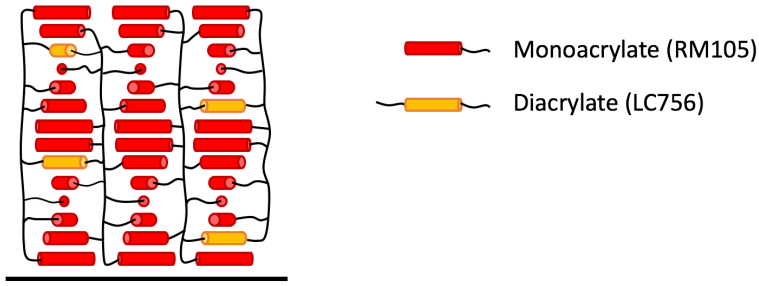

Figure 6.2- Schematic representation of CLC film made from mixture 1.

Mixture 2

RM105 liquid crystalline monomer was mixed with nematic mixture E7 in a 5:4 weight ratio. Cholesteric structure was achieved by adding 5 wt.% LC756 to the mixture. The mixture was placed on a hot plate at 90 °C (isotropic phase) under vigorous stirring for 2 hours.

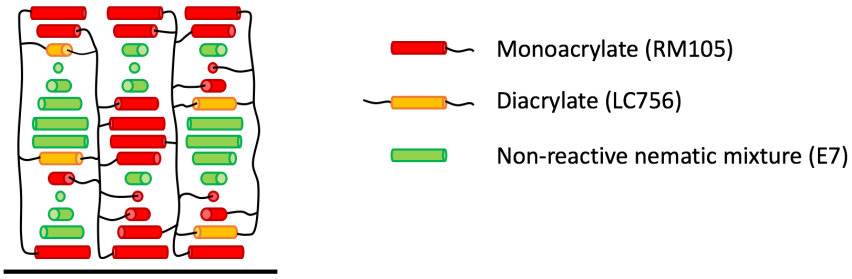

Figure 6.3- Schematic representation of CLC film made from mixture 2.

Mixture 3

Monoacrylate liquid crystalline monomer RM105 was mixed with nematic mixture E7 in a 5:4 weight ratio. Diacrylate monomers LC756 and RM 82 with concentrations of 5 wt.% and 2.5 wt.% were added into the mixture respectively. The concentration of RM82 depended upon the concentration of chiral dopant and should add up to 7.5 wt.% of diacrylate monomers in total in order to get sufficient crosslinking into the polymer

network. The mixture was placed on a hot plate at 90 °C (isotropic phase) under vigorous stirring for 2 hours.

Figure 6.4- Schematic representation of CLC film made from mixture 3.

6.2.2 Reference substrate

Commercially available Homogeneous Cells (Instec) are used as the reference substrate. The cell is composed of top and bottom glass which are glued together around the edges. The cell has dimensions 15.25 × 17 × 1.5 mm with variable cell spacing and an antiparallel alignment layer. The cells are filled with different sized glass microspheres depending on the cell spacing. There are two injection ports on the cell. By placing a very small amount of liquid crystal material on one opening of an empty cell, the capillary force will pull liquid crystal material into the cell and it takes only a few minutes before the cell is fully filled.

For this experiment commercial 9 microns thick cells (LC2-9.0) were used. First the liquid crystal mixture was heated on a hot plate at 90 °C to achieve the isotropic phase. Then a drop of mixture was placed on one injection port while the cell was also placed on the hot plate to maintain the isotropic phase as the LC mixture is filling the cell.

Figure 6.5- Image of 9 microns thick cell with dimensions 15.25 × 17 × 1.5 mm.

6.2.3 Transfer print technique

In order to stick the LCE thin film to the acrylic tape, a transfer printing technique was used (Figure 6.6). First the top glass of the cell was removed which resulted in LCE film sticking to the bottom glass (Figure 6.6 a). The backing paper of acrylic elastomer was removed from one side and the sticky side of the tape was placed on the LCE film and was pressed firmly by fingers to ensure adhesion between the two films (Figure 6.6 b). Then the acrylic tape was removed by applying force in one direction which automatically peeled off the LCE film from the bottom glass (Figure 6.6 c).

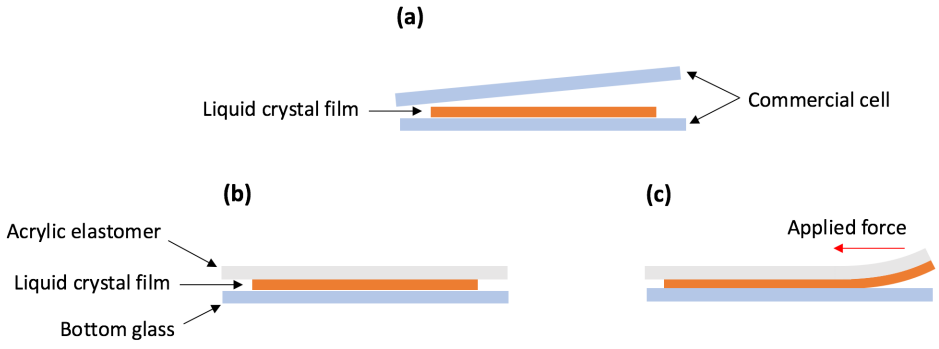

Figure 6.6- Schematic representation of the transfer print technique.

6.2.4 Preparation of antiparallel aligned PVA cells

PVA solution of 5 wt.% PVA in water was spin coated (SCS 6800 Spin Coater Series) on two microscopic glass slides with dimensions 25 × 25 mm at 1000 rpm for 30 seconds, then were placed on a hot plate at 80 °C for 30 minutes to be cured. The surface of the PVA on both glass slides were rubbed ten times smoothly with a velvet cloth in one direction for the planar alignment of the CLCs. LC mixture was mixed with xylene 1:0.2 ratio by weight. LC mixture was then spin coated on one rubbed PVA coated glass at 750 rpm for 30 seconds. LC coated glass was placed in the oven for 30 seconds for the solvent to evaporate. The other PVA coated glass was placed on top of the LC coating where the alignment layer was on the opposite direction (antiparallel alignment). Therefore, when the top and bottom substrates were aligned antiparallel to each other, a homogenous planar alignment of the liquid crystals was achieved.

The cell was placed into the oven for a few seconds to reach isotropic temperature for the alignment of the LC molecules. The cell was then taken out from the oven and pressed by fingers for few seconds to ensure contact between top PVA coated glass and LC coating and this was cooled down to room temperature (nematic phase). The LC coating in the cell was photopolymerised using a mercury lamp (EXFO Omnicure S2000 λ= 350-450 nm) under nitrogen at room temperature for 200 seconds.

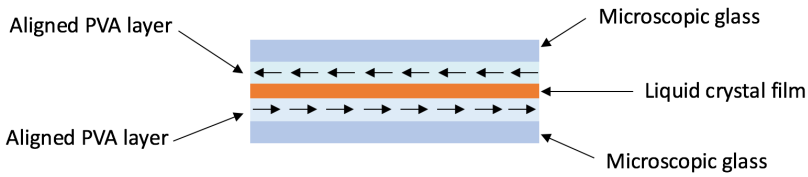

Figure 6.7- Schematic representation of the LC film sandwiched in between antiparallel aligned PVA cells.

6.2.5 Characterisation

Differential Scanning Calorimetry (DSC) measurement was performed using PerkinElmer DSC 4000 for uncured mixtures in the powder form to look into their phase transition temperature. A further thermal analysis of the uncured mixture was done using a Linkam HFS600 heating stage that was fitted to an Olympus BX60 optical microscope to look at the transition temperature.

Ultraviolet-visible (UV/Vis) spectroscopy was used to check the optical properties of the samples. The measurements were taken in transmission mode using Lambda 950 UV/Vis Spectrometer, integrating sphere. The wavelength was set to 400-800 nm.

6.3 Results and Discussion

6.3.1 Mixture 1

DSC measurement was performed on the LC host (RM105/LC756) to determine the transition temperatures. Table 6.1 shows the temperature profile used for this measurement.

Table 6.1- Temperature profile for DSC measurement.

	Temperature/ °C	**Temperature rate °C/ min**	**Holding time at final temp/ min**
Room temp cooling	25 to -40	-10	10
1st heating	-40 to 130	10	5
1st cooling	130 to -40	-10	10
2nd heating	-40 to 130	10	5

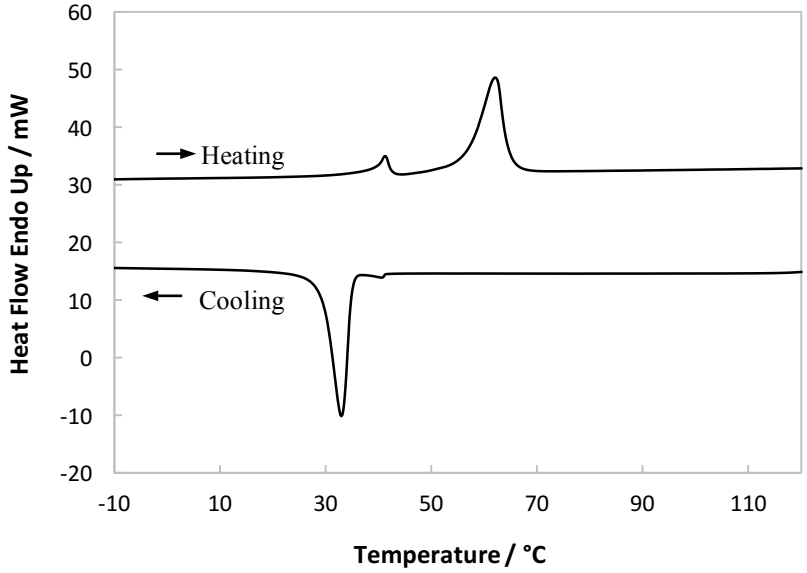

Figure 6.8- DSC thermogram of the mixture RM105/LC756 during the first cooling and second heating.

The first heating was performed in order to remove any processing artefacts. The blend showed first nematic transition upon first cooling at 41 °C followed by crystalline transition at 33 °C. Upon second heating the blend showed second nematic transition at 41 °C followed by the isotropic transition at 61 °C. From the results it was seen that the working temperature range for the nematic phase was very narrow (Figure 6.8).

The mixture was infused into a homogeneous cell with the thickness of 9 microns and was placed on a heating stage to look at phase transition of the mixture upon first cooling (Table 6.2) and second heating (Table 6.3) under the optical microscope in reflection mode without the use of polarisers.

Table 6.2- Thermal analysis of the mixture RM105/LC756 upon first cooling.

Temperature / °C	Transition	Optical Microscopy Images
63	Isotropic phase	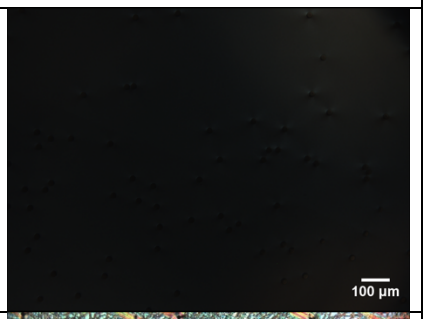
33	Chiral nematic phase	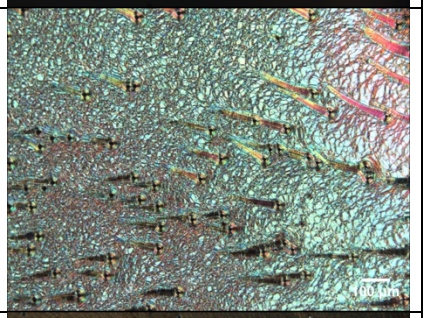
26	Crystalline phase	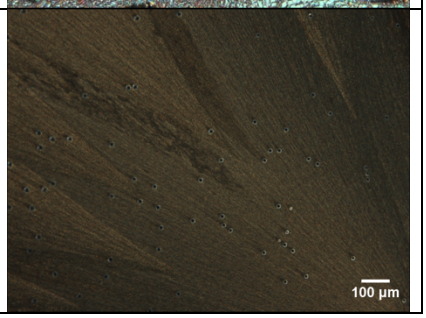

The results in Table 6.2 support the transition phases deduced from the DSC thermogram results in Figure 6.8. From the DSC results, the nematic transition peak was at 41 °C. The optical microscopy results showed that a strong green reflection band in the nematic range was achieved as the molecules become highly aligned with the substrate at a lower temperature (31-33 °C) which was close to the crystallisation temperature.

Table 6.3- Thermal analysis of the mixture RM105/LC756 upon second heating.

Temperature / °C	Transition	Optical Microscopy Images
26	Crystalline phase	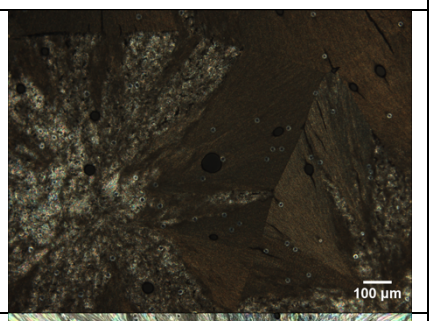
45	Morphology change	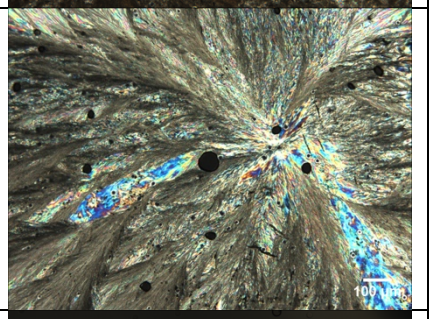
63	Isotropic phase	

Upon second heating, the optical microscopy images in Table 6.3 show two transitions with roughly same transition temperatures as found in the DSC thermogram of the mixture in Figure 6.8. The first transition was expected to be chiral nematic phase but the optical microscopy image shows a different transition possibly a smectic phase with some parts of nematic phase which are blue/green colour at 45 °C. The reason why there is no chiral nematic phase could be that the sample on the heating stage did not cool down to room temperature compared to DSC sample that cooled down to -40 °C and hence this significant additional cooling resulted in the appearance of a different phase.

Taking into account the temperature dependence of the order parameter *S* in nematic liquid crystal phase in Figure 6.9, the order parameter of the liquid crystal increases with decreasing temperature.

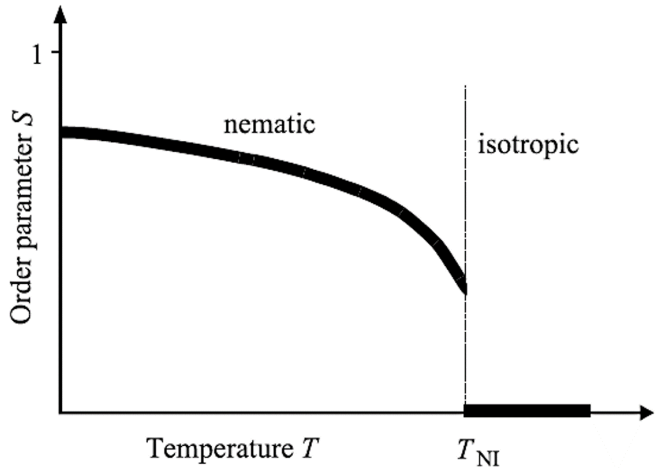

Figure 6.9- Order parameter variation with temperature in the nematic liquid crystal phase. T_{NI} is the phase transition temperature from Nematic to Isotropic (Scharf, 2007).

This agrees well with the optical microscopy images in Table 6.2 showing the molecules became more ordered at lower temperatures close to the crystallisation temperature. Therefore, to get highly ordered liquid crystalline molecules that have a strong reflection band, the mixture had to be photopolymerised in the very narrow temperature window (31-33 °C) and hence photopolymerisation at room temperature was not possible.

6.3.2 Mixture 2

To overcome the problem of narrow temperature range of the nematic phase in mixture 1, a nematic mixture (E7) is added to the monomer mixture 2. The mixing ratio of RM105 and E7 was 5:4 by weight. The DSC measurement with the same temperature profile was performed on the mixture RM105/E7/LC756.

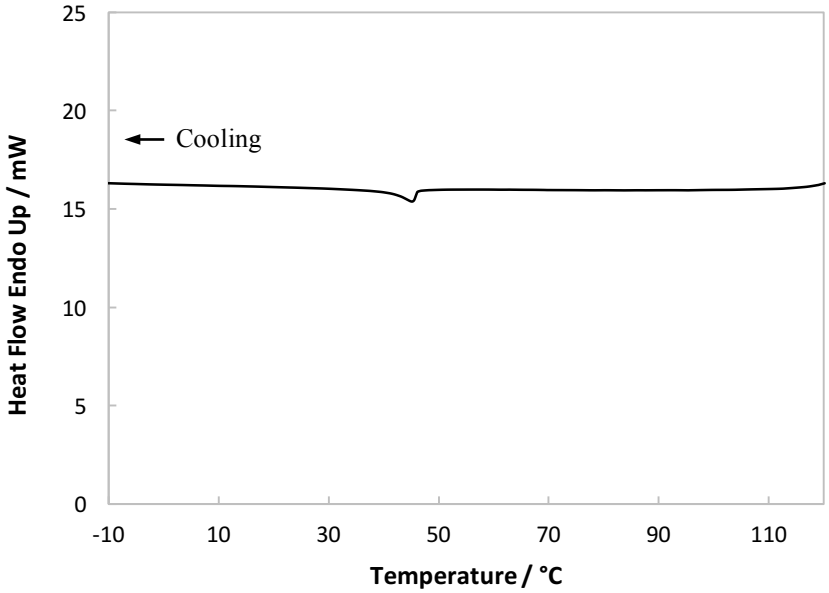

Figure 6.10- DSC thermogram of the mixture RM105/E7/LC756 during the first cooling.

During first cooling, a single transition from isotropic to nematic was observed at 45 °C. This nematic phase was found to be stable over a broad range of temperatures. This allowed for photopolymerisation of this LC at room temperature.

6.3.3 Mixture 3

With the addition of nematic mixture to the LC host in mixture 2, 2.5 wt.% diacrylate monomer (RM82) was added into mixture 3 to ensure there were enough crosslinks in the LC network after curing. Together with 5 wt.% LC756, this gave a total cross linker concentration of 7.5 wt.% in the mixture. To cover the whole visible spectrum, the concentration of the LC756 was reduced from 5 wt.% to 4.8 wt.% which resulted in a shift in the reflection band towards higher wavelength (from green to red) (Figure 6.11) compared with mixtures 1 and 2.

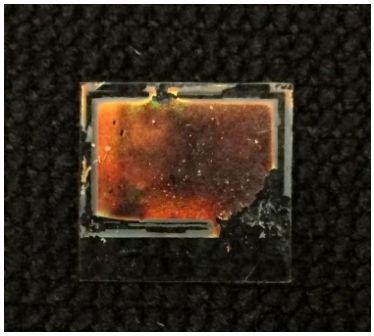

Figure 6.11- Image of the commercial cell filled with liquid crystal mixture 3 (top view).

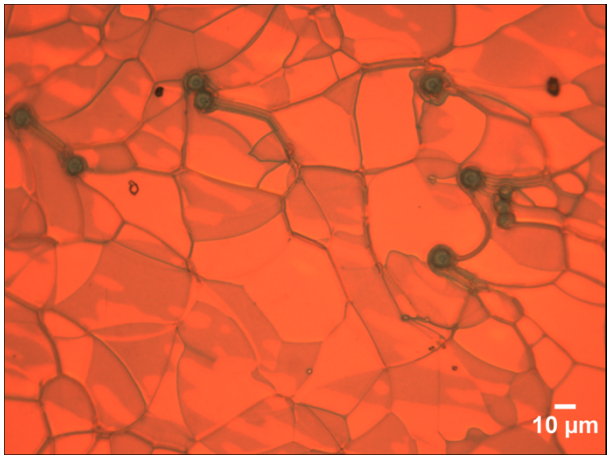

Figure 6.12- Optical microscopy image of red reflecting LCE film (mixture 3) in the homogenous cell in reflection mode without polarisers.

The optical microscopy observations of the film inside the cell showed the characteristic oily streak morphology with a planar alignment (Figure 6.12). The black lines running through the red background are the *disclinations* which are defects in the orientation of the director. The round domains are the glass microspheres of diameter around 9 microns which are spread randomly inside the cell to maintain the cell thickness. To measure reflective propertied of the film UV/Vis spectroscopy was performed in transmission (400-800 nm) with non-polarised light at normal incident. The film showed a strong reflection band centred λ_0= 669 nm (red) and a width $\Delta\lambda$= 98 nm (Figure 6.13).

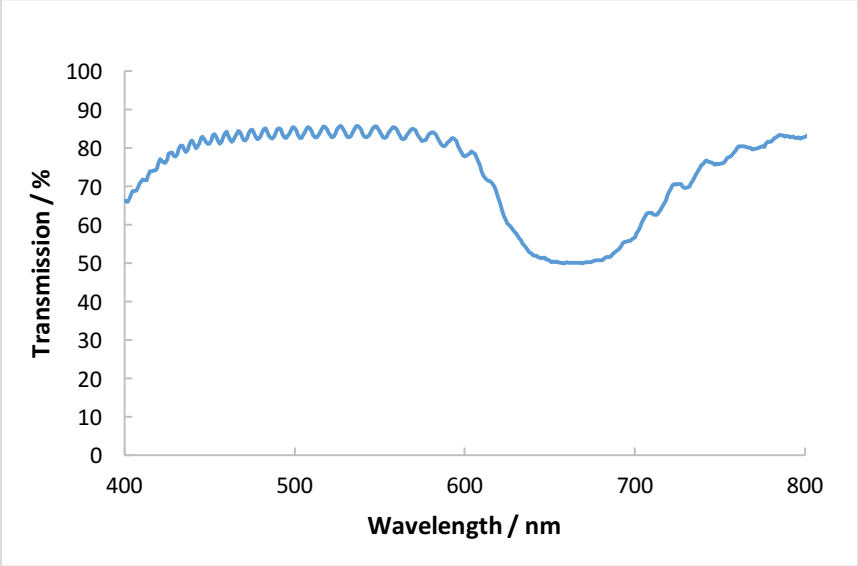

Figure 6.13- Transmission spectra of crosslinked LCE film (mixture 3) with 4.8 wt.% LC756 made in the homogenous cell.

The top glass substrate was removed from the bottom glass and transfer print technique was used to transfer the LCE film onto acrylic tape (Figure 6.6).

6.3.4 Colour shift with time

When a film was made from mixture 3 and was transfer printed onto an acrylic substrate, a shift in the reflected colour was observed over time (Figure 6.14).

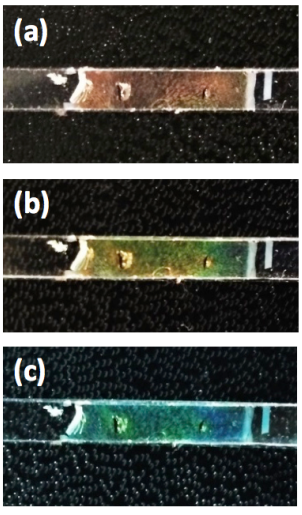

Figure 6.14- Images of LCE films transfer print on acrylic at normal incidence showing shift in reflected colour over time, (a) immediately, (b) after 2 hours and (c) after 24 hours.

The shift in colour is probably similar in nature to the phenomena described in section 4.3.5 for the PDLC materials. The diffusion of the volatile compounds in the acrylic required for its adhesive properties into the LC network causes the unreacted E7 to change from a nematic to isotropic phase. As the molecules in the isotropic state have no orientational and positional order, their refractive index changes and since the pitch length is fixed due to the crosslinks in the LC network, the change in the refractive index of the overall film results in a blue shift with time. After 24 hours the shift in the colour seemed to have stabilised.

The bandwidth ($\Delta\lambda$) of the LCE film was measured as a function of time after the LC film was transfer printed on an acrylic substrate.

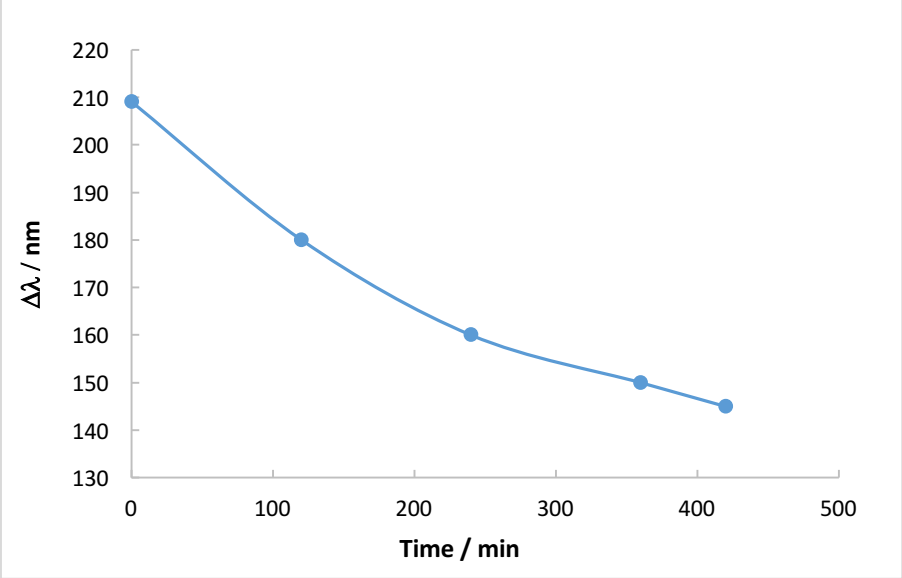

Figure 6.15- A plot of shift in the width of the reflection band as a function of time for LCE film immediately after transfer printed on acrylic substrate.

Figure 6.15 shows that the width of the reflection band decreases with time. As the LCE film is in contact with the acrylic substrate, the change in the state of E7 molecules from nematic to isotropic phase results in a reduction of the birefringence of the LC molecules that causes an overall decrease in the birefringence of the film. Since the width of the

reflection band is proportional to the birefringence (Δn) of the polymer [$\Delta\lambda = p\Delta$n], a decrease in the bandwidth is observed.

6.3.5 LCE film prepared in antiparallel aligned PVA cell

Due to the undesirable but unavoidable presence of microsphere spacers in the commercial homogenous cells, the LCE film was prepared using the PVA coated microscopic glass slides with antiparallel alignment layer as described in section 6.2.4.

After observation of a blue shift in the reflection band with time on LCE film that was transfer printed on acrylic substrate in Figure 6.14, the concentration of chiral dopant was reduced to 3.8 wt.% so that the whole visible spectrum could be covered after the blue shift had stabilised. 3.8 wt.% chiral dopant concentration shifted the reflection band to the infrared (IR) region of the electromagnetic spectrum.

To compare the reflective properties of the films made by antiparallel aligned PVA cell and homogenous cell, UV/Vis spectroscopy was performed in transmission mode (400-1200 nm) with non-polarised light at normal incident (Figure 6.16).

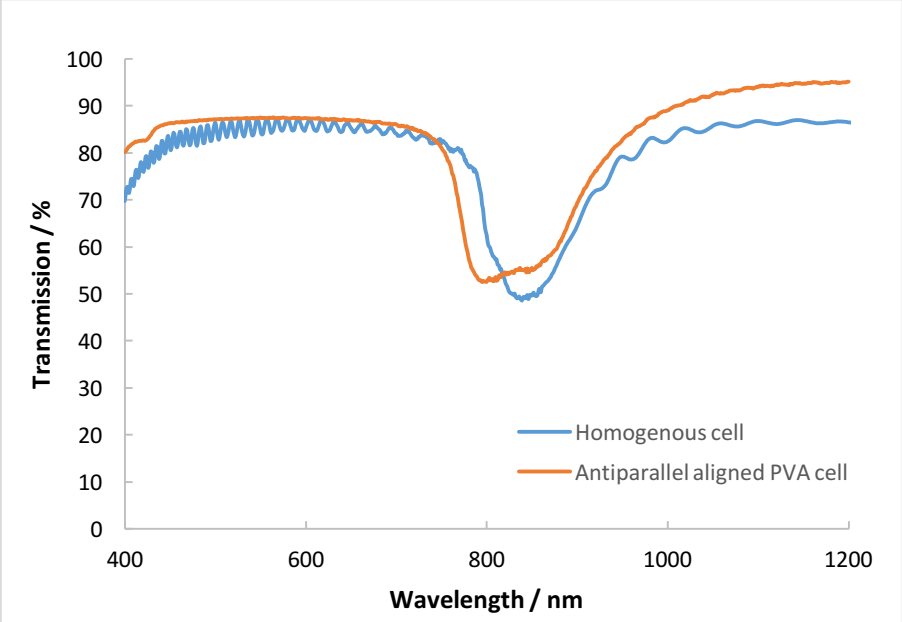

Figure 6.16- Transmission spectra of the crosslinked LCE film with 3.8 wt.% LC756 made in two different cells.

The film that was made in homogenous cell showed a reflection band centred λ_0 = 852 nm (IR) and a width $\Delta\lambda$ = 112 nm and antiparallel aligned PVA cell showed a reflection band centred λ_0 = 836 nm (IR) and a width $\Delta\lambda$ = 138 nm. Thus both films have reflection band that is centred in the IR region. Since the antiparallel aligned PVA cell is made by hand, a number of factors can affect the alignment of the LC molecules during processing including the presence of impurities such as dust particles in the air, inhomogeneity of alignment layer and the magnitude and uniformity of applied pressure to the cell.

The unreacted E7 mixture in the film was washed off with acetone to see how far the wavelength of the reflected colour shifted as the thickness of the film was reduced producing a decrease in the pitch length of the cholesteric helix as well as change in the overall refractive index of the film.

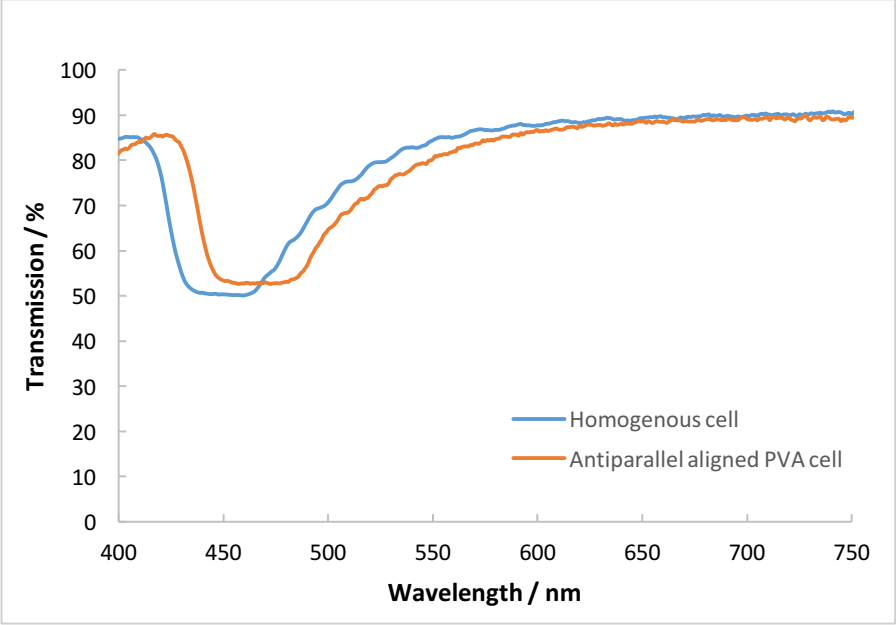

Figure 6.17- Transmission spectra of the LC film with 3.8 wt.% LC756 made in two different cells after removal of E7 by acetone.

The transmission spectra results showed a significant 395 nm shift in the central reflection band from λ_0= 852 to λ_0= 457 for homogenous cell and 354 nm shift from λ_0 = 836 to λ_0= 474 for antiparallel aligned PVA cell.

Optical microscopy observation of the films on both cells also showed the characteristic oily streak morphology with a planar alignment and showing a blue reflecting colour after removal of E7 (Figure 6.18).

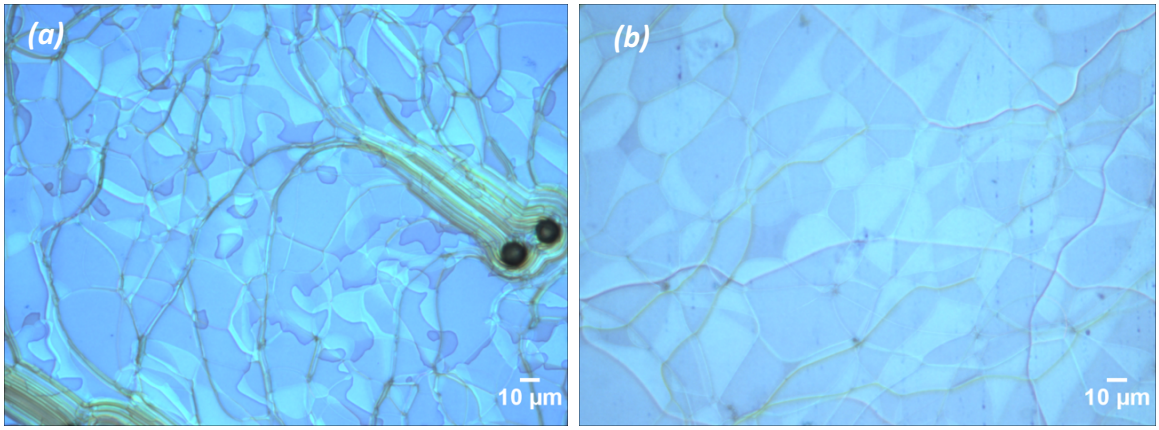

Figure 6.18- Optical microscopy image of blue reflecting LCE film made in (a) homogenous cell and (b) antiparallel aligned PVA cell in reflection mode without polarisers.

6.3.6 Shift in wavelength with the applied strain

LCE film prepared using antiparallel aligned PVA cell was transfer printed onto the acrylic elastomer substrate. The sample was left for 3 days so that the blue shift with time was stabilised. The sample was stretched using a custom-made strain rig. The frame produced a uniaxial extension. The transmission spectra of the bilayer were measured for each extension value using UV/Vis spectroscopy. Measurements were performed during both an initial loading and unloading cycle to see if any changes with strain are reversible. The extension was increased step-wise and the reflection band was measured during each step.

(a)

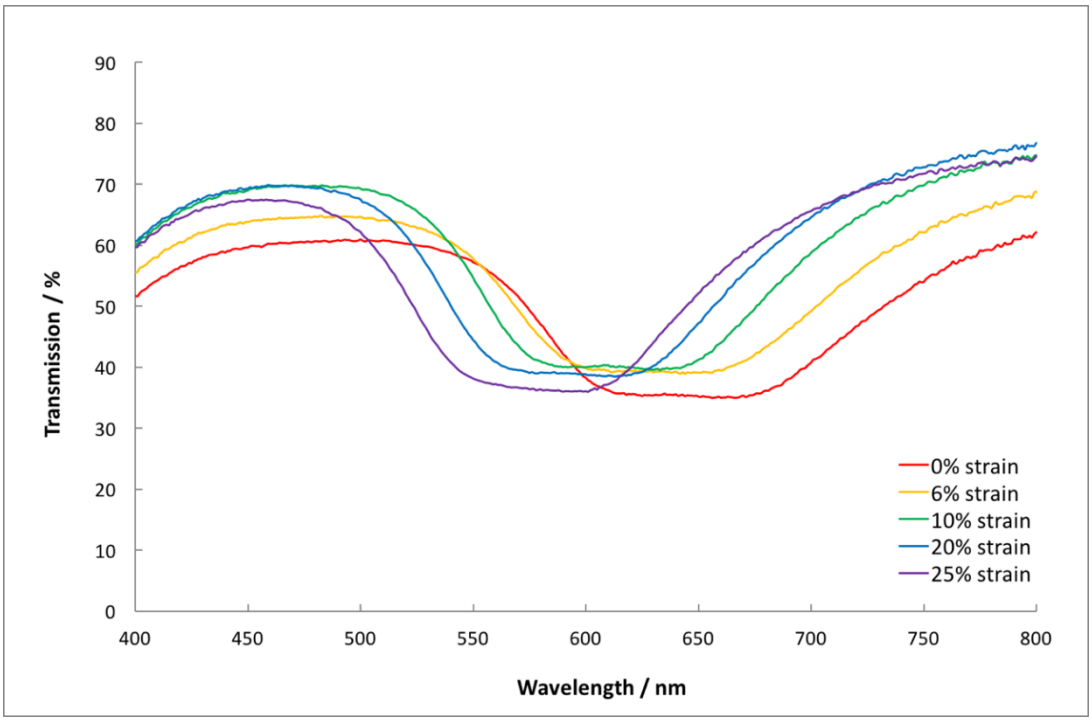

(b)

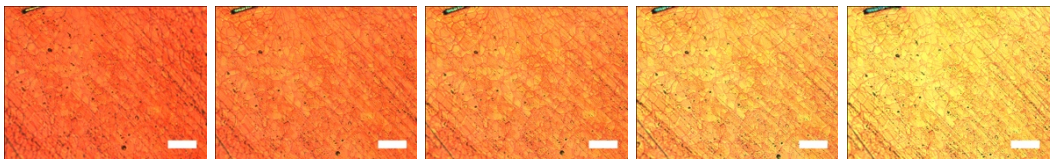

Figure 6.19- (a) transmission spectra of the LCE film on acrylic with loading strain, (b) microscopy pictures in reflection mode without polarisers showing the corresponding change in colour. The scale bars stand for 100 µm.

The central reflection band at 0% strain was λ_0= 656 nm (red) which shifted to lower wavelength λ_0= 587 nm (orange) with increasing strain. At a maximum strain of 25%, an overall shift of 69 nm of the central reflection band was achieved and an average sensitivity of approximately 2.8 nm/% strain was observed. Figure 6.19 b shows that a large shift in the wavelength generated an observed change in the colour of the film from red to orange. This change in the wavelength was consistent with research done by Picot et al. (2013a) on a flexible strain sensor based on a cholesteric liquid crystal network. In their experiment they achieved sensitivity of 3 nm/% strain for crosslinked cholesteric

liquid crystal layer that was spray-coated onto a uniaxially oriented polyamide 6 substrate (Picot et al., 2013a).

(a)

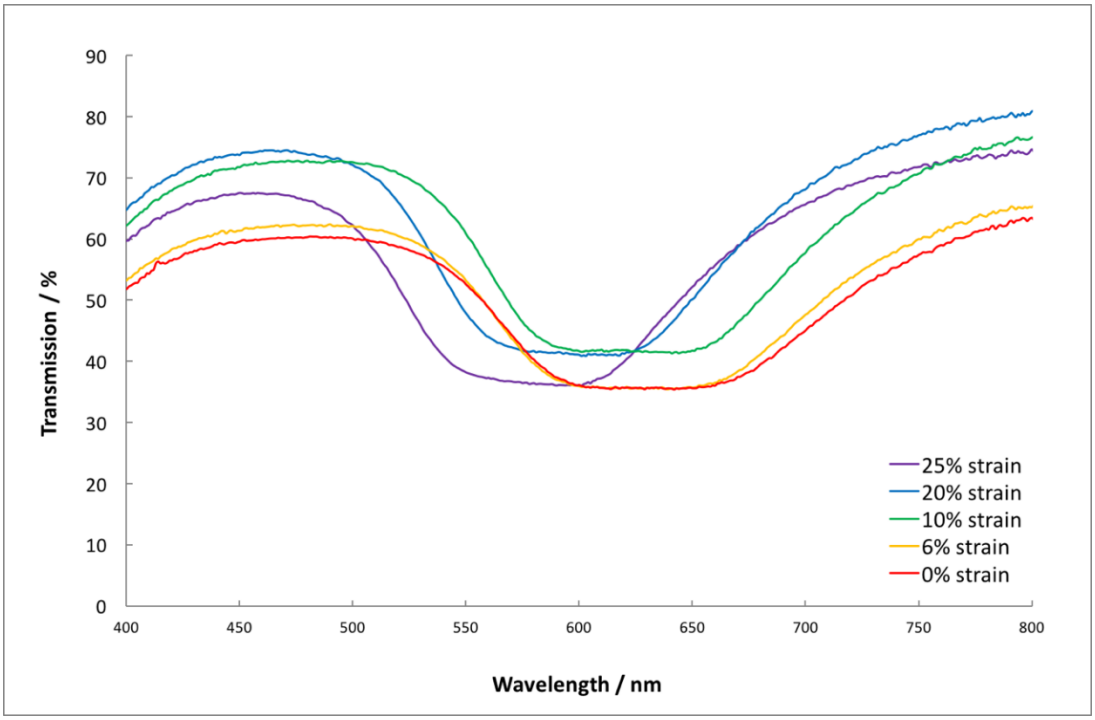

(b)

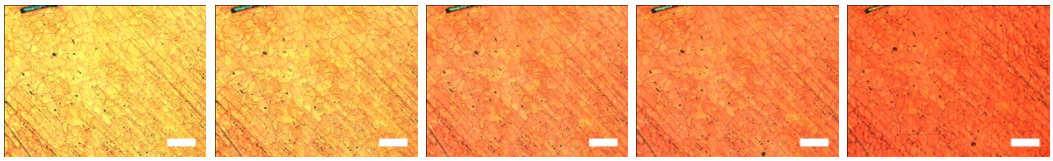

Figure 6.20- (a) transmission spectra of the LCE film on acrylic with unloading strain, (b) microscopy pictures in reflection mode without polarisers showing the corresponding change in colour. The scale bars stand for 100 µm.

The sample was unloaded in a stepwise manner and a reverse shift in the wavelength was observed (Figure 6.20). Upon unloading (at 0% strain) the red colour was restored but a 'permanent' shift of around 18 nm remained.

The reflection band during loading and unloading was further investigated to understand the reversible behaviour of the same sample. Figure 6.21 shows a plot of central

wavelength shift as a function of applied strain. The central wavelength shift is defined as the difference between the central wavelength at 0% strain and the central wavelength at x% strain (λ_0- λ_x). For each spectrum the central wavelength (λ_0) was measured. Measurements below 20% strain show a slight deviation between the loading curve behaviour and unloading data. The 18 nm residual shift could result from the imperfect elasticity of the acrylic elastomer substrate. Picot et al. (2013a) also reported a residual shift of 5 nm in wavelength of the polymer film at 0% strain after unloading (Picot et al., 2013a).

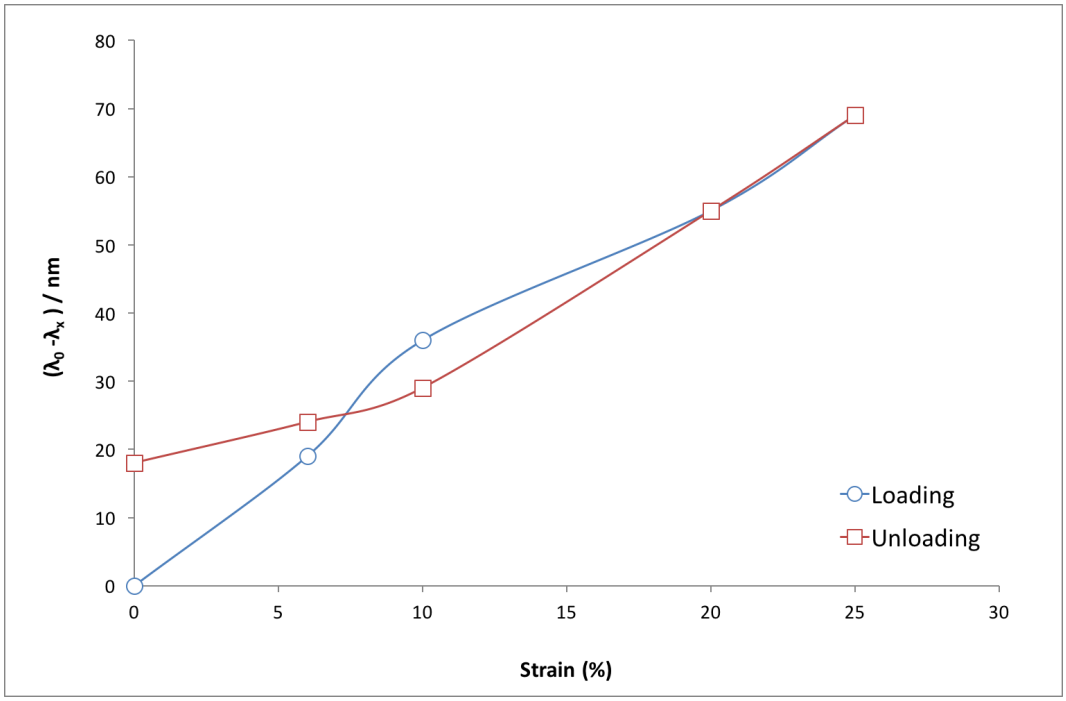

Figure 6.21- Wavelength shift as a function of strain during loading (○) and unloading (□) of the LCE film on acrylic for maximal strain of 25%.

To investigate this residual shift in the reflection band as a result of inelastic behaviour of the acrylic rubber, the test was repeated with a lower maximal strain of 15.2% applied to a new sample. The transmission spectra of the bilayer were measured for each extension value using UV/Vis spectroscopy 3 days after transfer printing (Figure 6.22).

(a)

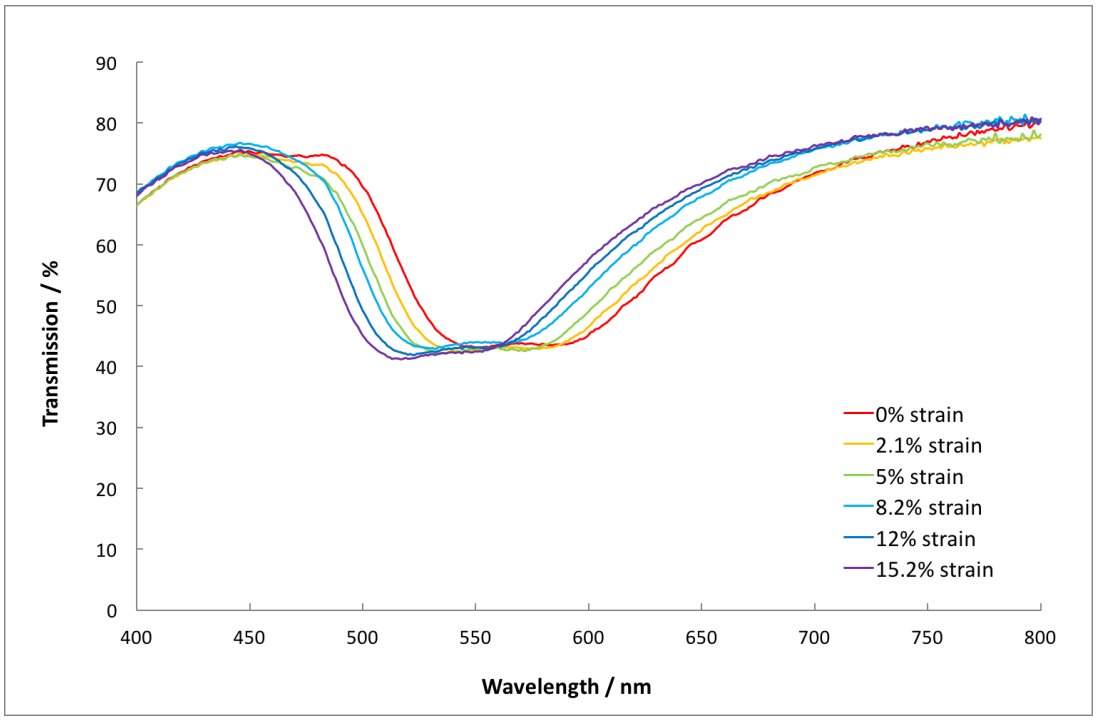

(b)

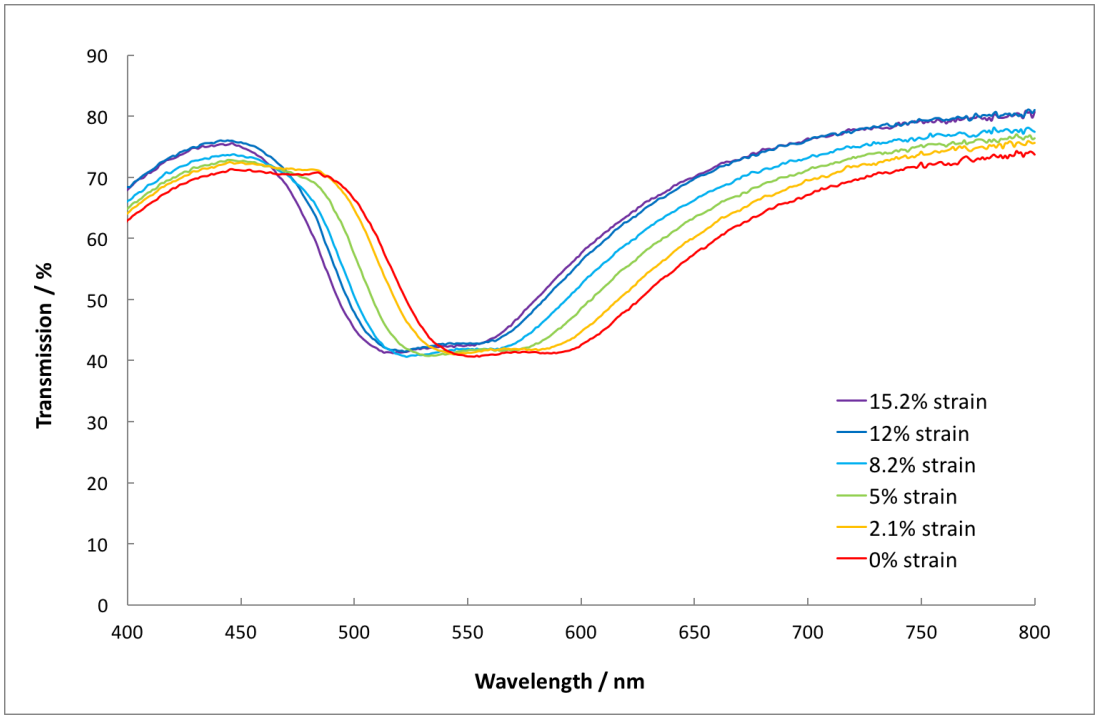

Figure 6.22- Transmission spectra of the LCE film on acrylic with (a) increasing strain, (b) reducing strain.

The central reflection band at 0% strain was λ_0= 578 nm (orange) which shifted to lower wavelength λ_0= 543 nm (green) with increasing strain. With maximal strain of 15.2%, an overall shift of 35 nm of the reflection band was achieved and an average sensitivity of approximately 2.3 nm/% strain was observed. Step-wise unloading of the film led to a reverse shift in the wavelength. Upon unloading (at 0% strain) the orange colour was fully and reversibly restored with less than 1 nm shift in the wavelength.

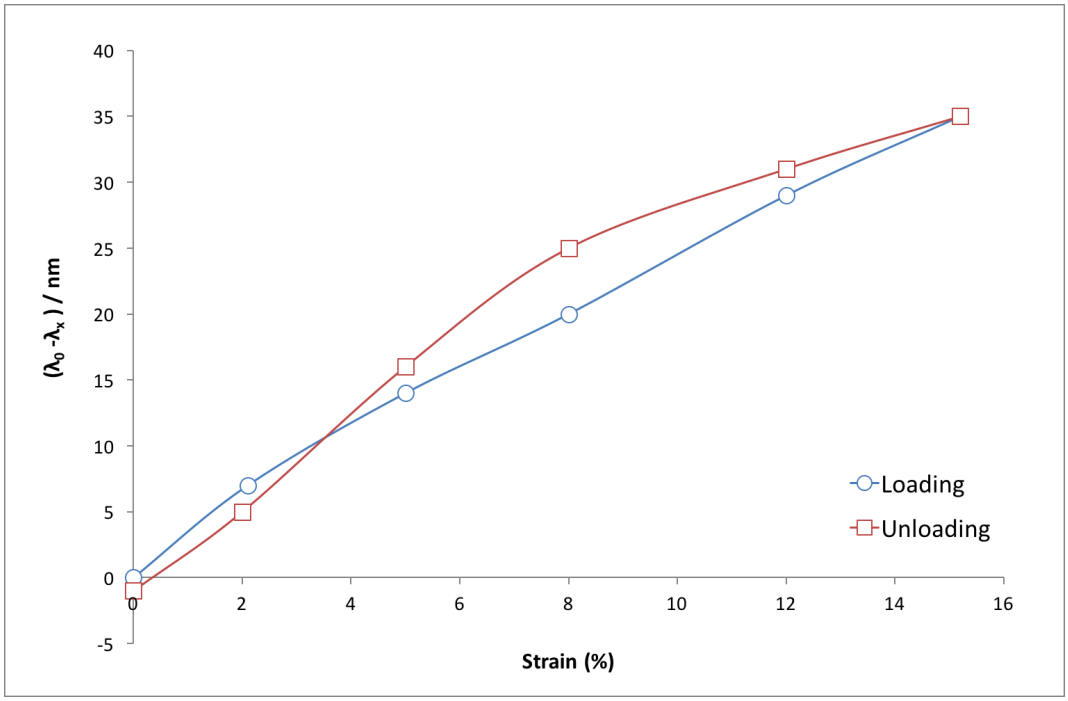

Figure 6.23- Wavelength shift as a function of strain during loading (○) and unloading (□) of the LCE film on acrylic for maximal strain of 15.2%.

A plot of wavelength shift as a function of applied strain is shown in Figure 6.23 for a system that has a maximal strain of 15.2%. Both the loading and unloading curves coincide closely and show almost linear behaviour. Any slight discrepancy for the loading and unloading data and the negative shift in the reflection band upon unloading at 0% strain can be attributed to the accuracy of the experimental data for example small changes in the position and angle of the film would produce similar shifts. From the

results it can be concluded that the residual shift seen in the previous experiment was because the acrylic was not fully recovered with time after a maximal strain of 25%. The behaviour of this initial LC sample that had been strained to 25% was reinvestigated during loading and unloading after a 49 day dwell time after the initial test.

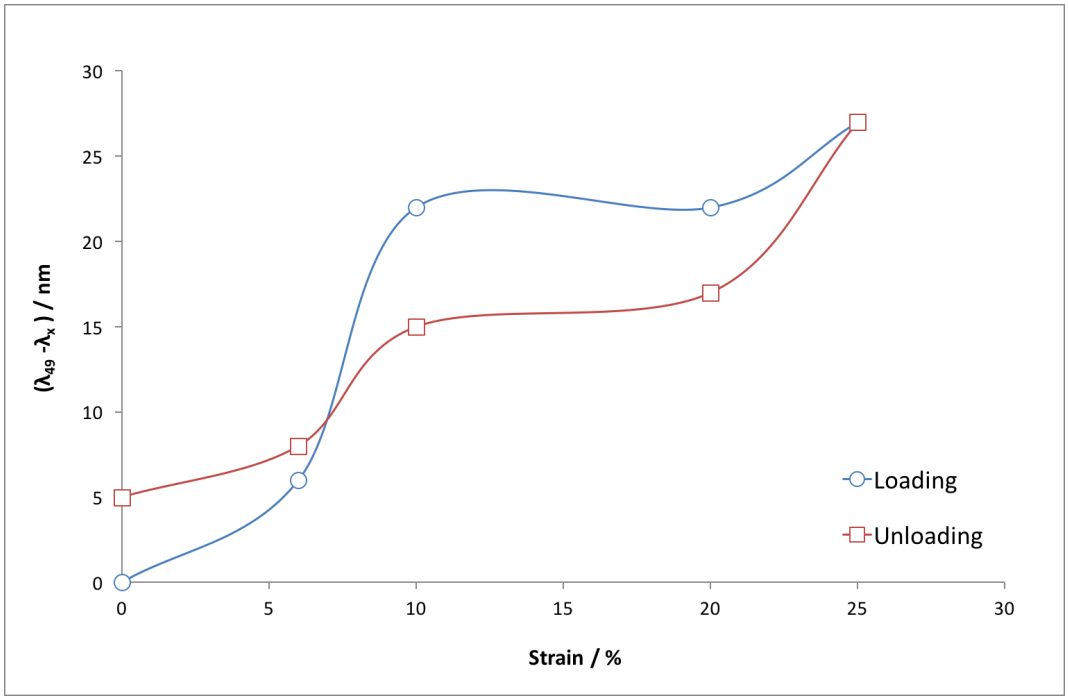

Figure 6.24- Wavelength shift as a function of strain during loading (○) and unloading (□) of the LCE film on acrylic for maximal strain of 25% after 49 days of transfer print.

During the reloading to a maximal strain of 25%, an overall shift of 27 nm of the central reflection band was achieved (Figure 6.24). The unloading of the film resulted in a reverse shift. Upon unloading (at 0% strain) a 'permanent' shift of around 5 nm remained. Comparing this to the same sample that was strained 3 days after transfer printing, the overall shift and the remaining shift upon unloading at 0% strain was around 42 nm and 13 nm less respectively. Also the loading and unloading data showed a more non-linear behaviour than previously. This could be due to change in alignment of the LC molecules over time as a result of change in the state of the E7 LC molecules from nematic to

isotropic and hence there being a less significant shift in the central wavelength. Also this non-linear behaviour could be due to delamination or slippage of the LCE film as the adhesive properties at the interface might be changing over time.

6.4 Discussion

Using antiparallel aligned PVA cells a lightly crosslinked thin LCE film was produced which showed a strong reflection and oily streak morphology. This suggested that the helical axis of the molecules was perpendicular to the surface of the substrate (CLC planar alignment). When the film was transfer printed onto the acrylic elastomer, a colour shift in the reflection band was observed over time which was found to be related to the diffusion of the volatile compounds in the acrylic required for its adhesive properties on the surface into LCE film and changing the state of unreacted E7 LC molecules from nematic to isotropic. This then results in a change in the overall refractive index of the LCE film as the molecules in the isotropic phase are no longer birefringent and resulting in a blue shift over time.

When uniaxial strain was applied to the bilayer along the orientation direction, a shift in the reflection band was observed. For large deformation ~15% the corresponding shift in the wavelength was large enough to result in a visible colour change to the eye. The proposed colour change mechanism is shown in Figure 6.25.

The uniaxial extension of the bilayer caused a reduction in the thickness of the LCE film ($t' < t$) due to Poisson's contraction which then leads to a decrease in the cholesteric helical pitch ($P' < P$).

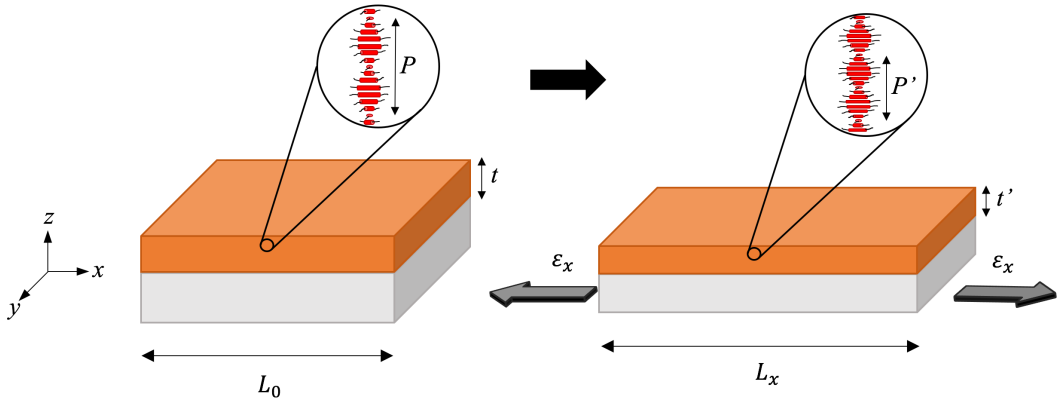

Figure 6.25- Schematic representation of the cholesteric liquid crystal strain sensing mechanism.

The colour shift was reversible and the initial wavelength was fully restored during unloading from a deformation strain of about 15%. Higher deformation resulted in the initial wavelength not to be fully restored after unloading the bilayer. It is assumed that the acrylic substrate was not fully recovered to its initial length within the time frame of the experiment and hence resulting in a residual wavelength shift. The same effect was also reported on CLC coating on a polyamide 6 substrate by Picot et al. (2013a).

6.5 Conclusion

In this chapter a lightly crosslinked CLC elastomer has been produced using a bespoke antiparallel PVA aligned cell. The thin LCE was then transfer printed onto an acrylic elastomer and which was left for at least 24 hours until any resulting colour shift had stabilised. When the bilayer was stretched in tension, a reversible colour shift was observed. The colour shift was directly related to the reduction in the cholesteric helix's pitch as a result of change in the thickness of the LCE. Thus the optical response was found to be entirely dependent on the mechanical deformation of the bilayer. As such this was an entirely novel material that had been developed that exhibited a strain dependent

colour shift in transmission mode. If time had permitted then this proof of concept discovery would have been extended further. The aim would have been to optimise the substrate so that any colour change resulting from either the leaching out of unreacted E7 from the LCE film or the swelling in of any plasticising materials from the elastomer substrate was avoided. Ideally this substrate would also have the required properties for high performance dielectric transduction, have adhesive properties that are not influenced by the state of the unreacted LC molecules when adhered to the surface of LCE film and whose adhesive properties to LC did not change with time.

Chapter 7: Conclusions and Future Work

7.1 Conclusions

The aim of this study was to develop a new approach to create a strain actuated compliant colour changing device that is controlled using dielectric elastomer actuators (DEAs).

An initial approach was aimed at creating colour changes using dielectric elastomer actuators that drove a masked positioner. This method showed colour change since the mask changes the colour visualisation. The movement of the spots on the actuator was analysed and the results showed that in the central region, where the displacement was highest, the movement of the spots was mostly unidirectional. Spots further away from the electrode displaced significantly less than their central equivalents whilst the spots

closest to the frame exhibited the smallest displacement as the frame restricted their movement. Since a large portion of the device was covered by the mask and only a small portion showed colour and the colour change was dominated by the mask, it was decided to consider an alternative approach to produce a more significant colour changing device using DEAs.

The second approach used polymer dispersed liquid crystals, such as a nematic liquid crystal within a reactive silicone resin. The immiscibility of these compounds resulted in a dispersion of the liquid crystal droplets in the silicone matrix. To create this system a wide range of processing parameters, such as the ideal concentration for the various components and the solvents, were explored. Different spin coating speeds produced films with different liquid crystal droplet sizes and distributions. The presence of the LC droplets in the material also served to significantly reduce the transmittance of the PDLC film compared to the silicone rubber. The alignment of the dispersed liquid crystal droplets was investigated using two chemically different liquid crystal molecules. It was found that the alignment of the LC molecules inside the droplets are directly influenced by their chemical nature and their anchoring force against the wall surface of the droplets. It was found that the PDLC film has a much lower Young's modulus and a slightly lower glass transition temperature value when compared to the pure silicone elastomer. Since E7 is a nematic liquid crystal that acts as a Newtonian fluid, its Young's modulus is essentially zero. Thus this large reduction in the Young's modulus of the PDLC film was explained by this. Also it is presumed that either residual xylene or a small amount of LC molecules within the elastomer phase act as a plasticiser, reducing slightly the Tg and modulus of the rubber phase. The effect of a mechanical deformation on the alignment of the molecules inside the droplets was examined. It was found that the alignment of the LC molecules inside the droplets could not be controlled through mechanical deformation.

Intriguingly, the silicone matrix did not become significantly anisotropic along the direction of the applied deformation and this rather disappointingly resulted in no change in the director configuration of the liquid crystal dispersed droplets. However, the alignment of resulting LC droplets in the PDLC films was sensitive to the elastomeric substrate (acrylic) used to perform the actuation. From the results it is concluded that some of the molecules within the elastomeric substrate diffused into the PDLC film causing it to change the state of the LC molecules inside the droplets from a nematic to an isotropic phase. This resulted in the PDLC film becoming transparent as the refractive index of the isotropic LC molecules inside the droplets was closer to the refractive index of the silicone matrix and hence less light was scattered. Due to these complications it was decided to attempt to create a colour changing elastomer film using an alternative approach.

The next approach was to develop thin film coatings on PVA and acrylic aligned substrates using reactive cholesteric liquid crystals (CLC) through spray deposition technique. Unlike PVA, the acrylic substrate showed no planar alignment. Potentially this was due to the swelling of the elastomer with the xylene and hence this caused the small molecules in the mixture to diffuse into the elastomer before curing and this changed the concentration of the chiral dopant in CLC the mixture.

In free standing films a planar cholesteric alignment was obtained with mesogens aligned parallel to the substrate and colour was achieved based on the selective reflection of light. A transfer print technique was introduced to combine CLC coatings with an elastomeric substrate (acrylic) that can be stretched. However, no colour change was achieved in response to mechanical deformation primarily due to the modulus and strength mismatch between the CLC thin film and the elastomeric substrate material.

Finally, lightly crosslinked liquid crystal elastomers using a combination of reactive and non-reactive liquid crystals were produced using a bespoke antiparallel PVA aligned cell. The thin CLC elastomer was then transfer printed onto an acrylic elastomer and which was left for at least 24 hours until any resulting colour shift had stabilised. When the bilayer was stretched in tension, a reversible colour shift was observed. The colour shift was directly related to the reduction in the cholesteric helix's pitch as a result of change in the thickness of the CLC elastomer. Thus the optical response was found to be entirely dependent on the mechanical deformation of the bilayer. As such this was an entirely novel material that had been developed that exhibited a strain dependent colour shift.

7.2 Future Work

Due to lack of time it was not possible to extend the proof of concept demonstrated in Chapter 6 further. The aim would have been to optimise the substrate so that any colour change resulting from either the leaching out of unreacted E7 from the LCE film or the swelling in of any plasticising materials from the elastomer substrate was avoided. Ideally this substrate would also have the required properties for high performance dielectric transduction, have adhesive properties that are not influenced by the state of the unreacted LC molecules when adhered to the surface of LC film and whose adhesive properties to LC did not change with time.

CLC elastomer can then be adhered to the optimised elastomeric substrate which can then be incorporated in a dielectric elastomer actuator to investigate their colour response as a function of applied voltage. There are three potential DEA configurations for this application that are described below.

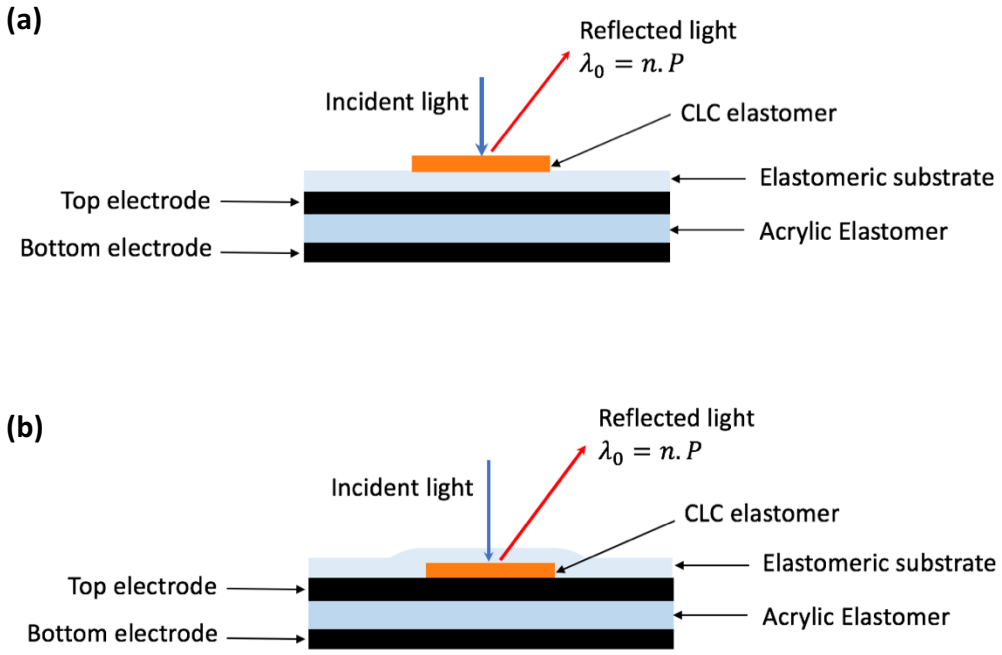

Figure 7.1- Schematic representation of first proposed DEA device (side view), where CLC layer and elastomeric substrate are adhered on top of the device (a) CLC elastomer facing up and (b) CLC elastomer facing down on the top electrode.

The first proposed configuration is shown in Figure 7.1 a or face down as shown in Figure 7.1 b on the top electrode. When a voltage difference is applied between the electrodes, the acrylic substrate is squeezed in thickness and increases in area, resulting in a decrease in thickness and stretching in area of both the elastomeric substrate and the CLC elastomer that are adhered on top of the DEA. Hence the top electrode must be very uniform and should adhere well to the elastomeric substrate/CLC elastomer.

The second proposed configuration is shown in Figure 7.2. Here the elastomeric substrate is used as the DE membrane. To achieve colour in reflection mode, the top electrode must be transparent so that any change in colour due to change in the thickness of the CLC elastomer as a result of applied voltage is observable through the top electrode.

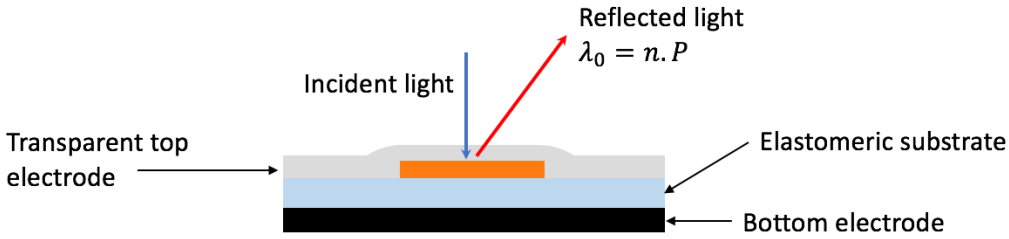

Figure 7.2- Schematic representation of second proposed DEA device with transparent top electrode.

A third proposed configuration is shown in Figure 7.3. Here the CLC elastomer is transfer printed onto the central region of the DEA directly on the elastomeric substrate whilst the device is in the actuated state. This results in CLC elastomer that can be stretched in area and reduced in thickness when the voltage is turned off and the DEA is at rest. This DEA configuration has an additional advantage that it can be operated not only in a reflection mode but also in transmission.

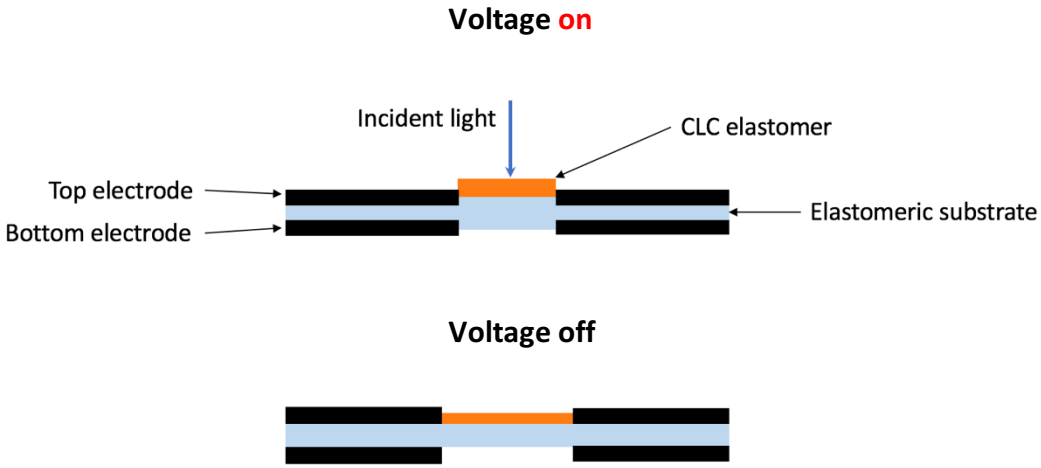

Figure 7.3- Schematic representation of third proposed DEA device showing activation state and at rest.

References

AKBARI, S., ROSSET, S. & SHEA, H. R. 2013. Improved electromechanical behavior in castable dielectric elastomer actuators. *Applied Physics Letters,* 102**,** 071906.

ALAM, M. Z., YOSHIOKA, T., OGATA, T., NONAKA, T. & KURIHARA, S. 2007. Influence of helical twisting power on the photoswitching behavior of chiral azobenzene compounds: applications to high-performance switching devices. *Chemistry,* 13**,** 2641-7.

AMIMORI, I., PRIEZJEV, N. V., PELCOVITS, R. A. & CRAWFORD, G. P. 2003. Optomechanical properties of stretched polymer dispersed liquid crystal films for scattering polarizer applications. *Journal of Applied Physics,* 93**,** 3248.

ANDERSON, I. A., GISBY, T. A., MCKAY, T. G., O'BRIEN, B. M. & CALIUS, E. P. 2012. Multi-functional dielectric elastomer artificial muscles for soft and smart machines. *Journal of Applied Physics,* 112**,** 041101.

ASCHWANDEN, M., NIEDERER, D. & STEMMER, A. 2008. Tunable transmission grating based on dielectric elastomer actuators. *Electroactive Polymer Actuators and Devices (EAPAD),* 6927**,** 69271R-69271R-12.

BLEILE, D. M. 1997. Immunoassay. Eleftherios P. Diamandis and Theodore K. Christopoulos, eds. San Diego: Academic Press, 1996, 579 pp, Paperback. ISBN 0-12-214730-8. *Clinical Chemistry,* 43**,** 550-550.

BROCHU, P. & PEI, Q. 2010. Advances in dielectric elastomers for actuators and artificial muscles. *Macromol Rapid Commun,* 31**,** 10-36.

BROER, D. J., FOUASSIER, J. P. & RABEK, J. F. 1993. *Radiation Curing in Polymer Science and Technology*.

BROER, D. J., MOL, G. N. & CHALLA, G. 1991. *Makromol. Chem.,* 192**,** 59.

CARPI, F. & DE ROSSI, D. 2005. Electroactive polymer-based devices for e-textiles in biomedicine. *Ieee Transactions on Information Technology in Biomedicine,* 9**,** 295-318.

CARPI, F. & DE ROSSI, D. 2007. Bioinspired actuation of the eyeballs of an android robotic face: concept and preliminary investigations. *Bioinspir Biomim*, 2, S50-63.

CARPI, F., DE ROSSI, D., KORNBLUH, R., PELRINE, R. & SOMMER-LARSEN, P. 2008. Dielectric Elastomers as Electromechanical Transducers. 1 ed. Oxford: Elsevier.

CARPI, F., FREDIANI, G. & DE ROSSI, D. 2012. Electroactive elastomeric actuators for biomrdical and bioinspired systems. *The Fourth IEEE RAS/EMBS International Conference on Biomedical Robotics and Biomechatronics.* Roma, Italy.

CARPI, F., FREDIANI, G., TURCO, S. & DE ROSSI, D. 2011. Bioinspired Tunable Lens with Muscle-Like Electroactive Elastomers. *Advanced Functional Materials,* 21**,** 4152-4158.

COLLINGS, P. J. 1990. *Liquid Crystals: Nature's Delicate Phase of Matter*, Published by Princeton University.

COLLINGS, P. J. & HIRD, M. 1997. *Introduction to Liquid Crystals: chemistry and physics*, Taylor & Francis Group.

DAVIS, F. J. 1993. Liquid-crystalline elastomers. *Journal of Materials Chemistry,* 3**,** 551-562.

DE GENNES, P.-G. 1997. Un muscle artificiel semi-rapide. *Comptes Rendus de l'Académie des Sciences - Series IIB - Mechanics-Physics-Chemistry-Astronomy,* 324**,** 343-348.

DIERKING, I. 2003. *Textures of Liquid Crystals*, Wiley and Sons.

DISSADO, I. A. & FOTHERGILL, J. C. 1992. *Electrical degradation and breakdown in polymers,* London, United Kingdom, Peter Peregrinus.

DOANE, J. W., GOLEMME, A., WEST, J. L., WHITEHEAD, J. B. & WU, B. G. 1988. Polymer Dispersed Liquid-Crystals for Display Application. *Molecular Crystals and Liquid Crystals,* 165**,** 511-532.

DRZAIC, P. S. 1995. *Liquid crystal dispersions,* Singapore; River Edge, NJ, World Scientific.

ELIAS, A. L., HARRIS, K. D., BASTIAANSEN, C. W. M., BROER, D. J. & BRETT, M. J. 2006. Photopatterned liquid crystalline polymers for microactuators. *Journal of Materials Chemistry,* 16**,** 2903.

FANG, Z. H., PUNCKT, C., LEUNG, E. Y., SCHNIEPP, H. C. & AKSAY, I. A. 2010. Tuning of structural color using a dielectric actuator and multifunctional compliant electrodes. *Applied Optics,* 49**,** 6689-6696.

FINKELMANN, H. 1987. Liquid Crystalline Polymers. *Angew. Chem. Int. Ed,* 26**,** 816–824.

FINKELMANN, H. 1988. Liquid Crystals—State of the Art. *Angew. Chem.,* 100**,** 1019-1020.

FINKELMANN, H., KIM, S. T., MUNOZ, A., MUHORAY, P. P. & TAHERI, B. 2001. Tunable mirrorless lasing in cholesteric crystalline elastomers. *Advance Materilas,* 13**,** 1069-1072.

FUDOUZI, H. 2016. Tunable structural color in organisms and photonic materials for design of bioinspired materials. *Science and Technology of Advanced Materials,* 12**,** 064704.

FUDOUZI, H. & SAWADA, T. 2006. Photonic Rubber Sheets with Tunable Color by Elastic Deformation. *Langmuir,* 22**,** 1365-1368.

HU, L. B., YUAN, W., BROCHU, P., GRUNER, G. & PEI, Q. B. 2009. Highly stretchable, conductive, and transparent nanotube thin films. *Applied Physics Letters,* 94.

HU, W., NIU, X., LI, L., YUN, S., YU, Z. & PEI, Q. 2012. Intrinsically stretchable transparent electrodes based on silver-nanowire-crosslinked-polyacrylate composites. *Nanotechnology,* 23**,** 344002.

ISABEL, A., PETROVA, K., TERESA, M. & SOTOMAYOR, J. 2012. New Polymer Networks for PDLC Films Application.

JORDI, C., MICHEL, S. & FINK, E. 2010. Fish-like propulsion of an airship with planar membrane dielectric elastomer actuators. *Bioinspir Biomim,* 5**,** 026007.

KEPLINGER, C., KALTENBRUNNER, M., ARNOLD, N. & BAUER, S. 2010. Rontgen's electrode-free elastomer actuators without electromechanical pull-in instability. *Proc Natl Acad Sci U S A,* 107**,** 4505-10.

KEPLINGER, C., SUN, J.-Y., FOO, C.C., ROTHEMUND, P., WHITESIDES, G. M. & SUO, Z. 2013. Stretchable, Transparent, Ionic Conductors. *Science*, 341**,** 984-987.

KIM, Y., JUNG, D., JEONG, S., KIM, K., CHOI, W. & SEO, Y. 2015. Optical properties and optimized conditions for polymer dispersed liquid crystal containing UV curable polymer and nematic liquid crystal. *Current Applied Physics,* 15**,** 292-297.

KINOSHITA, S. & YOSHIOKA, S. 2005. Structural colors in nature: the role of regularity and irregularity in the structure. *Chemphyschem,* 6**,** 1442-59.

KOFOD, G., SOMMER-LARSEN, P., KORNBLUH, R. & PELRINE, R. 2003. Actuation Response of Polyacrylate Dielectric Elastomers. *Journal of Intelligent Materials Systems and Structures,* 14**,** 787-793.

KOFOD, G., PAAJANEN, M. & BAUER, S. 2006. Self-organized minimum-energy structures for dielectric elastomer actuators. *Applied Physics A,* 85**,** 141-143.

KOH, S. J. A., LI, T., ZHOU, J., ZHAO, X., HONG, W., ZHU, J. & SUO, Z. 2011. Mechanisms of large actuation strain in dielectric elastomers. *Journal of Polymer Science Part B: Polymer Physics,* 49**,** 504-515.

KOLLE, M., SALGARD-CUNHA, P. M., SCHERER, M. R. J., HUANG, F., VUKUSIC, P., MAHAJAN, S., BAUMBERG, J. J. & STEINER, U. 2010. Mimicking the colourful wing scale structure of the Papilio blumei butterfly. *Nat Nano,* 5**,** 511-515.

KORNBLUH, R., PELRINE, R., PEI, Q. B., HEYDT, R., STANFORD, S., OH, S. J. & ECKERLE, J. 2002. Electroelastomers: Applications of dielectric elastomer transducers for actuation, generation and smart structures. *Smart Structures and Materials 2002: Industrial and Commercial Applications of Smart Structures Technologies,* 4698**,** 254-270.

KOVACS, G. & DURING, L. 2009. Contractive tension force stack actuator based on soft dielectric EAP. *Electroactive Polymer Actuators and Devices (EAPAD),* 7287.

KOVACS, G., DÜRING, L., MICHEL, S. & TERRASI, G. 2009. Stacked dielectric elastomer actuator for tensile force transmission. *Sensors and Actuators A: Physical,* 155**,** 299-307.

KUPFER, J. & FINKELMANN, H. 1991. Nematic Liquid Single-Crystal Elastomers. *Makromolekulare Chemie-Rapid Communications,* 12**,** 717-726.

LI, M. H. & KELLER, P. 2006. Artificial muscles based on liquid crystal elastomers. *Philos Trans A Math Phys Eng Sci,* 364**,** 2763-77.

LIU, D. & BROER, D. J. 2014. Liquid Crystal Polymer Networks: Preparation, Properties, and Applications of Films with Patterned Molecular Alignment. *Langmuir,* 30**,** 13499-13509.

MAFFLI, L. 2014. *Fluidically-coupled dielectric elastomer actuator structures for tunable optics and microfluidics.* École polytechnique fédérale de Lausanne (EPFL).

MALIK, P. & RAINA, K. K. 2004. Droplet orientation and optical properties of polymer dispersed liquid crystal composite films. *Optical Materials,* 27**,** 613-617.

MITOV, M. 2012. Cholesteric liquid crystals with a broad light reflection band. *Adv Mater,* 24**,** 6260-76.

MULDER, D. J., SCHENNING, A. P. H. J. & BASTIAANSEN, C. W. M. 2014. Chiral-nematic liquid crystals as one dimensional photonic materials in optical sensors. *Journal of Materials Chemistry C,* 2**,** 6695-6705.

O'HALLORAN, A., O'MALLEY, F. & MCHUGH, P. 2008. A review on dielectric elastomer actuators, technology, applications, and challenges. *Journal of Applied Physics,* 104**,** 071101.

OHM, C., BREHMER, M. & ZENTEL, R. 2010. Liquid crystalline elastomers as actuators and sensors. *Adv Mater,* 22**,** 3366-87.

OSWALD, P. & PIERANSKI, P. 2005. *Nematic and Cholesteric Liquid Crystals,* United States of America, Taylor & Francis Group.

OUYANG, G., WANG, K., HENRIKSEN, L., AKRAM, M. N. & CHEN, X. Y. 2010. A novel tunable grating fabricated with viscoelastic polymer (PDMS) and conductive polymer (PEDOT). *Sensors and Actuators A: Physical,* 158**,** 313-319.

PARAB, S. S., MALIK, M. K., BHATIA, P. G. & DESHMUKH, R. R. 2014. Investigation of liquid crystal dispersion and dielectric relaxation behavior in polymer dispersed liquid crystal composite films. *Journal of Molecular Liquids,* 199**,** 287-293.

PARK, L. Y. 1999. *Light and colour in liquid crystalline materials* [Online]. Anaheim, CA: Journal of Chemical Education. Available: http://education.mrsec.wisc.edu/courses/colorsymp/park/index.html [Accessed June 2016.

PARK, S. & HONG, J. W. 2009. Polymer dispersed liquid crystal film for variable-transparency glazing. *Thin Solid Films,* 517**,** 3183-3186.

PARKER, A. R. 2000. 515 million years of structural colour. *Journal of Optics A: Pure and Applied Optics,* 2**,** R15.

PELRINE, R., KORNBLUH, R., PEI, Q. & JOSEPH, J. 2000. High-Speed Electrically Actuated Elastomers with Strain Greater Than 100%. *Science,* 287**,** 836-839.

PELRINE, R. E., KORNBLUH, R. D. & JOSEPH, J. P. 1998. Electrostriction of polymer dielectrics with compliant electrodes as a means of actuation. *Sensors and Actuators a-Physical,* 64**,** 77-85.

PICOT, O. 2014. *Functional Films and Fibres based on Liquid Crystal Coatings.* Doctor of Philosophy, Queen Mary University of London.

PICOT, O., PEIJS, T. & BASTIAANSEN, K. 2012. Production of reflective fibres for smart textile applications.

PICOT, O. T., DAI, M., BILLOTI, E., BROER, D. J., PEIJS, T. & BASTIAANSEN, C. W. M. 2013a. A real time optical strain sensor based on a cholesteric liquid crystal network. *Rsc Advances,* 3**,** 18794-18798.

PICOT, O. T., DAI, M., BROER, D. J., PEIJS, T. & BASTIAANSEN, C. W. 2013b. New approach toward reflective films and fibers using cholesteric liquid-crystal coatings. *ACS Appl Mater Interfaces,* 5**,** 7117-21.

PLANTE, J.-S. & DUBOWSKY, S. 2006. Large-scale failure modes of dielectric elastomer actuators. *International Journal of Solids and Structures,* 43**,** 7727-7751.

RAETHER, H. 1988. Surface-Plasmons on Smooth and Rough Surfaces and on Gratings. *Springer Tracts in Modern Physics,* 111**,** 1-133.

RAINA, K. K. & KUMAR, P. 2009. Polymer dispersed liquid crystal composite films-droplet orientation and optical responses. *Journal of the Indian Institute of Science,* 89.

RICHARD, J. P. 2007. Advances in Physical Organic Chemistry. Academic Press.

ROSSET, S. & SHEA, H. R. 2012. Flexible and stretchable electrodes for dielectric elastomer actuators. *Applied Physics A*.

ROSSITER, J., CONN, A., CERRUTO, A., WINTERS, A. & ROKE, C. Colour gamuts in polychromatic dielectric elastomer artificial chromatophores. 2014. 905620-905620-8.

ROSSITER, J., YAP, B. & CONN, A. 2012. Biomimetic chromatophores for camouflage and soft active surfaces. *Bioinspir Biomim,* 7**,** 036009.

SAWA, Y., YE, F., URAYAMA, K., TAKIGAWA, T., GIMENEZ-PINTO, V., SELINGER, R. L. B. & SELINGER, J. V. 2011. Shape selection of twist-nematic-elastomer ribbons. *Proceedings of the National Academy of Sciences of the United States of America,* 108**,** 6364-6368.

SCHARF, T. 2007. *Polarized Light in Liquid Crystals and Polymers,* New Jersey, John Wiley & Sons.

SCHARF., T. 2007. *Polarized light in liquid crystals and polymers,* Canada, Wiley.

SHARMA, V., CRNE, M., PARK, J. O. & SRINIVASARAO, M. 2009. Structural Origin of Circularly Polarized Iridescence in Jeweled Beetles. *Science,* 325**,** 449-451.

SHIBAEV, P. V., RIVERA, P., TETER, D., MARSICO, S., SANZARI, M., RAMAKRISHNAN, V. & HANELT, E. 2008. Color changing and lasing stretchable cholesteric films. *Optics Express,* 16**,** 2965-2970.

SHIBAEV, P. V., UHRLASS, R., WOODWARD, S., SCHLESIER, C., ALI, M. R. & HANELT, E. 2010. Mechanism of colour changes in stretchable cholesteric films. *Liquid Crystals,* 37**,** 587-592.

SHIEH, J. Y., KUO, J. Y., WENG, H. P. & YU, H. H. 2013. Preparation and evaluation of the bioinspired PS/PDMS photochromic films by the self-assembly dip-drawing method. *Langmuir,* 29**,** 667-72.

SON, S.-I., PUGAL, D., HWANG, T., CHOI, H. R., KOO, J. C., LEE, Y., KIM, K. & NAM, J. D. 2012. Electromechanically driven variable-focus lens based on transparent dielectric elastomer. *Applied Optics,* 51**,** 2987-2995.

ST. JOHN, W. D., FRITZ, W. J., LU, Z. J. & YANG, D. K. 1995. Bragg reflection from cholesteric liquid crystals. *Physical Review E,* 51**,** 1191-1198.

STARK, K. H. & GARTON, C. G. 1955. Electric Strength of Irradiated Polythene. *Nature,* 176**,** 1225-1226.

SUZUMORI, K., MIHARA, M. & WAKIMOTO, S. Beautiful Flexible Microactuator changing its structural color with variable pitch grating. Robotics and Automation (ICRA), 2011 IEEE International Conference on, 9-13 May 2011 2011. 2771-2776.

THAKUR, V. K. & KESSLER, M. R. 2015. *Liquid Crystalline Polymers: Volume 1– Structure and Chemistry*, Springer International Publishing.

VUKUSIC, P. & SAMBLES, J. R. 2003. Photonic structures in biology. *Nature,* 424**,** 852-855.

WARNER, M. & TERENTJEV, E. M. 2003. Liquid Crystal Elastomers. 422.

WINKLER, M., KAISER, A., KRAUSE, S., FINKELMANN, H. & SCHMIDT, A. M. 2010. Liquid Crystal Elastomers with Magnetic Actuation. *Macromolecular Symposia,* 291-292**,** 186-192.

XIE, P. & ZHANG, R. 2005. Liquid crystal elastomers, networks and gels: advanced smart materials. *Journal of Materials Chemistry,* 15**,** 2529.

YUN, S., NIU, X. F., YU, Z. B., HU, W. L., BROCHU, P. & PEI, Q. B. 2012. Compliant Silver Nanowire-Polymer Composite Electrodes for Bistable Large Strain Actuation. *Advanced Materials,* 24**,** 1321-1327.

ZHANG, S. & CHEN, Y. 2015. Nanofabrication and coloration study of artificial Morpho butterfly wings with aligned lamellae layers. *Sci Rep,* 5**,** 16637.

ZHAO, Y., XIE, Z., GU, H., ZHU, C. & GU, Z. 2012. Bio-inspired variable structural color materials. *Chem Soc Rev,* 41**,** 3297-317.

ZHU, X., SHI, L., LIU, X., ZI, J. & WANG, Z. 2010. A mechanically tunable plasmonic structure composed of a monolayer array of metal-capped colloidal spheres on an elastomeric substrate. *Nano Research,* 3**,** 807-812.

ZOU, J. & FANG, J. 2011. Adhesive polymer-dispersed liquid crystal films. *Journal of Materials Chemistry,* 21**,** 9149.